INAUGURAL - DISSERTATION
zur
Erlangung der Doktorwürde
der
Naturwissenschaftlich - Mathematischen Gesamtfakultät
der
Ruprecht - Karls - Universität
Heidelberg

vorgelegt von
Dipl.-Math. Volkmar Reinhardt
aus Essen

Tag der mündlichen Prüfung: 21. November 2008

On the Application of Trajectory-based Optimization for Nonlinear Kinetic Model Reduction

Gutachter: Prof. Dr. Dr. h.c. Hans Georg Bock
PD Dr. Dirk Lebiedz

To my wife Heidi and my daughter Johanna

and to

Prof. Dr. Dr. h.c. Jürgen Warnatz, who passed away too early

Only love has no limits. In contrast, our predictions can fail, our communication can fail, and our knowledge can fail. For our knowledge is patchwork, and our predictive power is limited. But when perfection comes, all patchwork will disappear.

(*Prof. Dr. Arnold Neumaier's* paraphrase to *1 Cor. 13:8-10*)

Abstract

The use of increasingly detailed reaction mechanisms for the chemistry description in computational fluid dynamics simulations plays a major role in combustion research. Model reduction adresses the discrepancy between the need to develop detailed high-dimensional multi-scale models (e.g. in chemical kinetics) and the inefficiency of their use in computationally demanding numerical simulations. Many modern model reduction approaches are based on the approximation of slow invariant manifolds of lower dimension than the original system. Pursuing the work of Lebiedz on Minimum Entropy Production Trajectories (MEPT), this work presents a way to approximate slow invariant manifolds based on the optimization of trajectories. This work particularly covers the generalization of the MEPT concept for the construction of invariant manifolds of arbitrary dimension and guides the way for the construction of general relaxation criteria. Especially the minimization of curvature of trajectories – used for model reduction purposes for the first time within the scope of this work – leads to highly encouraging results, where the optimized trajectories are close to the slow invariant manifold. For the derivation of a reliable method for the construction of low-dimensional manifolds to be used in chemical kinetics, this work deals with advanced numerical methods, ideas from thermodynamics and differential geometry.

Kurzfassung

Für die Beschreibung chemischer Reaktionen für Simulationen numerischer Strömungsmechanik in der Verbrennungsforschung wird die Benutzung immer detaillierterer Reaktionsmechanismen zunehmend wichtiger. Die Modellreduktion befasst sich mit der Diskrepanz zwischen der Notwendigkeit solcher hochdimensionalen Multiskalenmodelle (z.B. in der chemischen Reaktionskinetik) und deren Limitierung in der Anwendung in hohe Rechenleistung erfordernden numerischen Simulationen. Viele moderne Modellreduktionsansätze fußen auf der Approximation langsamer invarianter Mannigfaltigkeiten, die gegenüber dem ursprünglichen System eine niedrigere Dimension aufweisen. Basierend auf der Arbeit von Lebiedz über Trajektorien minimaler Entropieproduktion (Minimum Entropy Production Trajectories – MEPT) befasst diese Arbeit sich mit der Approximation langsamer invarianter Mannigfaltigkeiten durch die Optimierung von Trajektorien. Insbesondere wird dabei das MEPT-Konzept für die Konstruktion invarianter Mannigfaltigkeiten beliebiger Dimension verallgemeinert und Wege zur Konstruktion allgemeiner Relaxationskriterien aufgezeigt. Vor allem die Minimierung der Krümmung von Trajektorien, die im Rahmen dieser Arbeit das erste mal für Zwecke der Modellreduktion angewendet wird, führt zu viel versprechenden Ergebnissen, bei denen die optimierten Trajektorien sehr nah an der langsamen invarianten Mannigfaltigkeit liegen. Um eine zuverlässige Methode für die Konstruktion niedrigdimensionaler Mannigfaltigkeiten für chemische Reaktionskinetik zu entwickeln, befasst sich diese Arbeit mit hochentwickelten numerischen Methoden, Ideen aus der Thermodynamik und der Differentialgeometrie.

Acknowledgements

There are many people I want to thank for their direct or indirect help and support along the way towards the completion of this work.
First, I want to thank Prof. Dr. Dr. h.c. Hans Georg Bock for the supervision and assessment of this work and for providing mathematical software from his research group "Simulation and Optimization" at the IWR.
I want to express my heartfelt gratitude to my mentor PD Dr. Dirk Lebiedz. For one thing I want to thank him for putting his trust in me to pursue this exciting project initiated by him, but more than this for many conversations far beyond the scientific support.
My deeply felt thanks to Prof. Dr. Dr. h.c. Jürgen Warnatz for making the employment at the Interdisciplinary Center for Scientific Computing (IWR) possible and giving me the opportunity to do be involved in this fascinating research. It is my deepest grief to be forced to express this gratitude postmortem.
The funding of the German Research Foundation (DFG) through the Special Resarch Area (SFB) 568 is gratefully acknowledged.
For his help with the embedding of this work's model reduction approach in his parametric optimization code I cordially thank Prof. Dr. Moritz Diehl, who is now at K.U. Leuven. Andreas Potschka deserves many thanks for his continual help with software problems and the advice to use the "complex-step derivative approximation" for the computation of curvature and Dr. Mario Mommer for fruitful mathematical discussions.
For the careful proofreading of the manuscript of this work, I sincerely thank Jochen Siehr, Andrea Wilming and Miriam Winckler, the latter is moreover gratefully acknowledged for her commitment during the work on her diploma thesis about the matter this work is concerned with.
I also want to thank my colleagues from the SFB 568 for the collaboration and interesting discussions and the whole research group "Reactive Flows" for the extraordinary friendly work climate. I particularly thank PD Dr. Uwe Riedel for all administrative, Ingrid Hellwig for all organizational issues and Jürgen Moldenhauer, Joachim Simon and Jens Marquetand for the computer administration.
With all my heart I would like to thank my parents for their support in every sense without which my studies would not have been possible. Sincere thanks are given to all my friends who supported me in my studies, particularly to my friends from the Karlstorgemeinde Heidelberg for their prayers and God for answering them.
Finally, I want to thank my wife Heidi and my daughter Johanna – your patience, support and encouragement helped more than you might know.

Contents

Acronyms

BDF	Backward Differentiation Formula
BVP	Boundary Value Problem
CSP	Computational Singular Perturbation
DAE	Differential Algebraic Equation
FGM	Flamelet Generated Manifold
ICE-PIC	Invariant Constrained Equilibrium Edge Preimage Curve
ILDM	Intrinsic Low-Dimensional Manifold
IVP	Initial Value Problem
NLP	Nonlinear Programming Problem
NMPC	Nonlinear Model-Predictive Control
MEPT	Minimal Entropy Production Trajectory
ODE	Ordinary Differential Equation
PEA	Partial Equilibrium Assumption
QSSA	Quasi Steady-State Assumption
RCCE	Rate-Controlled Constrained Equilibrium
r.h.s.	right hand side
SIM	Slow Invariant Manifold
SQP	Sequential Quadratic Programming
w.r.t.	with respect to

Chapter 1

Introduction

The scientific examination of combustion is motivated by the fact that combustion is, by far, the main energy source of today's world. Driven by economical and ecological needs, the optimization of combustion processes plays a major role in combustion research.
Early combustion research was rather directed to fluid dynamics, often under the assumption of infinitely fast chemistry. While this approach may be successful for stationary combustion, it is not sufficient to treat e.g. pollutant formation or transient processes, which require a detailed chemistry treatment. Since the late seventies of the last century numerical simulations of combustion including chemical reaction kinetics have developed from laminar flat flame calculations [91, 92, 93] to modern computational fluid dynamics that can resolve turbulent structures [1].
Along with this development, reaction mechanisms for the detailed description of chemistry in combustion processes are on the increase. Modern reaction mechanisms may contain hundreds of species and thousands of reactions. Despite growing computer power, a solution of these detailed reaction mechanisms in a full spatiotemporal reactive flow simulation is not in sight.
This is where model reduction comes into application. A key issue of model reduction is to address the discrepancy between the need to develop detailed high-dimensional models (e.g. in chemical kinetics) and the inefficiency of their use in computationally demanding multi-scale numerical simulations. The ultimate goal of all model reduction techniques in chemical kinetics is to find a low-dimensional approximation of a reaction mechanism which contains essential information to still describe the system accurately enough. For models of chemical kinetics this is equivalent to identifying the essential degrees of freedom with respect to (w.r.t.) the system properties of interest. Those properties of interest are often related to long-term dynamics. To construct low-dimensional approximations, many model reduction tech-

niques therefore make use of intrinsic multiple time scales. If the long-term behaviour of a system is to be studied, fast transient dynamical modes are assumed to be relaxed within the reduced model approximation replacing the original system of differential equations by one of lower dimension without losing too much key information about the long-term system dynamics.
An important point in simulations of technical processes is that usually all species are relevant for the properties of interest and therefore have to be considered, not only the ones that parametrize the reduced reaction mechanism. Hence the concentrations for the species of the full mechanism need to be calculated automatically as functions of the species parametrizing the reduced mechanism. This so-called *automatic species reconstruction* is implemented in most of the model reduction algorithms, independently of the concepts the methods are based on.
Algorithms for model reduction in chemical kinetics range from "manual" methods like quasi steady-state or partial equilibrium assumptions to modern methods approximating slow invariant manifolds. Many of the model reduction methods are not generally restricted to the application in chemical kinetics. However, the methods benefit from the large number of fast transient processes in chemical reaction mechanisms which enable a very efficient reduction without imposing too large errors.
While many model reduction methods have been introduced in the past and most modern ones are based on the approximation of slow invariant manifolds, the problem of a simple and robust method to compute such manifolds still remains. For example many methods suffer from their local character.
Nowadays, sophisticated mathematical tools allow for the computation of optimal trajectories for dynamical systems such as chemical reaction mechanisms. Mathematically, this computation of optimal trajectories corresponds to a so-called *variational boundary-value problem*. As the original formulation of such a problem is of infinite dimension, a discretization provides a finite dimensional Nonlinear Programming Problem (NLP), which can be solved using standard approaches, e.g. Sequential Quadratic Programming (SQP).
Based on these tools, Lebiedz [50] presented a novel approach to model reduction in chemical kinetics. The resulting trajectories are supposed to be maximally relaxed with respect to an optimization criterion which, for these calculations, was chosen to be minimal entropy production rate in [50]. The variables parametrizing the low-dimensional manifold – the so-called progress variables – find a fully natural realization as initial values of the trajectory in this context. This approach assures that at least an approximation of slow attracting manifolds that is "as good as possible" in the sense of the optimization criterion is found, even in regions where other model reduction methods requiring a clear time scale separation – as for example the Intrinsic

Low-Dimensional Manifold (ILDM) [60] – fail.
Pursuing Lebiedz's optimality concept, this work presents a generalized trajectory-based optimization approach suitable for the accurate computational approximation of slow invariant manifolds and its application to increasingly realistic kinetic models. In particular, this work covers the derivation of alternative criteria for the optimization of trajectories and the efficient evaluation of the variational boundary value problems to improve the quality of the resulting approximations of slow attracting manifolds. The approach is also adapted for the computation of higher-dimensional manifolds, where optimal trajectories are computed for different initial values. A parametric embedding of the optimization problem serves for an efficient solution of these neighbouring problems.
In summary, this work brings together highly sophisticated numerical methods, ideas from thermodynamics and differential geometry to derive a reliable method for the construction of low-dimensional manifolds to be used in chemical kinetics.

1.1 Outline

The structure of this thesis is as follows:
In Chapter 2 a detailed overview of methods for the reduction of chemical kinetics modeled by Ordinary Differential Equation (ODE) systems is given. The methods presented range from quasi steady-state and partial equilibrium assumptions to modern manifold methods.
Chapter 3 introduces the theoretical background which is used for both the description and reduction of models in chemical kinetics in this work. These comprise chemical kinetics for the description of chemical reactions in terms of ODE systems, basic theory of dynamical systems for the solution of these ODE systems and elements from thermodynamics and differential geometry which are used for the reduction of ODE models in this work.
The trajectory-based optimization approach for model reduction that is employed in this work is described by a variational boundary value problem. Chapter 4 introduces the methods for the numerical solution of this problem. These methods cover the computation of single optimal trajectories as well as the embedding of these computations in a parametric optimization setting.
Bringing together the ideas from the previous chapters, a general strategy for model reduction by trajectory-optimization is presented in Chapter 5. Along with a numerical continuation strategy and a detailed description of the relaxation criteria to be used in this framework, this strategy constitutes

the methodological focus of this work.
The main results achieved with this strategy are presented in Chapter 6. The variety of underlying dynamical systems, for which results are presented, ranges from small two-dimensional systems to a realistic hydrogen combustion mechanism. These examples can also be found in the Appendix.
The thesis is summarized in Chapter 7 along with an extended outlook. This extended outlook has its focus on the extension of the developed method for large-scale model reduction.

Chapter 2

Model Reduction in Chemical Kinetics

"It is useful to solve invariance equations."
Alexander N. Gorban (following Newton)
at a workshop on model reduction

Model reduction is situated at the discrepancy between increasingly detailed models for chemical kinetics and high-resolution spatiotemporal numerical calculations that need to rely on these models at every grid-point.
The aim of model reduction therefore is the low-dimensional description of high-dimensional models while preserving the most important features such as the long term dynamics.
In this chapter, common model reduction techniques for chemical and biochemical systems modeled by Ordinary Differential Equation (ODE) systems

$$\dot{x_i} = F_i(x) = \sum_{j=1}^{m} \nu_{ij} v_j(x), \quad i = 1, ..., n \tag{2.1}$$

and their applications in practical simulations are reviewed.
In practical applications, the components x_i of the vector x usually denote (bio)chemical *species* and v_j denotes the velocity of the j-th *reaction*. The *stoichiometric coefficients* ν_{ij} determine the reactions that contribute to the formation and consumption of the i-th species. The aim of a lower-dimensional description is usually met by reducing the number of differential variables x_i.
As the presentation of the model reduction methods in this chapter is designed to be a summary, the reader is referred to [33, 68] for comprehensive overviews of the most common model reduction techniques and their underlying concepts. Comparisons of different methods for the construction of invariant manifolds can be found in [14].

2.1 Model Reduction Methods – Overview

2.1.1 QSSA and PEA

The Quasi Steady-State Assumption (QSSA) [9, 10, 13] (or Quasi-Stationary Assumption) and the Partial Equilibrium Assumption (PEA) [62] have been among the first ideas to reduce chemical reaction mechanisms [45, 46, 84, 88]. The key idea of both assumptions is similar. The QSSA assumes certain *species* to be in a steady-state, while the PEA assumes certain *reactions* to be in equilibrium.
A good explanation of the QSSA is found in the following simple example from [95]:

Example 2.1 (QSSA)
Consider the reaction

$$\mathrm{S}_1 \overset{k_{12}}{\rightarrow} \mathrm{S}_2 \overset{k_{23}}{\rightarrow} S_3 \tag{2.2}$$

described by the ODE system

$$\frac{\mathrm{d}[\mathrm{S}_1]}{\mathrm{d}t} = -k_{12}[\mathrm{S}_1] \tag{2.3a}$$

$$\frac{\mathrm{d}[\mathrm{S}_2]}{\mathrm{d}t} = k_{12}[\mathrm{S}_1] - k_{23}[\mathrm{S}_2] \tag{2.3b}$$

$$\frac{\mathrm{d}[\mathrm{S}_3]}{\mathrm{d}t} = k_{23}[\mathrm{S}_2]. \tag{2.3c}$$

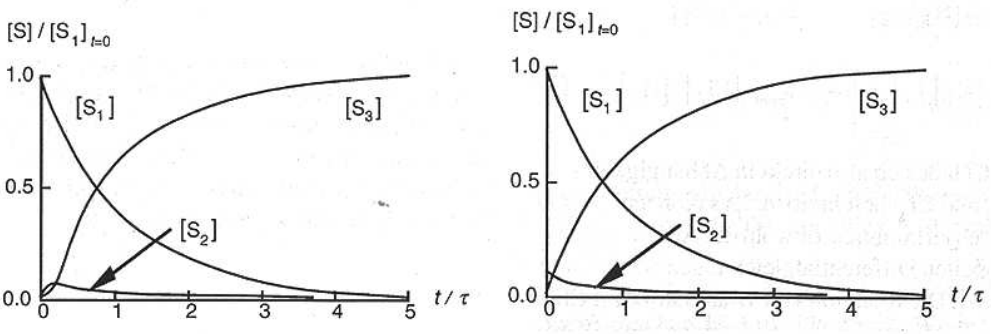

Figure 2.1: Left: Exact solution of ODE system 2.3, right: Temporal evolution of the reaction $\mathrm{S}_1 \rightarrow \mathrm{S}_2 \rightarrow S_3$ with assumed quasi-stationarity for $[\mathrm{S}_2]$ [95].

If S_2 is assumed to be a reactive particle, its formation and decomposition can be assumed to have similar velocity

$$\frac{\mathrm{d}[\mathrm{S}_2]}{\mathrm{d}t} = k_{12}[\mathrm{S}_1] - k_{23}[\mathrm{S}_2] \approx 0 \tag{2.4}$$

and hence (2.3b) can be replaced by

$$[S_2] = \frac{k_{12}}{k_{23}}[S_1]. \tag{2.5}$$

Figure 2.1 shows a comparison of the exact solution of the linear ODE system (2.3) and the solution assuming quasi-stationarity for $[S_2]$.

Another common example for the QSSA is the Michaelis-Menten kinetics [62], where – similar to the above example – the concentration of an intermediate species is assumed to be in steady-state.
As stated above, the PEA is conceptually similar to the QSSA, except that the major assumption is on reactions as opposed to species. This idea again is explained by an example from [95]:

Example 2.2 (PEA)
The analysis of experiments or simulations with reaction mechanisms for the combustion of hydrogen shows that for large temperatures (e.g. $T > 1800\,\mathrm{K}$ at $p = 1\,\mathrm{bar}$) reaction velocities of forward and reverse reactions are so high that the reactions

$$\mathrm{OH} + \mathrm{H_2} \rightleftharpoons \mathrm{H_2O} + \mathrm{H} \tag{2.6a}$$
$$\mathrm{H} + \mathrm{O_2} \rightleftharpoons \mathrm{OH} + \mathrm{O} \tag{2.6b}$$
$$\mathrm{O} + \mathrm{H_2} \rightleftharpoons \mathrm{OH} + \mathrm{H} \tag{2.6c}$$

are in a so-called *partial equilibrium*, i.e. their forward and reverse reactions have (approximately) equal velocity. Equating the reaction velocities yields the algebraic expressions

$$\begin{aligned} k_1[\mathrm{OH}][\mathrm{H_2}] &= k_2[\mathrm{H_2O}][\mathrm{H}] \\ k_3[\mathrm{H}][\mathrm{O_2}] &= k_4[\mathrm{OH}][\mathrm{O}] \\ k_5[\mathrm{O}][\mathrm{H_2}] &= k_6[\mathrm{OH}][\mathrm{H}] \end{aligned}$$

that can be solved for the radical species O, H and OH

$$[\mathrm{H}] = \left(\frac{k_1^2 k_3 k_5 [\mathrm{O_2}][\mathrm{H_2}]^3}{k_2^2 k_4 k_6 [\mathrm{H_2O}]^2}\right)^{\frac{1}{2}} \tag{2.7a}$$
$$[\mathrm{O}] = \frac{k_1 k_3 [\mathrm{O_2}][\mathrm{H_2}]}{k_2 k_4 [\mathrm{H_2O}]} \tag{2.7b}$$
$$[\mathrm{OH}] = \left(\frac{k_3 k_5}{k_4 k_6}[\mathrm{O_2}][\mathrm{H_2}]\right)^{\frac{1}{2}}. \tag{2.7c}$$

Hence the radical particles are expressed in terms of the more stable particles $[H_2]$, $[O_2]$ and $[H_2O]$. In [94] this procedure has been compared to a detailed reaction mechanism. Figure 2.2 shows that the PEA yields satisfactory results only for high temperatures.

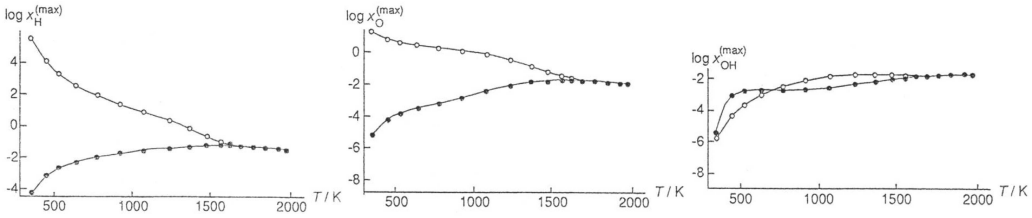

Figure 2.2: Maximal mole fractions of the radical species H, O, OH in premixed stoichiometric H_2-Air-Flames from [94], computed by a detailed reaction mechanism (black dots) and with the partial equilibrium assumption (white dots).

Despite the development of more sophisticated model reduction methods, both the QSSA and the PEA are still used nowadays due to their conceptual simplicity [69]. However, it has to be noted that usually both methods require detailed knowledge of the mechanism to decide which species a quasi-stationarity or which reactions a partial equilibrium can be assumed for. A technique for the automatic choice of these species or reactions is presented in [88].

2.1.2 Time-Scale Analysis

While the background of the QSSA and PEA lies in a "by-hand" time-scale analysis, modern time-scale analysis based methods try to automatize this process by computing approximations of invariant manifolds [32].

The basis for this procedure is the fact that chemical kinetics are based on largely different time scales. The QSSA and the PEA try to exploit this fact by finding (and eliminating) the fast reactions or fast chemical source terms. The methods presented in this section have a more general view on the underlying chemical systems. The main difference is that the *processes* which are assumed (or computed) to be relaxed are not directly related to either *reactions* or *species*, but to generalized mathematical or physical properties of the underlying ODE system (2.1).

Intrinsic Low-Dimensional Manifold

In 1992, Maas and Pope [60] introduced a way of approximating slow manifolds by applying a time-scale analysis to the underlying ODE-system $\dot{\psi} = S(\psi)$ with the state vector $\psi = (T, p, w_1, ..., w_n)^T$, where p denotes pressure, T temperature and w_i the mass fraction of species i.
The local time scales of this system can be determined as the inverse eigenvalues of the Jacobian $J(\psi_0) = \frac{\partial S(\psi_0)}{\partial \psi}$. By linear algebra transformations explained in more detail in [19], this Jacobian can be written as

$$J(\psi) = L\tilde{T}L^{-1} = L \begin{pmatrix} \tilde{T}_{\text{slow}} & 0 \\ 0 & \tilde{T}_{\text{fast}} \end{pmatrix} L^{-1} \tag{2.8}$$

where $\tilde{T}_{\text{slow}}$ and $\tilde{T}_{\text{fast}}$ are the real Schur matrices with the slow and fast eigenvalues as diagonal entries. In the case of complex eigenvalues these diagonal entries have a 2-by-2 block structure.
The aim of the Intrinsic Low-Dimensional Manifold (ILDM) method is to represent the fast variables as a function of the slow ones, under the assumption that the fast processes are already relaxed. In combustion processes, most eigenvalues of the Jacobian have large negative real parts, which means that there is a large number of fast modes and a small number of slow ones. With the decoupling from (2.8), the ODE system can be transformed into

$$\frac{\mathrm{d}x_{\text{slow}}}{\mathrm{d}t} = g_{\text{slow}}(x) \qquad \frac{\mathrm{d}x_{\text{fast}}}{\mathrm{d}t} = g_{\text{fast}}(x) \stackrel{!}{=} 0 \tag{2.9}$$

for $x = \begin{pmatrix} x_{\text{slow}} \\ x_{\text{fast}} \end{pmatrix} = L^{-1}\psi$ and $g = \begin{pmatrix} g_{\text{slow}} \\ g_{\text{fast}} \end{pmatrix} = L^{-1}S$, where $g_{\text{fast}} = 0$ is the relaxation assumption defining the ILDM.
Denoting E_{fast} the part of L^{-1} corresponding to the fast variables (i.e. $g_{\text{fast}} = E_{\text{fast}}S$), the full ILDM equation system to be solved is given by

$$E_{\text{fast}}S(x) = 0, \qquad P(x, c) = 0. \tag{2.10}$$

The parametrization $P(x, c) = 0$ closes the algebraic equation system. It contains the mass conservation relations associated with the chemical reaction system and specifies a single point on the manifold in terms of given concentration values of the chosen reaction progress variables.
For the application of reduced mechanisms, the computationally expensive solution of the ILDM equation (2.10) is performed a priori and the ILDM is tabulated on a numerical grid defined by appropriate step sizes for the reaction progress variables. The computation of the ILDM is then accomplished by using a continuation method, taking previously calculated ILDM

points as initial guesses for subsequent ones. As a starting point for this procedure usually a point near the chemical equilibrium is taken which is a zero-dimensional ILDM by definition.
Roussel and Tang [79] recently developed a new algorithm for the computation of ILDM-points by functional iteration. More information on the practical realization of ILDM and its applications can be found in [1, 15, 58, 59, 64].

Computational Singular Perturbation

The Computational Singular Perturbation (CSP) method [49] has first been presented by Lam in 1985 [48].
The CSP method is based on a reformulation of the ODE system

$$\dot{x}_i = F_i(x) = \sum_{j=1}^{m} \nu_{ij} v_j(x), \qquad i = 1, ..., n \tag{2.11}$$

in terms of a new (orthogonal) basis with the basis vectors $a_i, i = 1, ..., n$, $b_i, i = 1, ..., n$, $b_i^T a_j = \delta_{ij}, i, j = 1, ..., n$, i.e.

$$F(x) = \sum_{i=1}^{n} a_i c_i \tag{2.12}$$

$$c_i = b_i^T F(x) = \sum_{j=1}^{m} B_{ij} v_j(x), \ \forall i \tag{2.13}$$

$$B_{ij} = b_i^T \nu_{ij}, \ \forall i. \tag{2.14}$$

After this choice of basis, the modes c_i are reordered according to their timescales. Differentiating $c_i = b_i^T F(x)$ w.r.t. time one obtains

$$\frac{\mathrm{d}c_i}{\mathrm{d}t} = \sum_{j=1}^{n} \Lambda_{ij} c_j, \forall i \ \text{ with } \ \Lambda_{ij} = \left(\frac{\mathrm{d}b_i}{\mathrm{d}t} + b_i^T J \right)^T a_j, \tag{2.15}$$

where J is the Jacobian of the original system (2.11).
Based on eigenvectors of the Jacobian of the original system, CSP refines the new basis vectors to approximate a set of "ideal" basis vectors. The aim of this refinement procedure is a representation of the original system in a basis such that the slow and fast modes are decoupled. Essentially the refinement procedure is a generalization of the so-called "power-method" for computing eigenvectors and produces a block-diagonal Λ_{ij} when converged.
An analysis of the CSP method can be found in [99].

2.1.3 Iterative Methods

Apart from methods based on the explicit separation of time-scales, methods based on a functional equation that can be obtained from the original ODE formulation have been introduced in the past.

Fraser's algorithm

In [26, 63], Fraser introduced an iterative way to compute a "slow manifold" – a term that has also been introduced in this context. Singh et al. [83] later named this manifold Slow Invariant Manifold (SIM). Here Fraser's algorithm is introduced in terms of the modified version presented in [16]. The basis for this procedure is the elimination of time from the model equation (2.1). For a two-dimensional system

$$\begin{pmatrix} \dot{x} \\ \dot{y} \end{pmatrix} = \begin{pmatrix} F_1(x,y) \\ F_2(x,y) \end{pmatrix}$$

this yields

$$F_2(x,y)\mathrm{d}x - F_1(x,y)\mathrm{d}y = 0. \tag{2.16}$$

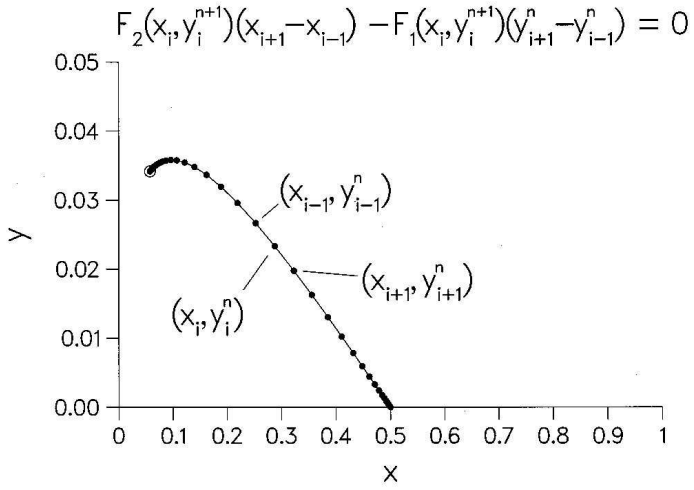

Figure 2.3: Illustration of Fraser's algorithm in 2D from [16]. Points on the slow manifold are computed iteratively by solving (2.17).

Note that the extension to more dimensions is straightforward. The fixed point equation (2.16) can be rewritten in an iterative form as

$$F_2(x_i, y_i^{n+1})\mathrm{d}x_i - F_1(x_i, y_i^{n+1})\mathrm{d}y_i^n = g(y_i^{n+1}) = 0, \quad i = 1, ..., m, \tag{2.17}$$

which has to be solved at each of the m points of the manifold. Note different from the usual notation m and n do not denote the numbers of chemical reactions and species respectively, but m denotes the number of points on the manifold and n is the iteration index.

The idea of using the fixed point equation (2.17) is depicted in Figure 2.3 from [16].

The applicability of this method for the construction of manifolds of higher dimensions has been demonstrated in [77, 78].

A comparison of the ILDM and the Roussel-Fraser algorithm can be found in [42].

Constrained Runs

Another iterative approach that has been introduced recently in [27] and analysed for accuracy and convergence in [98] is the so-called Constrained Runs algorithm.

The basic idea is that (2.1) is described by

$$\dot{u} = p(u, v) \tag{2.18}$$

$$\dot{v} = q(u, v), \tag{2.19}$$

with initial conditions $u(0)$ specified only for u, which in other words simply means that the progress variables or variables parametrizing the "slow manifold" are collected in u.

Assuming the existence of a singular perturbation form, the Constrained Runs scheme proposes the iterative solution of

$$\frac{\mathrm{d}^{m+1} v}{\mathrm{d}t^{m+1}} = 0, \tag{2.20}$$

i.e. the $(m+1)^{\text{st}}$ (time) derivative of the free variables is computed as being zero (note that the iteration does not take place in m, but in the computation of the zero of (2.20)). The intuition behind this condition is that differentiation "amplifies" rapidly varying components more than slowly varying components.

For the practical implementation, the authors of [27] suggest the use of forward differences to approximate the $(m+1)$st derivative, an approach which even has some theoretical advantages in this context.

2.1.4 Other Approaches

Rate-Controlled Constrained Equilibrium

In 1971 Keck and Gillespie proposed in [43] the Rate-Controlled Constrained Equilibrium (RCCE) method, which later was further developed by Hamiroune et al. [40]. The method is based on locally maximizing the entropy or minimizing the Gibbs free energy of the mixture. This optimization (subject to a set of constraints fixing the reaction progress variables) is achieved by using the Lagrange multipliers method.
Subsequently, the species composition can be computed as a function of the Lagrange multipliers. While the method is appealing in its simplicity, a conceptual problem of the RCCE method is the question of the physical relevance of the computed optimal solutions as they generally do not lie on – or even close to – slow manifolds.

Invariant Constrained Equilibrium Edge Preimage Curve

In [75, 76] Ren, Pope et al. introduced a new species reconstruction method called Invariant Constrained Equilibrium Edge Preimage Curve (ICE-PIC). This method uses the RCCE method on the boundary of a predefined realizable region. More precisely, the "ICE-Manifold is the union of all reaction trajectories emanating from boundary points in the edge of the constrained equilibrium manifold". The invariance of the resulting manifold is guaranteed by the fact that it is constructed from reaction trajectories.
By using preimage curves (PIC), Ren and Pope [75] then realize "species reconstruction" locally, i.e. without having to construct a complete manifold in advance.

Method of Invariant Grids

In [32], Gorban and Karlin comprehensively studied invariant manifolds for physical and chemical kinetics. The basis for their analysis is the invariance equation

$$\Delta = (1 - P)F = 0, \tag{2.21}$$

where P is a projection on an invariant manifold. This projection actually defines the invariant manifold to be computed.
Based on this theoretical approach, Gorban et al. present the Method of Invariant Grids in [31]. For this method, the choice of the projector is based on the second law of thermodynamics: it is chosen in such a way that entropy grows in the fast motion. For the realization of this idea, the authors use

the "entropic scalar product", which is used in this work as the Riemannian metric in Subsection 5.2.3.
The Method of Invariant Grids has been further pursued and compared to other methods in [14].

Flamelet-Generated Manifold

For combustion applications, van Oijen and de Goey introduced the Flamelet Generated Manifold (FGM) method in [67]. This method combines the idea of flamelet approaches – that a multidimensional flame can be considered as an ensemble of one-dimensional flames – with the precomputation and storage from manifold approaches.
However, even though recent research [17] tries to extend the FGM from 2D to 3D, the extension of this method to arbitrary dimensions remains a problem.

2.1.5 Yet Another Approach?

As can be seen in this section, many conceptually different approaches to model reduction have been presented in the past and the most modern ones are based on finding or approximating invariant manifolds.
However, the computation of invariant manifolds is not a trivial task and most of the methods presented in this section have disadvantages by some means or other.
One of the problems that is often encountered is the fact that some model reduction methods depend on the explicit separation of the time-scales. Problems arise under conditions where the requirement of clear timescale separation does not hold. Low temperatures, for example may impede the solution of time scale decoupling equations, e.g. in the computation of ILDM-points.
Another drawback of many model reduction approaches is the fact that they often depend on the computation of the complete manifold or at least large parts of it. However, from the application point of view it is highly desirable to find reduced descriptions on the manifold locally. The computation of single manifold points without having to construct a complete manifold first is called "local species reconstruction" or "in-situ approach".
The approach developed in this work can overcome some of the problems in the computation or approximation of slow invariant manifolds. Particularly the optimization basis of the approach guarantees solvability by computing "optimally reduced" models even in cases where other approaches fail.
For consistent optimization criteria (see Definition 5.1), the approach presented here is also capable of local species reconstruction.

Finally, approaches like the ILDM exploit only local information for their time-scale analysis, the approach presented in this work uses global information by considering trajectories instead of points in phase space, hence making use of the nonlinearities of the underlying dynamical systems.
Considering all this, the trajectory-based optimization approach for model reduction presented in this work bears promise for a fast and robust constructive approximation and application of invariant manifolds.

2.2 Model Reduction and Complexity Analysis

A field that is closely related to model reduction is complexity analysis. While the aim of model reduction lies in the explicit expression of a large system in dependence of only a few degrees of freedom, complexity analysis aims at finding the essential system dynamics and coupling relations. In other words, complexity analysis tries to find the necessary degrees of freedom (minimal dimension) of a system within a given error tolerance, while model reduction tries to explicitly compute and apply attracting manifolds of a given dimension (usually neglecting errors).
Although both fields show different aims, they often share their key algorithms. For example [100] uses an ILDM-related strategy to find the active modes of a biochemical system (the PO reaction). A similar strategy is used in [82] to find the essential dynamics of the photosensitive Belousov-Zhabotinsky reaction and subsequently reduce the dimension of its model. This way, [82] combines complexity analysis and model reduction. However, the *by-hand model reduction* used by [82] is only very loosely related to the automatic model reduction treated in this thesis.
Lebiedz et al. [52] use a mathematically more sophisticated strategy for complexity analysis. In principal, this strategy (based on a singular value decomposition of sensitivity matrices) could also be applicable for model reduction; for large systems however, the computation of sensitivities becomes too demanding. The complexity analysis in [52] of the Michaelis-Menten [62] kinetics in a way justifies the QSSA for this system (see Subsection 2.1.1).
More results of research in the field of complexity analysis can be found in [41].

Chapter 3

Theoretical Background

> "It is useful to solve differential equations."
>
> *V. Arnold's* translation of
>
> "Data aequatione quotcunque fluentes quantitae involvente fluxiones invenire et vice versa."
>
> *Sir Isaac Newton*

This chapter deals with the theoretical background necessary for the discussion and application of the trajectory-based optimization approach for model reduction that is pursued in this work. Section 3.1 introduces some aspects from the general theory of dynamical systems and ordinary differential equations, whereas Section 3.2 discusses properties of the solutions of these systems. The physical background for the systems dealt with in this work is introduced in Sections 3.3 and 3.4.

3.1 Dynamical Systems

The theory of dynamical systems aims at analyzing qualitative properties of mathematical models describing the behaviour of time-dependent processes.

Definition 3.1 (Autonomous Differential Equation (System))
An ordinary differential equation or a system of ordinary differential equations (ODE system) $\dot{c} = f(c,t)$ *is said to be* autonomous*, if it does not explicitly depend on time* t*, i.e.*

$$\dot{c}(t) := \frac{\mathrm{d}c(t)}{\mathrm{d}t} = f(c(t)),\ c(t) \in \mathbb{R}^n. \tag{3.1}$$

The dynamical systems considered in this work are chemical reaction mechanisms, which can be described by autonomous ordinary differential equations with a continuous (in c) vector function $f : U \to \mathbb{R}^n$, where U is an open set in $\mathbb{R}^n$. The right hand side (r.h.s.) of equation (3.1) can also be referred to as a *vector field*, as c can be geometrically interpreted as a curve in $\mathbb{R}^n$ with its tangent vectors given by $f(c(t))$ at each point.
A solution of (3.1) is a mapping

$$\begin{aligned} c : I &\to \mathbb{R}^n \\ t &\mapsto c(t) \end{aligned}$$

from some interval $I \subset \mathbb{R}$ into $\mathbb{R}^n$, such that $c(t)$ satisfies equation (3.1). Note that – together with the continuity of $f(c(t))$ – this implies that $c(t)$ is continuously differentiable in c.

Definition 3.2 (Phase Space)
The space of all possible states of the dependent variables $c(t)$ of the autonomous ODE (system) (3.1) is called phase space*. A point in phase space is called* phase point*.*

A solution of (3.1) for a given initial condition $c(t_0) = c_0$ is often denoted by $c(t, c_0)$.

Definition 3.3 (Trajectory)
The solution $c(t, c_0)$ of (3.1) with the initial value c_0 is called trajectory *or* phase curve *through the point c_0 at $t = t_0$.*

Definition 3.4 (Orbit)
For a point c_0 in the phase space of (3.1), the orbit $O(c_0)$ through c_0 *is defined as the set of points in phase space which lie on a trajectory passing through c_0. For $c_0 \in U \subset \mathbb{R}^n$, the orbit through c_0 is given by*

$$O(c_0) = \{c \in \mathbb{R}^n | c = c(t, c_0), t \in I\}\,. \tag{3.2}$$

The motion of a set of phase points along the corresponding orbits is called the phase flow *or* flow*.*

Different solutions of the ODE (3.1) are distinguished by specifying initial conditions:

Definition 3.5 (Initial Value Problem (IVP))
The ODE system (3.1) together with a specified initial condition

$$\begin{aligned} \dot{c}(t) &= f(c(t)),\ t \in I \\ c(t_0) &= c_0 \end{aligned} \tag{3.3}$$

is called initial value problem.

The solution to an initial value problem is unique under certain regularity conditions imposed on the right hand side f.

Definition 3.6 (Lipschitz condition)
A vector valued function $f(c)$ is said to satisfy a Lipschitz-condition *in the interval $[t_0, t_\mathrm{f}]$ with respect to c (with the* Lipschitz-constant *$L \geq 0$), if for $c_1, c_2 \in \mathbb{R}^n$*

$$\|f(c_1(t)) - f(c_2(t))\| \leq L\|c_1(t) - c_2(t)\| \tag{3.4}$$

holds for all $t \in [t_0, t_\mathrm{f}]$.
The function is said to satisfy a local Lipschitz condition *if for every $c \in \mathbb{R}^n$ there exists a neighbourhood $U(c)$ such that f restricted to U satisfies a Lipschitz condition (the Lipschitz constant L may take different values on different neighbourhoods).*

Theorem 3.7 (Existence and Uniqueness Theorem)
Let f be continuous on the strip $S := \{(t, c) | t_0 \leq t \leq t_\mathrm{f}, c \in \mathbb{R}^n\}$ with finite t_0 and t_f and satisfy a local Lipschitz-condition with respect to c.
Then for every pair (t, c_0) with $t \in [t_0, t_\mathrm{f}]$ and $c \in \mathbb{R}^n$ there exists exactly one function $c(t)$ with

$$\dot{c}(t) = f(c(t)) \text{ for } t \in [t_0, t_\mathrm{f}] \text{ and } c(t_0) = c_0. \tag{3.5}$$

Proof. See e.g. Walter [90]. □

Remark 3.8
If f is continuously differentiable with respect to c, then f satisfies a local Lipschitz condition with respect to c. Hence a solution to an initial value problem (3.3) always exists and is unique, if f is continuously differentiable with respect to c, which is given for the ODE systems considered in this work.

Definition 3.9 (Equilibrium Solution)
A solution $\bar{c}(t) : I \to \mathbb{R}^n$ of (3.1) satisfying

$$f(\bar{c}(t)) = 0 \; \forall t \in I$$

is called equilibrium solution.

As an equilibrium solution does not change in time, it is often referred to as *fixed point, critical point* or *steady-state* and will in the sequel be denoted by $\bar{c}$ (omitting t).

Equilibrium solutions are of particular interest for dynamical systems, as they can be used to analyze the structure of the system's phase space in their neighbourhood. A property of interest regarding equilibrium solutions is stability. There are two important definitions of stability for equilibrium solutions that will be introduced here:

Definition 3.10 (Lyapunov Stability)
An equilibrium solution $\bar{c}$ of (3.1) is called stable *or* Lyapunov stable*, if for any given $\varepsilon > 0$ there exists a $\delta = \delta(\varepsilon) > 0$, such that $\|\bar{c} - c(t)\| < \varepsilon$ for any solution $c(t)$ of (3.1) that satisfies $\|\bar{c} - c(t_0)\| < \delta$ with $t > t_0$, $t_0 \in \mathbb{R}$.*

Definition 3.11 (Asymptotic Stability)
An equilibrium solution $\bar{c}$ of (3.1) is called asymptotically stable*, if it is Lyapunov stable and if there exists a constant $b > 0$ such that $\lim_{t\to\infty} \|\bar{c} - c(t)\| = 0$ follows from $\|\bar{c} - c(t_0)\| < b$.*

In other words, Lyapunov stability means that solutions starting "close" to $\bar{c}$ will remain close to $\bar{c}$ for all time, while asymptotical stability means that trajectories starting nearby $\bar{c}$ all converge to $\bar{c}$ eventually.

Definition 3.12 (Lyapunov function)
Consider a dynamical system governed by the ODE system $\dot{c}(t) = f(c(t))$, $c(t) \in \mathbb{R}^n$ with a fixed point $\bar{c}$. A C^1-function $V : U \to \mathbb{R}$ in a neighbourhood U of $\bar{c}$ is called Lyapunov function*, if the following properties are satisfied*

1. *$V(\bar{c}) = 0$*
2. *$V(c) > 0$ if $c \neq \bar{c}$*
3. *$\frac{\mathrm{d}V(c)}{\mathrm{d}t} \leq 0$ in $U \setminus \{\bar{c}\}$*

There is no general way to find a Lyapunov function for arbitrary systems, but for some systems Lyapunov functions are known. An important implication of the existence of a Lyapunov function is given in the following

Theorem 3.13
If a Lyapunov function V exists for a dynamical system $\dot{c} = f(c)$ with a fixed point $\bar{c}$, then $\bar{c}$ is a stable fixed point. If further strict inequality holds for 3. in Definition 3.12, $\bar{c}$ is asymptotically stable.

Proof. See Wiggins [96]. □

Definition 3.14 (Invariant Set / Manifold)

1. *A set $S \subset \mathbb{R}^n$ is called* invariant under *$\dot{c} = f(c)$, if for any $c_0 \in S$ it holds that $c(t, c_0) \in S$ for all $t \in \mathbb{R}$.*

2. *An invariant set $S \subset \mathbb{R}^n$ is said to be a $C^k (k \geq 1)$* invariant manifold, *if S has the structure of a C^k differentiable manifold.*

Definition 3.15 (Attracting Set / Attractor)
A closed and invariant set $\mathcal{A}$ is called an attracting set, *if there exists an open neighbourhood U of $\mathcal{A}$, such that all solutions $c(t)$ with initial solution in U will eventually enter $\mathcal{A}$, i.e.*

$$\lim_{t \to \infty} d(c(t), \mathcal{A}) = 0 \tag{3.6}$$

for a given metric d.
An attractor *of (3.1) is an attracting set which contains a dense orbit.*

Remark 3.16
Every asymptotically stable fixed point is an attractor.

Definition 3.17 (Dissipative / Conservative System)
A dynamical system $\dot{c} = f(c)$ is called dissipative, *if the volume of its phase space contracts along a trajectory. If the phase space volume of a dynamical system is preserved along a trajectory, it is called* conservative.

For dissipative systems the generalized divergence is less than zero, i.e.

$$\sum_{i=1}^{n} \frac{\partial f_i}{\partial c_i} < 0. \tag{3.7}$$

The change of the volume of an element in phase space caused by the flow of an autonomous differential equation (3.1) can be characterized by the following lemma:

Lemma 3.18 (Phase space contraction)
Consider the equation $\dot{c} = f(c)$ in $\mathbb{R}^n$ and a domain $D(0)$ in $\mathbb{R}^n$ which has the volume $v(0)$. The flow defines a mapping g of $D(0)$ into $\mathbb{R}^n$, $g : \mathbb{R}^n \to \mathbb{R}^n$, $D(t) = g^t D(0)$. For the volume $v(t)$ of the domain $D(t)$ we have

$$\left. \frac{\mathrm{d}v}{\mathrm{d}t} \right|_{t=0} = \int_{D(0)} \nabla \cdot f \mathrm{d}c, \tag{3.8}$$

where $\nabla \cdot f = \frac{\partial f_1}{\partial c_1} + \frac{\partial f_2}{\partial c_2} + ... + \frac{\partial f_n}{\partial c_n} = \mathrm{div} f$.

Proof. See Verhulst [89]. □

Remark 3.19
Lemma 3.18 can be used for the proof of Liouville's theorem which states that the flow generated by a time-independent Hamiltonian system is volume-preserving (see [89]). In mathematics, Lemma 3.18 itself is sometimes named Liouville's theorem.

3.2 Differential Geometry of Curves

The solutions of the ODE systems described in the previous section are curves in phase space. In this section some properties of these curves that can be of importance in the model reduction context are described.
While the most interesting part of differential geometry may be the study of *manifolds*, in the context of trajectory-based optimization *curves* are of special interest. This section will focus on the differential geometry of curves only. An extensive overview of differential geometry in physics can be found in [25].
The material presented here is mainly based on [6, 12]. Although the presentation in these textbooks mainly deals with $\mathbb{R}^3$, some ideas can be directly transferred to $\mathbb{R}^n$. As the context of this work is based on dynamical systems of arbitrary dimension, the definitions here will be given in $\mathbb{R}^n$.
Some basic definitions for differential geometry of curves are given in the following definition. As the curves that are analyzed in this work are given as solutions of ODE systems, the same notation $c(t)$ is chosen for solutions of ODE systems and parametrized differentiable curves.

Definition 3.20 (Regular Curve)

- *A* parametrized differentiable curve *is a differentiable map* $c : I \to \mathbb{R}^n$ *of an open interval* $I = (a, b) \in \mathbb{R}$ *into* $\mathbb{R}^n$.
- *Given* $t \in I$, *the* velocity vector (or tangent vector) *of a parametrized differentiable curve is* $\dot{c}(t)$ *and the* speed *at* t *is* $\|\dot{c}(t)\|$. *A curve is said to be* unit speed *if* $\|\dot{c}(t)\| = 1$ *for all* $t \in I$.
- *A point* t *of a parametrized differentiable curve* $c : I \to \mathbb{R}^n$ *is called* singular point *of* c, *if* $\dot{c}(t) = 0$.
- *A parametrized differentiable curve* $c : I \to \mathbb{R}^n$ *is said to be* regular *if* $\dot{c}(t) \neq 0 \quad \forall t \in I$.

An important property of a curve is its arc length.

Definition 3.21 (Arc Length)
Given $t \in I$, *the* arc length *of a regular parametrized differentiable curve* $c : I \to \mathbb{R}^n$ *from the point* t_0 *is*

$$s(t) = \int_{t_0}^{t} \|\dot{c}(\tau)\| \mathrm{d}\tau. \tag{3.9}$$

Definition 3.22 (Energy of a Curve)
Given $t \in I$, the energy E *of a regular parametrized differentiable curve $c : I \to \mathbb{R}^n$ is*

$$E(t) = \int_{t_0}^{t} \|\dot{c}(\tau)\|^2 \mathrm{d}\tau. \tag{3.10}$$

Lemma 3.23 (Energy-Length Inequality)
Given $t \in I$, the energy $E(t)$ *of a regular parametrized differentiable curve $c : I \to \mathbb{R}^n$ can be related to its* length $s(t)$ *by the inequality*

$$s(t)^2 \leq (t - t_0)E(c). \tag{3.11}$$

Equality holds if and only if the parameter t is proportional to the arc length.

Proof. The proof is based on the integral form of the Cauchy-Schwarz inequality:

$$\begin{aligned} s(t) &= \int_{t_0}^{t} \|\dot{c}(\tau)\| \mathrm{d}\tau = \int_{t_0}^{t} \|\dot{c}(\tau)\| \|1\| \mathrm{d}\tau \\ &\leq \underbrace{\left(\int_{t_0}^{t} \|\dot{c}(\tau)\|^2 \mathrm{d}\tau \right)^{\frac{1}{2}}}_{=\sqrt{E(t)}} \underbrace{\left(\int_{t_0}^{t} \|1\|^2 \mathrm{d}\tau \right)^{\frac{1}{2}}}_{=\sqrt{t-t_0}}. \end{aligned} \tag{3.12}$$

By squaring (3.12) the desired inequality is proven.
Now if (and only if) t is proportional to the arc length, it follows that $\|\dot{c}(\tau)\|$ is constant and hence equality holds in the integral form of the Cauchy-Schwarz inequality. □

Definition 3.24 (Reparametrization)
Let $c : I \to \mathbb{R}^n$ and $\tilde{c} : \tilde{I} \to \mathbb{R}^n$ be parametrized differentiable curves. $\tilde{c}$ is called a reparametrization *of c, if there exists a diffeomorphism $h : \tilde{I} \to I$ such that $\tilde{c} = c \circ h$.*

Note that a curve has the same image set in $\mathbb{R}^n$ as any reparametrization of it.
An important special case of a reparametrization is given in the following definition:

Definition 3.25 (Natural Parametrization)
For a regular parametrized differentiable curve $c : I \to \mathbb{R}^n$ the natural, arc length *or* unit speed parametrization $\hat{c} : \hat{I} \to \mathbb{R}^n$ *is defined by*

$$c(t) = \hat{c}(s(t)),$$

where $s(t)$ is the arc length from Definition 3.21. $s(t)$ is also called the natural parameter *of c.*

Definition 3.26 (Curvature)
Let $c : I \to \mathbb{R}^n$ be a curve parametrized by arc length $s \in I$. The real number $k(s) = \|c''(s)\|$ is called the curvature *of c at s.*

Remark 3.27 (Arc length in ODE context)
Note that in general the solutions to the ODE systems treated in this work will not be parametrized by arc length. However, an arc length reparametrization is simple in the ODE context, as arc length can be computed from the right hand side of the ODE by

$$s(t) = \int_{t_0}^{t} \|\dot{c}(\tau)\| \mathrm{d}\tau = \int_{t_0}^{t} \|f(c(\tau))\| \mathrm{d}\tau. \tag{3.13}$$

3.3 Chemical Kinetics

While the previous sections gave introductions to the mathematical fields of dynamical systems and differential geometry, this section and the subsequent one give basic overviews over the chemical and physical processes ruling the dynamical systems that are dealt with in this work.
The temporal behaviour of chemical reaction systems can be modeled by systems of ordinary differential equations.
In a general case, a chemical reaction can be described by the equation

$$\mathrm{A} + \mathrm{B} + \mathrm{C} + ... \underset{k^{(\mathrm{r})}}{\overset{k^{(\mathrm{f})}}{\rightleftharpoons}} \mathrm{D} + \mathrm{E} + \mathrm{F} + ..., \tag{3.14}$$

where $\mathrm{A}, ..., \mathrm{F}$ denote the species involved in the reaction and the superscripts (f) and (r) denote forward and backward reactions respectively. The rate of formation or consumption of a species can be expressed by a *rate law*, e.g.

$$\frac{\mathrm{d}[\mathrm{A}]^{(\mathrm{f})}}{\mathrm{d}t} = -k^{(\mathrm{f})} \cdot [\mathrm{A}]^a [\mathrm{B}]^b [\mathrm{C}]^c ... \tag{3.15}$$

for species A. There $a, b, c, ...$ are the *reaction orders* with respect to the species $\mathrm{A}, \mathrm{B}, \mathrm{C}$ and k is the *rate coefficient* of the reaction.
Accordingly, the rate law for the production of A is obtained as

$$\frac{\mathrm{d}[\mathrm{A}]^{(\mathrm{r})}}{\mathrm{d}t} = k^{(\mathrm{r})} \cdot [\mathrm{D}]^d [\mathrm{E}]^e [\mathrm{F}]^f ... \tag{3.16}$$

and hence the overall change of A is

$$\frac{\mathrm{d}[\mathrm{A}]}{\mathrm{d}t} = -k^{(\mathrm{f})} \cdot [\mathrm{A}]^a [\mathrm{B}]^b [\mathrm{C}]^c ... + k^{(\mathrm{r})} \cdot [\mathrm{D}]^d [\mathrm{E}]^e [\mathrm{F}]^f ... \tag{3.17}$$

At chemical equilibrium, forward and backward reactions have the same rate, therefore one has

$$k^{(\mathrm{f})} \cdot [\mathrm{A}]^a[\mathrm{B}]^b[\mathrm{C}]^c... = k^{(\mathrm{r})} \cdot [\mathrm{D}]^d[\mathrm{E}]^e[\mathrm{F}]^f... \tag{3.18}$$

or

$$\frac{k^{(\mathrm{f})}}{k^{(\mathrm{r})}} = \frac{[\mathrm{D}]^d[\mathrm{E}]^e[\mathrm{F}]^f...}{[\mathrm{A}]^a[\mathrm{B}]^b[\mathrm{C}]^c...}. \tag{3.19}$$

The expression on the right hand side of this equation corresponds to the *equilibrium constant* K:

$$K := \frac{k^{(\mathrm{f})}}{k^{(\mathrm{r})}} = \frac{[\mathrm{D}]^d[\mathrm{E}]^e[\mathrm{F}]^f...}{[\mathrm{A}]^a[\mathrm{B}]^b[\mathrm{C}]^c...} \tag{3.20}$$

The equilibrium constant can also be calculated from thermodynamic data. For details see [95] and equation (3.39).

3.3.1 Elementary Reactions

An *elementary reaction* is one that occurs on a molecular level exactly in the way which is described by the kinetic rate law. Generally the equation of an elementary reaction r can be written as

$$\sum_{s=1}^{n} \nu_{rs}^{(\mathrm{e})} \mathrm{A}_s \xrightarrow{k_r} \sum_{s=1}^{n} \nu_{rs}^{(\mathrm{p})} \mathrm{A}_s, \tag{3.21}$$

and the rate law for the formation of species i in reaction r is then given by the equation

$$\left(\frac{\mathrm{d}c_i}{\mathrm{d}t}\right)_r = k_r \left(\nu_{ri}^{(\mathrm{p})} - \nu_{ri}^{(\mathrm{e})}\right) \prod_{s=1}^{n} c_s^{\nu_{rs}^{(\mathrm{e})}}. \tag{3.22}$$

Here $\nu_{rs}^{(\mathrm{e})}$ and $\nu_{rs}^{(\mathrm{p})}$ denote stoichiometric coefficients of *educts/reactants* and *products* in reaction r and c_s are the *concentrations* of the n different species A_s.

3.3.2 Reaction Mechanisms

Generally one is rather interested in more complex reactions than in elementary ones. To describe such reactions, they can be decomposed into elementary reactions (3.21), which in turn can be combined to an elementary

reaction mechanism. For an elementary mechanism composed of m reactions of n species, given by

$$\sum_{s=1}^{n} \nu_{rs}^{(e)} \mathrm{A}_s \xrightarrow{k_r} \sum_{s=1}^{n} \nu_{rs}^{(p)} \mathrm{A}_s, \quad r = 1, ..., m, \tag{3.23}$$

the rate of formation of species i is simply given by summation over the rate equations of all elementary reactions,

$$\frac{\mathrm{d}c_i}{\mathrm{d}t} = \sum_{r=1}^{m} k_r \left(\nu_{ri}^{(p)} - \nu_{ri}^{(e)}\right) \prod_{s=1}^{n} c_s^{\nu_{rs}^{(e)}}. \tag{3.24}$$

An important relation in the description of chemical reactions is the temperature dependence of the rate coefficients. This dependence is most easily described as $k = \tilde{A} \exp\left(-\frac{E_\mathrm{a}}{RT}\right)$ by the Arrhenius law, but generally the formulation

$$k = AT^b \exp\left(-\frac{E_\mathrm{a}}{RT}\right) \tag{3.25}$$

is used, which additionally includes a temperature dependence of the preexponential factor $\tilde{A}$.
With (3.25) the rate coefficient for a reaction at a given temperature can be computed from three characteristic quantities: The *activation energy* E_a, which corresponds to an energy barrier to be overcome during reaction, and the quantities A and b, forming the preexponential factor, which has different physical meanings in uni-, bi- and termolecular reactions – i.e. for reactions which involve one, two or three molecules respectively.
These three quantities E_a, A, b and the reaction equations for all elementary reactions (which are the basis for the stoichiometric coefficients) form the reaction mechanism.
Apart from the temperature dependence, rate coefficients can also show dependence on pressure. As the example mechanisms used in this work do not exhibit a pressure dependence this topic is not treated here and the reader is referred to [29, 87, 95] for more details.
More detailed introductions to chemical reaction kinetics can be found in [3, 95] e.g.

3.4 Thermodynamics

The field of thermodynamics studies – on a macroscopic scale – the energetic changes of a physical system as effects of changes in the system state.

The changes in the system state can be due to changes of e.g. temperature, pressure or volume.
Much of the material presented in this section follows the book of Kondepudi and Prigogine [47].
Systems in thermodynamics are usually discriminated according to their boundary conditions:

Definition 3.28 (Isolated / Closed / Open System)
Isolated systems *exchange neither energy nor matter with their exterior.*
Closed systems *exchange energy, but not matter with their exterior.*
Open systems *exchange both energy and matter with their exterior.*

All systems considered in this work are isolated, which is a simplification for real systems.

3.4.1 The Fundamental Laws of Thermodynamics

Thermodynamics is based on four laws which axiomatically postulate that and how energy can be exchanged between physical systems as heat or work. The two most important laws will be stated here.

Theorem 3.29 (The First Law of Thermodynamics)
In an isolated system, the internal energy is conserved in any state change.

The first law does not yield any information about the directionality of state changes (e.g. in chemical reaction systems) and hence does not give any information on irreversible processes as e.g. chemical reactions, which is the main interest in this work.
The explanation of irreversibility is the main idea of the Second Law, that can be stated in a number of different fashions. For reasons of comprehensibility some common formulations of the Second Law are stated here.

Theorem 3.30 (The Second Law of Thermodynamics)
"It is impossible that, at the end of a cycle of changes, heat has been transferred from a colder to a hotter body without at the same time converting a certain amount of work into heat." Clausius (1822-1888).
"A perpetual motion machine of the second kind is impossible." Max Planck (1858-1947)

Theorem 3.31 (The Second Law (in terms of entropy))
The entropy S of an isolated system not at equilibrium will tend to increase over time, approaching a maximum value at equilibrium.

3.4.2 "Driving Force" for Chemical Reactions

Irreversible processes in thermodynamics can be described in terms of *thermodynamic forces* and *thermodynamic flows*, i.e. a change in entropy due to irreversible chemical reactions in an isolated system can be written as

$$\mathrm{d_i}S = F\,\mathrm{d}X, \tag{3.26}$$

where the change in entropy $\mathrm{d_i}S$ is written in terms of the *force* F and the *flow* $\mathrm{d}X$ and the subscript $_\mathrm{i}$ denotes the change due to irreversible processes, whereas the subscript $_\mathrm{e}$ will denote changes due to the exchange of matter with the exterior in the sequel.
In the context of this work, we are mainly interested in driving forces for chemical reactions. Such "driving forces" for chemical reactions have been called *affinities* by chemists in the nineteenth century, but it was not until 1927, that a clear definition of affinities had been given.
The thermodynamic formulation of affinity which is used today has been introduced by de Donder and can be found in [22]. Its basis lies in the concept of chemical potential introduced by Gibbs.
Gibbs introduced an equation for changes in the *internal energy* U that was similar* to

$$\mathrm{d}U = T\,\mathrm{d}S - p\,\mathrm{d}V + \sum_{k=1}^{n} \mu_k\,\mathrm{d}N_k, \tag{3.27}$$

with temperature T, pressure p, volume V and the species *mole numbers* N_k. The coefficients μ_k are called *chemical potentials*. Gibbs did not take into account irreversible chemical reactions in his concept, but considered transformations between equilibrium states. Despite of that, equation (3.27) forms the fundament to de Donder's formulation of the thermodynamics of irreversible transformations.
A distinction between the entropy change $\mathrm{d_e}S$ due to the exchange of matter and energy with the exterior (entropy flow) and the irreversible increase of entropy $\mathrm{d_i}S$ due to chemical reactions (entropy production) was introduced. Using this distinction, the change in mole numbers $\mathrm{d}N_k$ can be expressed as a sum of two parts

$$\mathrm{d}N_k = \mathrm{d_i}N_k + \mathrm{d_e}N_k. \tag{3.28}$$

As Gibbs considered only the *reversible* exchange of heat and matter, his equation (3.27) could also be written as

$$\mathrm{d_e}S = \frac{\mathrm{d}U + p\,\mathrm{d}V}{T} - \frac{\sum_{k=1}^{n} \mu_k \mathrm{d_e}N_k}{T}. \tag{3.29}$$

*Gibbs actually wrote this equation in terms of the masses $m_1, ..., m_n$ of the substances. However, as chemical reaction rates are most easily formulated in terms of mole numbers, the reformulation (3.27) is used here.

De Donder formulated the entropy production due to a change in mole numbers $\mathrm{d}N_k$ by irreversible chemical reactions, $\mathrm{d_i}S$ as

$$\mathrm{d_i}S = -\frac{\sum_{k=1}^{n} \mu_k \mathrm{d_i}N_k}{T}. \tag{3.30}$$

This formulation is in accordance with the Second Law due to the fact that chemical reactions occur in such a way that $\mathrm{d_i}S$ is always positive. For the total change of entropy $\mathrm{d}S$ we have

$$\mathrm{d}S = \mathrm{d_e}S + \mathrm{d_i}S, \tag{3.31}$$

which by summing up (3.29) and (3.30) recovers (3.27). Hence (3.27) already included everything that was necessary for a description of irreversible thermodynamics.
Since the rate of chemical reaction specifies $\frac{\mathrm{d}N_k}{\mathrm{d}t}$, the rate of entropy production due to chemical reactions can be written as

$$\frac{\mathrm{d_i}S}{\mathrm{d}t} = -\frac{1}{T}\sum_{k=1}^{n} \mu_k \frac{\mathrm{d_i}N_k}{\mathrm{d}t} > 0. \tag{3.32}$$

Now, for a general chemical elementary reaction

$$a_1\mathrm{A}_1 + a_2\mathrm{A}_2 \rightleftharpoons b_1\mathrm{B}_1 + b_2\mathrm{B}_2 \tag{3.33}$$

the extent ξ of the reaction is defined as

$$\frac{\mathrm{d}N_{\mathrm{A}_1}}{-a_1} = \frac{\mathrm{d}N_{\mathrm{A}_2}}{-a_2} = \frac{\mathrm{d}N_{\mathrm{B}_1}}{b_1} = \frac{\mathrm{d}N_{\mathrm{B}_2}}{b_2} = d\xi \tag{3.34}$$

and the affinity A of the reaction is defined as

$$A \equiv \sum_{k=1}^{2} \mu_{\mathrm{A}_k} a_k - \sum_{k=1}^{2} \mu_{\mathrm{B}_k} b_k, \tag{3.35}$$

where the μ_i are *chemical potentials*.
The substitution of (3.34) and (3.35) in the equation for the rate of entropy production (3.32) yields

$$\frac{\mathrm{d_i}S}{\mathrm{d}t} = \left(\frac{A}{T}\right)\frac{\mathrm{d}\xi}{\mathrm{d}t} > 0, \tag{3.36}$$

which reflects the description of a thermodynamical property (entropy production) in terms of a thermodynamical force (affinity) and a thermodynamical flow (reaction rate) as in (3.26).

However, the purpose here is to look at the entropy production explicitly while chemical reactions are in progress, i.e. to look for explicit expressions for $\frac{\mathrm{d_i}S}{\mathrm{d}t}$ in terms of the rates of reaction (for the general problem of specifying rates of reactions see Section 3.3).
In equation (3.36), the entropy production rate has been expressed in terms of the extent of reaction ξ and the affinity A.
For a single reaction the time derivative of the extent ξ can be related to reaction rates by the relation

$$v = \frac{\mathrm{d}\xi}{V\mathrm{d}t} = R_\mathrm{f} - R_\mathrm{r} \tag{3.37}$$

where $v = R_\mathrm{f} - R_\mathrm{r}$ is the *reaction velocity*, R_f and R_r are the forward and reverse reaction rates and V is the volume of the system.
The next step towards an expression of entropy production in terms of reaction rates now is a relation of the affinity A to reaction rates.
A general chemical potential can be expressed as

$$\mu_k(T) = \mu_{k_0}(T) + RT\ln[\mathrm{A}_k], \tag{3.38}$$

where $[\mathrm{A}_k]$ is the concentration of A_k and $\mu_{k_0} = \Delta G_f^0[k]$ is the standard molar Gibbs free energy of formation which is a tabulated property. R denotes the universal gas constant. With this, the affinity can be rewritten as

$$A = \sum_{k=1}^{2} a_k\mu_{\mathrm{A}_{k,0}}(T) - \sum_{k=1}^{2} b_k\mu_{\mathrm{B}_{k,0}}(T) + \sum_{k=1}^{2} a_k RT\ln[\mathrm{A}_k] - \sum_{k=1}^{2} b_k RT\ln[\mathrm{B}_k].$$

Now, at equilibrium the thermodynamic forces and the corresponding flows become zero (i.e. $A = 0 \Leftrightarrow \sum_{k=1}^{2}\mu_{\mathrm{A}_k}a_k = \sum_{k=1}^{2}\mu_{\mathrm{B}_k}b_k$ and $v = 0 \Leftrightarrow R_\mathrm{f} = R_\mathrm{r}$).
By reformulating the condition $A = 0$ one obtains the *equilibrium constant*

$$K(T) = \exp\left(\frac{-\Delta G^0_\mathrm{rxn}}{RT}\right) \tag{3.39}$$

with

$$\Delta G^0_\mathrm{rxn} := \sum_{k=1}^{2} b_k\mu_{\mathrm{B}_{k_0}}(T) - \sum_{k=1}^{2} a_k\mu_{\mathrm{A}_{k_0}}(T)$$

the *Gibbs free energy of reaction* and hence

$$\Delta G^0_\mathrm{rxn} = -RT\ln K(T).$$

With this, the formula for the affinity is

$$A = RT \ln K(T) + RT \ln \left(\frac{[\mathrm{A}_1]^{a_1}[\mathrm{A}_2]^{a_2}}{[\mathrm{B}_1]^{b_1}[\mathrm{B}_2]^{b_2}} \right)$$

and since $K(T) = \frac{k^{(\mathrm{f})}}{k^{(\mathrm{r})}}$, combining the logarithms this can be written as

$$A = RT \ln \left(\frac{k^{(\mathrm{f})}[\mathrm{A}_1]^{a_1}[\mathrm{A}_2]^{a_2}}{k^{(\mathrm{r})}[\mathrm{B}_1]^{b_1}[\mathrm{B}_2]^{b_2}} \right) = RT \ln \left(\frac{R_\mathrm{f}}{R_\mathrm{r}} \right), \tag{3.40}$$

Substituting (3.37) and (3.40) into the expression (3.36) for the entropy production yields

$$\frac{1}{V}\frac{\mathrm{d_i}S}{\mathrm{d}t} = \frac{1}{V}\frac{A}{T}\frac{\mathrm{d}\xi}{\mathrm{d}t} = R(R_\mathrm{f} - R_\mathrm{r}) \ln \left(\frac{R_\mathrm{f}}{R_\mathrm{r}} \right) \geq 0. \tag{3.41}$$

This is an expression relating *entropy production per unit volume* to reaction rates which was the aim of the derivations in this section. As required by the Second Law, the right hand side is non-negative, as the two factors $R_\mathrm{f} - R_\mathrm{r}$ and $\ln \left(\frac{R_\mathrm{f}}{R_\mathrm{r}} \right)$ always have the same sign.
For several simultaneous (elementary) reactions equation (3.41) can be generalized by

$$\frac{1}{V}\frac{\mathrm{d_i}S}{\mathrm{d}t} = \frac{1}{V}\sum_{k=1}^{m}\frac{A_k}{T}\frac{\mathrm{d}\xi_k}{\mathrm{d}t} = R\sum_{k=1}^{m}(R_{k\mathrm{f}} - R_{k\mathrm{r}}) \ln \left(\frac{R_{k\mathrm{f}}}{R_{k\mathrm{r}}} \right) \geq 0, \tag{3.42}$$

where k is the index for a single reaction and $R_{k\mathrm{f}}$ and $R_{k\mathrm{r}}$ are the forward and reverse reaction rates for this reaction.

Chapter 4

Optimization

> "And this is my prayer: that your love may abound more and more in knowledge and depth of insight, so that you may be able to discern what is *best*."
>
> *Phil. 1,9-10*

In this chapter the numerical optimization methods used for solving the variational boundary value problems that occur in the novel model reduction approach are explained. The general problem formulation is introduced and explained in Section 4.1 whereas Sections 4.2 and 4.3 deal with the discretization of this formulation, such that a nonlinear programming problem (NLP) is obtained. Using the numerical integration from Section 4.4, this NLP can be solved using a numerical standard approach introduced in Section 4.5. Section 4.6 then introduces an embedding strategy for the efficient solution of neighbouring problems, which is of special interest as a continuation method in the model reduction context.

4.1 Problem Formulation

A variational boundary value problem as used in this work can be formulated as

$$\min_{x(\cdot),(t_\mathrm{f})} \int_{t_0}^{t_\mathrm{f}} L(x(t),p)\mathrm{d}t \tag{4.1a}$$

subject to

$$\dot{x}(t) - f(x(t),p) = 0, \qquad t \in [t_0, t_\mathrm{f}] \tag{4.1b}$$

$$g(x(t),p) \geq 0, \qquad t \in [t_0, t_\mathrm{f}] \tag{4.1c}$$

$$r_0(x(t_0),p) + r_\mathrm{f}(x(t_\mathrm{f}),p) = 0 \tag{4.1d}$$

Here t_0 and t_f denote the initial and final time respectively and can be chosen as $t_0 = 0$ and $t_\mathrm{f} = T$ without loss of generality. The functions L, r_0, r_f and g are assumed to be continuously differentiable. The right hand side f of the ODE (4.1b) is assumed to fulfil the usual smoothness conditions ensuring local existence and uniqueness of its solution x for given initial values $x(0) = x_0$.
The length T of the integration horizon $[0, T]$ can either be fixed or used as an additional degree of freedom subject to optimization.
In the sequel, these equations will be explained in more detail.

Objective Functional Generally the objective of an ODE-constrained optimization problem lies in the minimization of certain overall "costs" which are usually defined on a finite time horizon $[t_0, t_\mathrm{f}]$ with initial time t_0 and final time t_f by a general Bolza-type objective functional

$$\int_{t_0}^{t_\mathrm{f}} L(x(t), p)\mathrm{d}t + E(x(t_\mathrm{f}), p). \tag{4.2}$$

The terms $L(x(t), p)$ and $E(x(t_\mathrm{f}), p)$ are called *Lagrange term* and *Mayer term* of the objective function respectively. A Mayer term can be reformulated into a Lagrange term and vice versa. For the sake of brevity we will only use Lagrange-type objective functionals as in (4.1a) in the formulation of variational boundary value problems throughout this work.

ODE constraints In the context of variational boundary value problems, an ODE model usually enters the formulation of the general problem as a constraint. Homogeneous chemical reaction systems can be described by autonomous (see Definition 3.1) ODE models of the form (4.1b)

$$\dot{x}(t) = f(x(t), p), \tag{4.3}$$

where $x(t) \in \mathbb{R}^{n_x}$ denotes the differential state vector, $t \in \mathbb{R}$ time, and $p \in \mathbb{R}^{n_p}$ is a vector of constant system parameters such as for example reaction coefficients in chemical kinetics.

Path Constraints and Boundary Constraints Path constraints as formulated in (4.1c) are constraints that have to be satisfied by the state trajectories $x(t)$ on the given time horizon. For a chemical reaction system these constraints may reflect positivity of chemical species concentrations.
Boundary constraints in the variational boundary value problem can be written in the general form (4.1d). These constraints may include conservation equations (element conservation) or can be employed e.g. to fix initial or final species concentrations.

4.2 Problem Discretization

The optimization problem (4.1) has to be discretized to be solved numerically. Therefore the problem is transformed into a nonlinear programming problem (NLP) first, which then can be solved using standard approaches for the solution of NLPs. A standard approach for the solution of NLPs based on the successive solution of quadratic approximations of the NLP is the Sequential Quadratic Programming (SQP) which is explained in detail in Section 4.5.
Strategies for the formulation of the NLP can be divided into two different approaches, namely the *sequential* and the *simultaneous* approach. In the sequential approach simulations and optimization calculations are performed sequentially. However, especially for poor initial guesses and unstable systems this procedure might lead to strong nonlinearity of the resulting NLPs and a poor convergence behaviour.
The simultaneous approach avoids this drawback by first discretizing the state trajectory and then solving both the dynamic model equations and the optimization problem simultaneously in one large constrained NLP. As the discretized state variables become part of the optimization variables, nonlinearity and instability can be better controlled.

4.3 Multiple Shooting

All calculations in this work have been carried out by software based on the *direct multiple shooting* method which has been first presented by Bock [7, 8] and Plitt [70]. The term *direct* refers to the direct approach used for the discretization of infinite dimensional optimal control problems. However, as no control functions are used in this work, the presentation here is restricted to the explanation of the multiple shooting method which is described for the solution of two point boundary value problems in [44] e.g.
The idea of the multiple shooting method is to subdivide the integration interval $[0, T]$ into several subintervals on each of which an independent initial value problem is solved. Matching conditions which enter the optimization problem as additional equality constraints assure continuity of the state trajectory from one subinterval to the next one. A modern implementation of this idea is realized in the optimal control software package MUSCOD-II by Leineweber [54, 55, 56, 57]. In the sequel the multiple shooting method shall be described in more detail.
A multiple shooting grid with multiple shooting nodes at the time points $\tau_0, ..., \tau_N$,

$$0 = \tau_0 < \tau_1 < ... < \tau_N = T \tag{4.4}$$

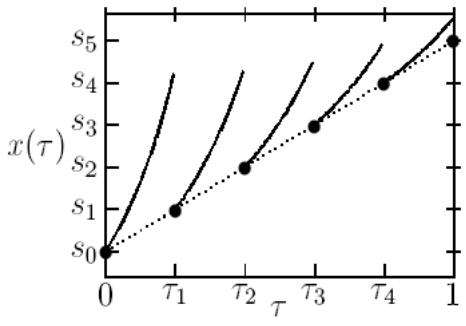

Figure 4.1: Multiple shooting discretization for $N = 5$ multiple shooting nodes. An initial value problem is solved on each multiple shooting interval.

is introduced for the discretization of the state trajectory as seen in Figure 4.1 for $T = 1$ and $N = 5$. On each of the intervals $[\tau_i, \tau_{i+1}], (i = 0, ..., N-1)$ introduced by this discretization an initial value problem

$$\begin{aligned} \dot{x}_i(\tau) &= f(x_i(\tau), p) \qquad\qquad \tau \in [\tau_i, \tau_{i+1}] \\ x_i(\tau_i) &= s_i, \end{aligned} \tag{4.5}$$

has to be solved. As the resulting trajectories $x_i(\tau)$ on $[\tau_i, \tau_{i+1}]$ depend only on the initial values s_i, these solutions can be computed simultaneously. As stated above, continuity of the solution state trajectory is enforced by imposing *matching conditions*

$$s_{i+1} = x_i(\tau_{i+1}; s_i), \qquad i = 0, ..., N-1. \tag{4.6}$$

These conditions assure that the initial value on the $i+1^{\text{st}}$ multiple shooting interval equals the final value on the i^{th} multiple shooting interval in the solution. Likewise by

$$s_0 = x_0 \tag{4.7}$$

the value of the first differential node s_0 should be equal to the initial value x_0 of the original problem.
On the same multiple shooting grid as introduced for the state trajectory, $\tau_0, ..., \tau_N$, the inequality path constraints (4.1c) are transformed into $N+1$ discrete vector inequality constraints

$$g(s_i, p) \geq 0, \qquad i = 0, 1, ..., N. \tag{4.8}$$

Having all this, a finite dimensional NLP can be formulated as

$$\min_{s_0,\ldots,s_N} \sum_{i=0}^{N-1} \int_{\tau_i}^{\tau_{i+1}} L(x_i(\tau), p)\mathrm{d}\tau \tag{4.9a}$$

subject to

$$x_i(\tau_{i+1}; s_i) - s_{i+1} = 0, \quad i = 0, ..., N-1 \tag{4.9b}$$

$$x_0 - s_0 = 0 \tag{4.9c}$$

$$g(s_i, p) \geq 0, \quad i = 0, ..., N \tag{4.9d}$$

$$r_0(s_0, p) + r_\mathrm{f}(s_N, p) = 0 \tag{4.9e}$$

and subject to the initial value problems (4.5). The solution of these IVPs is discussed in Section 4.4.
Using the multiple shooting discretization ($N > 1$), more variables and constraints are added to the NLP than by using single shooting ($N = 1$). However, the equality constraints in the matching conditions (4.9b) allow for the application of a condensing algorithm [7]. Using this algorithm, the computational costs for the numerical solution of the resulting condensed problem are only slightly higher than for the solution of the NLP set up by a single shooting discretization.

4.4 Numerical Integration

To solve the NLP (4.9), the solutions $x_i(\tau), \tau \in [\tau_i, \tau_{i+1}], i = 0, ..., N-1$ to the initial value problems (4.5), which occur within the integrals in (4.9a) have to be computed numerically. The underlying ODE models for chemical kinetics are generally stiff differential equation systems comprising multiple timescales. Employing explicit methods for the accurate solution of stiff differential equations requires too small step sizes. Hence for the efficient numerical solution of the initial value problems (4.5) the implicit Differential Algebraic Equation (DAE) solver DAESOL [2, 4, 5] is used which is integrated in the software package MUSCOD-II [54, 55]. The multistep Backward Differentiation Formula (BDF) methods implemented in DAESOL have beneficial stability properties (see [18]).
To explain the idea behind BDF methods, first a general linear multistep method is defined.

Definition 4.1 (Linear Multistep Method)
In a general linear multistep method (LMM) *for the numerical solution of an initial value problem an approximate value* η_{m+k} *of* $x(t_{m+k})$ *is computed from*

$k\,(k \geq 2)$ given approximate values η_j of $x(t_j)$, $j = m, m+1, ..., m+k-1$ at equidistant points $t_j = t_0 + jh$ by the general formula

$$\sum_{l=0}^{k} \alpha_l \eta_{m+l} = h \sum_{l=0}^{k} \beta_l f(\eta_{m+l}),\ m = 0, ..., N-k \tag{4.10}$$

with $\alpha_l, \beta_l \in \mathbb{R}, \alpha_k \neq 0$ and $|\alpha_0| + |\beta_0| \neq 0$.
If $\beta_k = 0$ then this is an explicit, otherwise an implicit method.

BDF methods are linear multistep methods defined by finding a polynomial that interpolates the $(k+1)$ values $\eta_m, ..., \eta_{m+k}$ and satisfies the differential equation at $t = t_{m+k}$.

Definition 4.2 (BDF method)
The k-step BDF method *is defined by the k starting values $\eta_m, ..., \eta_{m+k-1}$ specified and the formula*

$$\sum_{l=0}^{k} \alpha_l \eta_{m+l} = h\, f(\eta_{m+l}),\ m = 0, ..., N-k \tag{4.11}$$

with $\alpha_l \in \mathbb{R}$, and $\alpha_0, \alpha_k \neq 0$.

More detailed information about BDF methods including extensive stability analysis of multistep methods can be found in [37, 38].

4.5 Sequential Quadratic Programming

The finite dimensional NLP (4.9) from Section 4.2 can be solved by numerical standard approaches. In general a constrained NLP can be formulated as

$$\min_{w \in \mathbb{R}^{n_w}} F(w) \tag{4.12a}$$

subject to

$$\begin{aligned} G(w) &= 0 \\ H(w) &\geq 0 \end{aligned} \tag{4.12b}$$

where the functions $F : \mathbb{R}^{n_w} \to \mathbb{R}, G : \mathbb{R}^{n_w} \to \mathbb{R}^{n_G}$ and $H : \mathbb{R}^{n_w} \to \mathbb{R}^{n_H}$ are assumed to be twice continuously differentiable.
The solution of this problem can be based on meeting local optimality conditions.

Definition 4.3 (Feasibility and Optimality)

1. *The set* $S := \{w \in \mathbb{R}^{n_w} | G(w) = 0, H(w) \geq 0\}$ *is called* feasible set*, and* $w^* \in S$ *is called* feasible point*.*

2. *A feasible point* w^* *is called a* local minimizer *of the NLP (4.12) if there exists a neighbourhood* $U_\varepsilon(w^*)$ *of* w^* *such that* $F(w^*) \leq F(w)$ *for all* $w \in U_\varepsilon(w^*) \cap S$*.*

3. *The inequality constraint* $H_i(w) \geq 0$ *is called* active*, if* $H_i(w) = 0$*.*
All active inequality constraints at the feasible point w *are denoted by* $H^{\text{act}}(w)$*.*

4. *A feasible point* w *is called a* regular point*, if the Jacobian of the active constraints* $\nabla \tilde{G}(w)^T$ *has full rank.* $\tilde{G}(w) := \begin{pmatrix} G(w) \\ H^{\text{act}}(w) \end{pmatrix}$ *is the vector of equality and active inequality constraints.*

To formulate necessary conditions for the optimality of a feasible point w^* for (4.12), the *Lagrangian function* $\mathcal{L}$ is defined as

$$\mathcal{L}(w, \lambda, \mu) := F(w) - \lambda^T G(w) - \mu^T H(w). \tag{4.13}$$

Using this function, necessary conditions for the optimality of w^* for (4.12) can be formulated as given in the following theorem.

Theorem 4.4 (Karush-Kuhn-Tucker Necessary Conditions)
Let the regular point w^* *be a local minimizer of (4.12). Then there exist Lagrange multiplier vectors* $\lambda^* \in \mathbb{R}^{n_G}$ *and* $\mu^* \in \mathbb{R}^{n_H}$ *such that* (w^*, λ^*, μ^*) *satisfies the following necessary conditions:*

$$\nabla_w \mathcal{L}(w^*, \lambda^*, \mu^*) = 0 \tag{4.14a}$$
$$G(w^*) = 0 \tag{4.14b}$$
$$H(w^*) \geq 0 \tag{4.14c}$$
$$\mu^* \geq 0 \tag{4.14d}$$
$$\mu_j^* H_j(w^*) = 0, \qquad j = 1, ..., n_H. \tag{4.14e}$$

These conditions are called Karush-Kuhn-Tucker Necessary Conditions *or* KKT conditions*.*

Proof. See e.g. Nocedal and Wright [66]. □

Definition 4.5 (Karush-Kuhn-Tucker Point)
A triple (w^*, λ^*, μ^*) *satisfying the necessary Karush-Kuhn-Tucker conditions (4.14) is called a* stationary point *or* KKT point*.*

The active set vector function $H^{\text{act}}(w^*)$ at a KKT point (w^*, λ^*, μ^*) can be divided into *strongly active* parts (with strictly positive multipliers) and *weakly active* parts (with zero multipliers):

$$H^{\text{act}}(w^*) = \begin{pmatrix} H^{\text{s.act}} \\ H^{\text{w.act}} \end{pmatrix}(w^*). \tag{4.15}$$

A KKT point for which all active constraints are strongly active is said to satisfy the *strict complementarity condition.*
In Theorem 4.4, necessary conditions for the optimality of w^* have been treated. However, for a method based on meeting local optimality conditions, sufficient conditions are required. By the following theorem, sufficient conditions for w^* to be a local minimizer of (4.12) are given.

Theorem 4.6 (Strong Second Order Sufficient Conditions)
A regular point $w^* \in \mathbb{R}^{n_w}$ satisfying the necessary KKT conditions (4.14) is a local minimizer of (4.12) if and only if the Hessian matrix $\nabla_w^2 \mathcal{L}(w^*, \lambda^*, \mu^*) := \frac{\partial^2 \mathcal{L}}{\partial w^2}(w^*, \lambda^*, \mu^*)$ is positive definite on the null space

$$\mathcal{N}^{\text{s}} := \{\Delta w \in \mathbb{R}^{n_w} | \nabla_w \tilde{G}^{\text{s}}(w^*)^T \Delta w = 0\}$$

of the linearized strongly active constraints

$$\tilde{G}^{\text{s}}(w^*) := \begin{pmatrix} G \\ H^{\text{s.act}} \end{pmatrix}(w^*),$$

i.e. for every non-zero vector $\Delta w \in \mathcal{N}^{\text{s}}$

$$\Delta w^T \nabla_w^2 \mathcal{L}(w^*, \lambda^*, \mu^*) \Delta w > 0$$

holds.

Based on the sufficient conditions from Theorem 4.6, Sequential Quadratic Programming (SQP), going back to Powell [72], is an iterative procedure to find a KKT point (w^*, λ^*, μ^*) of an NLP (4.12).
A general SQP method replaces this NLP by a sequence of quadratic programs

$$\min_{\Delta w \in \Omega_k} \frac{1}{2} \Delta w^T A_k \Delta w + \nabla_w F(w_k)^T \Delta w \tag{4.16a}$$

subject to

$$\begin{aligned} G(w_k) + \nabla_w G(w_k)^T \Delta w &= 0 \\ H(w_k) + \nabla_w H(w_k)^T \Delta w &\geq 0 \end{aligned} \tag{4.16b}$$

with the solution point $(\Delta w_k, \tilde{\lambda}_k, \tilde{\mu}_k)$ that determine the directions

$$\Delta y_k = \begin{pmatrix} \Delta w_k \\ \Delta \lambda_k \\ \Delta \mu_k \end{pmatrix} := \begin{pmatrix} \Delta w_k \\ \tilde{\lambda}_k - \lambda_k \\ \tilde{\mu}_k - \mu_k \end{pmatrix} \tag{4.17}$$

for the SQP iteration

$$y_{k+1} = y_k + \alpha_k \Delta y_k \tag{4.18}$$

where $\alpha_k \in (0, 1]$ is a steplength and A_k in (4.16) is the so-called Hessian matrix (which need not be the exact Hessian, but can also be computed by update formulae such as BFGS – see [66, 86]). The SQP iteration is obviously subject to an initial guess $y_0 = (w_0, \lambda_0, \mu_0)$.
The iterates y_k from equation (4.18) form a sequence that is expected to converge towards a KKT point $y^* = (w^*, \lambda^*, \mu^*)$ of the original NLP. In practice, the iterations are stopped when a prespecified convergence criterion is fulfilled.
Practical realizations of SQP methods differ in steplength strategies for α_k, the choice (or update-strategy) of A_k and the choice of the set $\Omega_k \subset \mathbb{R}^{n_w}$. Particularly, if $\alpha_k := 1 \, \forall k, \Omega_k := \mathbb{R}^{n_w}$ and $A_k := \nabla_w^2 \mathcal{L}(w_k, \lambda_k, \mu_k)$ (i.e. the exact Hessian of the Lagrangian function) are chosen, the SQP method is called *Full Step Exact Hessian SQP Method* and can be proven to be locally convergent (see Fletcher [24], Section 12.4).
For practical applications update formulae are used for A_k rather than the exact Hessian. For details see any textbook on numerical optimiziation (e.g. [24, 28, 35, 66]).

4.6 Parametric Optimization and Initial Value Embedding

4.6.1 Parametric Optimization

Instead of a single optimization problem, now consider a parametrized family of optimization problems $P(p)$:

$$\min_{w \in \mathbb{R}^{n_w}} F(p, w) \tag{4.19a}$$

subject to

$$\begin{aligned} G(p, w) &= 0 \\ H(p, w) &\geq 0, \end{aligned} \tag{4.19b}$$

where $F : \mathbb{R} \times \mathbb{R}^{n_w} \to \mathbb{R}, G : \mathbb{R} \times \mathbb{R}^{n_w} \to \mathbb{R}^{n_G}$ and $H : \mathbb{R} \times \mathbb{R}^{n_w} \to \mathbb{R}^{n_H}$ are twice continuously differentiable.

Single optimization problems in (4.19) are distinguished by the parameter p and the interest of this section now focuses on the set of local minimizers for $P(p)$, i.e.

$$\Sigma_{\text{loc}} := \{(p, w) \in \mathbb{R} \times \mathbb{R}^{n_w} | w \text{ is a local minimizer for } P(p)\}, \tag{4.20}$$

restricting the attention to the subset of points $(p, w^*(p))$ of Σ_{loc} satisfying the strong second order sufficient conditions of Theorem 4.6.

The main result of interest in in this section is a statement on the differentiability of the solution $(w^*(p), \lambda^*(p), \mu^*(p))$ with respect to the parameter p. A detailed introduction to parametric optimization and the properties of Σ_{loc} can be found in [36].

The following theorem in its present form is taken from [21] where also a proof can be found. A similar formulation of the theorem and a proof can also be found in [36].

Theorem 4.7 (One Sided Differentiability)
Consider a parametrized family of optimization problems $P(p)$ as in (4.19). Assume that a KKT point $(w^*(0), \lambda^*(0), \mu^*(0))$ satisfying the sufficient optimality conditions from Theorem 4.6 with strongly and weakly active set vectors $H^{\text{s.act}}$ and $H^{\text{w.act}}$ has been found for problem $P(0)$. Assume further that the solution $(\delta w_*, \delta\lambda_*, \delta\mu_*^{\text{s.act}}, \delta\mu_*^{\text{w.act}})$ of the following quadratic program (with all derivatives evaluated at the solution point $(w^*(0), \lambda^*(0)\mu^*(0))$ for $p = 0$)

$$\min_{\delta w \in \mathbb{R}^{n_w}} \ \frac{1}{2}(\delta w)^T \nabla_w^2 \mathcal{L}(\delta w) + \left(\frac{\partial}{\partial t}\nabla_w \mathcal{L}\right)^T \delta w \tag{4.21a}$$

subject to

$$\begin{aligned} \frac{\partial G}{\partial p} + \nabla_w G^T \delta w &= 0 \\ \frac{\partial H^{\text{s.act}}}{\partial p} + (\nabla_w H^{\text{s.act}})^T \delta w &= 0 \\ \frac{\partial H^{\text{w.act}}}{\partial p} + (\nabla_w H^{\text{w.act}})^T \delta w &\geq 0. \end{aligned} \tag{4.21b}$$

satisfies the strict complementary condition for the multiplier vector $\delta\mu_*^{\text{w.act}}$ of the inequality constraints.

Then there exists an $\varepsilon > 0$ and a differentiable curve

$$v : [0, \varepsilon) \to \mathbb{R}^{n_w} \times \mathbb{R}^{n_G} \times \mathbb{R}^{n_H},$$
$$p \mapsto \begin{pmatrix} w^*(p) \\ \lambda^*(p) \\ \mu^*(p) \end{pmatrix}$$

of KKT points that satisfy the sufficient optimality conditions of Theorem 4.6 for the corresponding problems $P(p), p \in [0, \varepsilon)$. At $p = 0$, the one sided derivative of this curve is given by

$$\lim_{p \to 0, p > 0} \frac{1}{p} \begin{pmatrix} w^*(p) - w^*(0) \\ \lambda^*(p) - \lambda^*(0) \\ \mu^*(p) - \mu^*(0) \end{pmatrix} = \begin{pmatrix} \delta w_* \\ \delta \lambda_* \\ \begin{pmatrix} \\ \delta \mu_* \\ \\ \end{pmatrix} \end{pmatrix} := \begin{pmatrix} \delta w_* \\ \delta \lambda_* \\ \delta \mu_*^{\text{s.act}} \\ \delta \mu_*^{\text{w.act}} \\ 0 \end{pmatrix}.$$

Remark 4.8
Compared to Theorem 4.6, Theorem 4.7 needs only one additional condition, the assumption of strict complementarity in the solution of the QP (4.16), which is needed to guarantee that the active set of the local solutions of $P(p)$ does not change for $p \in [0, \varepsilon)$.

Remark 4.9
The theorem only assures existence for a solution curve for a positive change in p, i.e. for the solution curve $(w^*(p), \lambda^*(p), \mu^*(p))$ on the interval $p \in [0, \varepsilon)$. However, if the strict complementarity condition is also satisfied for the solution of an inverted version of the QP (4.16), the solution curve $p \in (-\varepsilon', 0] \mapsto (w^*(p), \lambda^*(p), \mu^*(p))$, $\varepsilon > 0$ also exists and has a one sided derivative.
This is an immediate consequence of the application of the same theorem to the reversed problem family $P'(p) = -P(p)$.

4.6.2 SQP for a Parameterized Problem Family

A family of augmented optimization problems that is equivalent to the family $P(p)$ defined by (4.19) can be written as the family $\breve{P}(\breve{p})$:

$$\min_{p \in \mathbb{R}, w \in \mathbb{R}^{n_w}} F(p, w) \tag{4.22a}$$

subject to

$$\begin{aligned} p - \breve{p} &= 0 \\ G(p, w) &= 0 \\ H(p, w) &\geq 0, \end{aligned} \tag{4.22b}$$

where again the functions $F : \mathbb{R} \times \mathbb{R}^{n_w} \to \mathbb{R}, G : \mathbb{R} \times \mathbb{R}^{n_w} \to \mathbb{R}^{n_G}$ and $H : \mathbb{R} \times \mathbb{R}^{n_w} \to \mathbb{R}^{n_H}$ are twice continuously differentiable. The only difference to the family $P(p)$ defined by (4.19) is the introduction of p as an additional variable, fixed by the constraint $p - \breve{p} = 0$. As a consequence of this addition of p to the SQP variables, derivatives with respect to p are evaluated in the SQP algorithm, hence allowing the transition between different optimization problems in such a way that a first order approximation of the solution manifold as in Theorem 4.7 is provided by the first iterate.

This can be subsumed in the following theorem:

Theorem 4.10
Assume that a KKT point $(\breve{w}^*(0), \breve{\lambda}^*(0), \breve{\mu}^*(0))$ of problem $\breve{P}(0)$ satisfying the sufficient optimality conditions of Theorem 4.6 has been found. If a full step exact Hessian SQP algorithm is applied for the solution of $P(\varepsilon)$ ($\varepsilon > 0$ sufficiently small) with this solution as an initial guess, then the nontrivial part of the first SQP step, $(\Delta w, \Delta\lambda, \Delta\mu)$, is identical to ε times the one-sided derivative of the solution manifold $(w^*(\cdot), \lambda^*(\cdot), \mu^*(\cdot))$ of Problems $P(p)$ as given in Theorem 4.7, i.e.

$$\frac{1}{\varepsilon}\begin{pmatrix} \Delta w \\ \Delta\lambda \\ \Delta\mu \end{pmatrix} = \begin{pmatrix} \delta w_* \\ \delta\lambda_* \\ \delta\mu_* \end{pmatrix} = \lim_{p\to 0, p>0} \frac{1}{p}\begin{pmatrix} w^*(p) - w^*(0) \\ \lambda^*(p) - \lambda^*(0) \\ \mu^*(p) - \mu^*(0) \end{pmatrix}. \tag{4.23}$$

A proof to this theorem can be found in [21]. The proof is based on making ε sufficiently small to ensure that the active set of the first QP corresponds to the active set in the immediate vicinity of the solution point $w^*(0)$.

However, Diehl [21] also demonstrates that the SQP method is also able to treat distant active set changes, which is the case that will be typically encountered in practice.

4.6.3 Embedded NLP Formulation

In the variational boundary value problems to be solved in this work, the distinguishing parameter of the NLPs $P(x_0)$ is the initial value x_0, which is constraining s_0^x by a trivial equality constraint $s_0^x - x_0 = 0$.

Therefore, the NLP formulation (4.9) can be regarded as an embedded formulation of the form

$$\min_{s_0^x \in \mathbb{R}^{n_x}, \tilde{w} \in R^{n_w - n_x}} F(s_0^x, \tilde{w}) \tag{4.24a}$$

subject to

$$\begin{aligned} s_0^x - x_0 &= 0 \\ \tilde{G}(s_0^x, \tilde{w}) &= 0 \\ H(s_0^x, \tilde{w}) &\geq 0, \end{aligned} \tag{4.24b}$$

with $w = (s_0^x, \tilde{w})$.
Assuming that a solution $y^*(x_0) = (w^*(x_0), \lambda^*(x_0), \mu^*(x_0))$ of problem $P(x_0)$ has been found and that the SQP algorithm for the solution of a neighbouring problem $P(x_0 + \varepsilon)$ is initialized with this solution, the first full step exact Hessian SQP iterate provides already an excellent (first order) approximation of the solution $y^*(x_0 + \varepsilon)$, as demonstrated by Diehl [21, Example 4.2].
This initial value embedding which was originally invented for Nonlinear Model-Predictive Control (NMPC) [20] will be exploited in Chapter 5 as a continuation strategy in model reduction.

Chapter 5

Force Relaxation Along Trajectories

"You are like a hurricane,
there's calm in your eye"

Neil Young, 1977

In [50], Lebiedz introduced a novel concept for model reduction, that can be interpreted as a minimization of relaxing forces along reaction trajectories. Lebiedz used entropy production, as described in Section 3.4, to measure chemical forces. However, to consider entropy production along trajectories is not sufficient and hence other measures of forces relaxing along trajectories have to be taken into account.
In Section 5.1 a general description of trajectory-based optimization approaches for model reduction is given and then in Section 5.2 the choice of different optimization criteria aimed at the description of relaxation of chemical forces is discussed.

5.1 Trajectory-based Optimization Approach

5.1.1 General Concept

Mathematically, Lebiedz' idea of Minimal Entropy Production Trajectories (MEPT) corresponds to a variational boundary value problem as given in (4.1). To be able to use other measures of forces within a trajectory-based optimization approach for model reduction, this concept can be written in a very general fashion.

This general trajectory-based optimization approach is written as

$$\min_{c} \int_0^T \Phi(c(t))\, \mathrm{d}t \tag{5.1a}$$

subject to

$$\frac{\mathrm{d}c_k}{\mathrm{d}t} = f_k(c),\ k = 1, ..., n \tag{5.1b}$$

$$c_k(0) = c_k^0, \qquad k \in I_{\text{fixed}} \tag{5.1c}$$

$$|c_k(T) - c_k^{\text{eq}}| \leq \varepsilon, \qquad k \in I_{\text{fixed}} \tag{5.1d}$$

and additionally is subject to conservation relations. The variables c_k denote the concentrations of chemical species, and I_{fixed} is the index set that contains the indices of variables with fixed initial values (the reaction progress variables). The system dynamics are described by (5.1b) and the initial concentrations of the reaction progress variables are fixed in (5.1c). When approaching the equilibrium point c^{eq}, the system dynamics become infinitely slow. Therefore the equilibrium point is approximated in (5.1d) within a surrounding of small radius ε for the concentration of the reaction progress variables. A priori the end time T is free and is determined within the optimization for (5.1d) to be fulfilled. Alternatively the time T can be fixed in such a way that the final state of the system is very close to the chemical equilibrium point. The objective functional $\Phi(c(t))$ in (5.1a) describes the optimization criterion related to the degree of relaxation of chemical forces. The key idea of using this approach for model reduction is found in the fact that trajectories can be used to span invariant manifolds. More precisely, a manifold spanned by trajectories is invariant by definition. The optimization in the formulation (5.1) assures that the spanned manifold is not only an invariant manifold but as close as possible to the Slow Invariant Manifold (SIM), if a suitable relaxation criterion Φ is chosen. The approximated SIM can then be used as a reduced model for the underlying ODE model. This reduced model can be parametrized by the progress variables which find a fully natural realization as initial concentrations in (5.1c).

5.1.2 Continuation Strategy

For a practical implementation of a model reduction method based on the considerations above, a sophisticated continuation strategy is essential to efficiently solve (5.1) for varying progress variable concentrations c_k^0. Based on the theory from Section 4.6, a very efficient continuation strategy can be employed for the initialization of neighbouring trajectories. Once an optimized

trajectory has been computed for given parameters $P(c_0)$, a neighbouring problem with parameters $P(c_0 + h)$ is initialized with this solution giving a good approximation of the desired solution, as described in Section 4.6. Passing through the whole computational domain, the initial values of the optimal trajectories can be stored in tables as reduced chemistry descriptions. In these tables the progress variable concentrations and other parameters as e.g. temperature, pressure or mixture fraction (see [95] e.g.) serve as tabulation axes, the species concentrations of the other variables are stored in dependence of these properties. For more details on the storage of tables of reduced chemistry, the reader is referred to [64, 71, 80]. Figure 5.1 illustrates

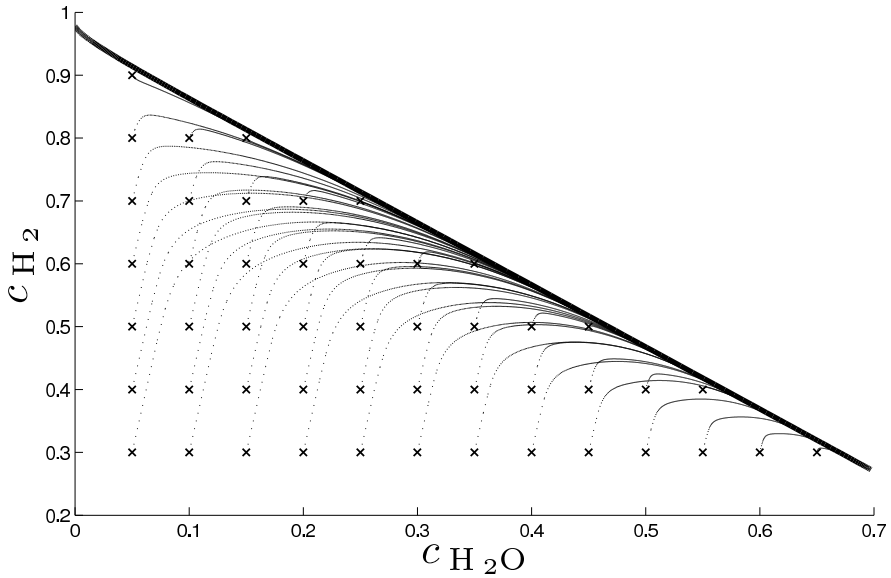

Figure 5.1: Continuation strategy: Neighbouring trajectories can be computed using an initialization from already computed trajectories.

the general continuation strategy.
Generally it is not necessary to compute all trajectories depicted in Figure 5.1. A manifold could also be composed of trajectories that emanate from the boundary of a predefined computational domain if an adequate storage strategy is used. This procedure has the additional advantage that the constructed manifold will at least be invariant, as it is composed of trajectories. However, as this work does not cover storage strategies for reduced chemistry, the simple strategy of computing reduced descriptions for parameter sets that are distributed equidistantly within the computational domain is chosen here.

5.2 Relaxation Criteria

As stated above, different criteria for the maximal relaxation of chemical forces can theoretically be applied. The background of some possible criteria has been described in Chapter 3.
The choice of the criterion $\Phi(c(t))$ affects both success and degree of accuracy of the resulting method. A suitable criterion $\Phi(c(t))$ should at least fulfil the following three requirements:

- Φ should describe the extent of relaxation of "chemical forces" in the evolution of trajectories to equilibrium – i.e. it should be minimal along a trajectory whose relaxation is as big as allowed by the initial constraints (5.1c).
- It should consist of easily accessible data (e.g. reaction rates, chemical source terms and their derivatives).
- It should be twice continuously differentiable along reaction trajectories.

Another desirable, but not necessary property is the following consistency property:

Definition 5.1 (Consistency property)
Suppose an optimal trajectory $\tilde{c}(t)$ has been computed as a solution of (5.1). Take the concentrations of the progress variables at some time $t_1 > 0$ as new initial concentrations and solve (5.1) again. If the resulting trajectory $\hat{c}(t)$ is the same as the part of the original trajectory that starts from t_1 (i.e. $\hat{c}(t) = \tilde{c}(t + t_1)$), we call the optimization criterion Φ consistent.

This property, which is illustrated in Figure 5.2 states a strong demand and will not be fulfilled in general. However, an invariant manifold can in principle be constructed without a consistent criterion by solving (5.1) for initial values $c_k^0,\ k \in I_{\text{fixed}}$ on the boundary of the desired domain and spanning the low-dimensional manifold by the resulting trajectories.
The theoretical background for the consistency property is found in the meaning of the Slow Invariant Manifold (SIM). The main characteristic of a SIM – regardless of its dimension – is, that it is attracting. In other words, trajectories from arbitrary (feasible) initial values converge towards a SIM. Additionally, once a trajectory has – at least approximately – reached the SIM, it remains on the SIM.
Using a relaxation criterion that fulfils the consistency property hence assures that trajectories are computed that fully reside on the SIM. An important

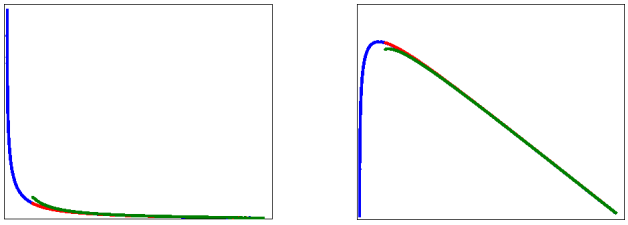

Figure 5.2: "Consistency property": If the blue trajectory has been computed as a solution $\tilde{c}(t)$ of problem (5.1), the red trajectory is the desired solution of problem (5.1) with the initial concentrations $c_k^0 = \tilde{c}_k(t_1)$, $k \in I_{\text{fixed}}$. That means if the red trajectory is a solution of problem (5.1) for a criterion $\tilde{\Phi}$, this criterion is *consistent*. The green trajectory depicts a solution of problem (5.1) with a criterion that does not fulfil the consistency property.

implication of such trajectories is that their initial values can be used for *local species reconstruction*, i.e. for a given combination of progress variables all other species can be reconstructed as the initial values of a trajectory computed as a solution of (5.1) with a relaxation criterion satisfying the consistency property.

5.2.1 Entropy Production

In order to derive a thermodynamic criterion which is related to maximal relaxation of "chemical forces" along phase space trajectories, Lebiedz [50] considered a generalized concept for the "distance" of a chemical system from its attractor. Under isolated conditions the attractor of a chemical system is the thermodynamic equilibrium. In Lebiedz' model reduction approach, a special trajectory (called **M**inimal **E**ntropy **P**roduction **T**rajectory (MEPT)) is calculated in such a way that the sum of affinities of the entropy production rates of single reaction steps is minimized [50, 51, 53]. The entropy production rate is closely related to the concept of chemical affinity which was first introduced by de Donder [22] as the driving force of chemical reactions. For an elementary reaction step j with the forward and backward reaction rates $R_{j\rightarrow}$ and $R_{j\leftarrow}$, the concept of chemical affinity can be related to the concept of entropy production by the following relation [47]:

$$\frac{\mathrm{d_i}S_j}{\mathrm{d}t} = R\,(R_{j\rightarrow} - R_{j\leftarrow}) \ln\left(\frac{R_{j\rightarrow}}{R_{j\leftarrow}}\right) , \tag{5.2}$$

where $\mathrm{d_i}S_j/\mathrm{d}t$ is the entropy production rate for reaction j and R is the gas constant. Entropy production rates are additive for several elementary reaction steps. Therefore the total entropy production rate (the sum of the entropy production rates of all n elementary reaction steps) can be computed for an arbitrary reaction system, if kinetic data are available and a detailed elementary reaction step mechanism is known.
An intuitive justification for the minimization of the total entropy production rate in the optimization problem (5.1) is provided by relation (5.2). In partial equilibrium the entropy production rate $\mathrm{d_i}S_j/\mathrm{d}t$ of a single elementary reaction step is zero, since in partial equilibrium forward and backward reaction rates are equal. This is equivalent to the thermodynamic driving force being fully relaxed, which in turn is an equivalent of the assumption of model reduction techniques based on time scale separation. Here it is assumed that fast reaction modes successively relax into partial equilibrium or quasi steady-states and the whole system can be satisfactorily described by the slow modes only. But unlike the methods explicitly based on time scale separation it is not necessary in the MEPT approach to actually identify and analyze the dynamical modes by e.g. numerically expensive eigenvalue decomposition and solve highly nonlinear algebraic "reduction equations". A configuration with as many elementary reaction steps as possible being close to quasi-equilibrium in terms of the objective functional is determined automatically by the optimization algorithm. The logarithmic ratio of forward and backward reaction rates in (5.2) has the meaning of a reaction affinity (see Subsection 3.4.2 or [47]). It is weighted by the absolute difference between the rates for forward and backward reactions. Thus fast processes produce more entropy than slow ones and the fast reactions have a stronger weighting factor in the optimization problem (5.1), which is fully natural for the purpose of this work. Moreover entropy production is a Lyapunov function (see Definition 3.12) for chemical systems [65].
In the context of the general optimization problem (5.1), using entropy production as an optimization functional means

$$\Phi(c(t)) = \sum_{j=1}^{n} \frac{\mathrm{d_i}S_j}{\mathrm{d}t}. \tag{5.3}$$

The details on the derivation of this criterion can be found in Section 3.4.

Remark 5.2
For isothermal isobaric systems, (negative) Gibbs free energy instead of entropy is the Lyapunov function. However, as

$$\frac{\mathrm{d}G}{\mathrm{d}t} = -T\frac{\mathrm{d_i}S}{\mathrm{d}t}, \tag{5.4}$$

the minimization of (negative) "Gibbs free energy production rate" along a trajectory is realized with the same criterion Φ from (5.3), making the MEPT approach valid for isothermal isobaric systems as well.

5.2.2 Curvature

As stated above, a suitable objective functional $\Phi(c(t))$ should characterize the relaxation of "chemical forces". A fundamentally rooted criterion in this context can be derived on the basis of the concept of curvature of trajectories in phase space and subsequently be combined with the entropy production [97]. From a physical point of view curvature is closely related to the geometric interpretation of a force.

One of the most popular examples is Einstein's general theory of relativity [23] which proposes the idea that gravitational force is replaced by a "geometric picture". Einstein's general theory of relativity relates the special theory of relativity and Newton's law of universal gravitation with the insight that gravitation can be described by curvature of space-time. Space-time is treated as a 4-dimensional manifold whose curvature is due to the presence of mass, energy and momentum.
But even long before Einstein, the concept of curvature has already been related to the concept of force in physics. In 1687 Sir Isaac Newton published the laws of motion in his work "Philosophiae Naturalis Principia Mathematica". In a differential formulation Newton's second law can be stated as

$$F = m \cdot a \ ,$$

where m is mass, a is acceleration and F is force. Since the acceleration a is the second derivative of the state variable $x(t)$ with respect to time, $a = \ddot{x}$, and thus contains information about the curvature of x, Newton's law is the first one to directly relate force to curvature.
In this context it is important to remark that equations of motion in classical mechanics can also be described by a variational principle, Hamilton's principle of least action. In Lagrangian mechanics, the trajectory of an object is determined in such a way that the action (which is defined as the integral of the Lagrangian over time, where the Lagrangian is the difference of kinetic energy and potential energy) is minimal. It can be shown by using the calculus of variations and the Legendre transformation technique, that Lagrange's equations of motion are equivalent to Hamilton's principle [30].
Another well-known variational principle is Fermat's principle of geometric optics. It states in its classical form that the actual path between two points taken by a beam of light is minimal.

The aim here is to transfer the principle of "force = curvature" to the field of chemical systems and look for a corresponding variational principle.
In chemical systems dissipative forces are active. Slow and fast dynamic modes result in an anisotropic force relaxation behaviour in phase space. To formally be able to describe this anisotropy for a chemical system whose dynamics are described by the ODE $\dot{c} = f(c)$, curvature of the trajectories $c(t)$ as geometrical objects in phase space is considered. The following relations hold:

$$\begin{aligned} \ddot{c}(t) = \frac{\mathrm{d}^2 c}{\mathrm{d}t^2} = \frac{\mathrm{d}\dot{c}}{\mathrm{d}t} = \frac{\mathrm{d}\dot{c}}{\mathrm{d}c} \cdot \frac{\mathrm{d}c}{\mathrm{d}t} = J(\dot{c}(t)) \cdot \dot{c}(t) \\ = J(f(c(t))) \cdot f(c(t)) \end{aligned} \tag{5.5}$$

with $J(f)$ being the Jacobian of the right hand side of the ODE $\dot{c}(t) = f(c(t))$. Hence the curvature of $c(t)$ can be defined as the vector norm

$$||\ddot{c}(t)|| = ||J(f(c(t))) \cdot f(c(t))|| \,. \tag{5.6}$$

Transferring the fundamental geometric principle of force being equivalent to curvature mentioned above, we relate the curvature of trajectories in a kinetic model $\dot{c} = f(c)$ to the forces driving the chemical system towards equilibrium by subsequent relaxation of dynamical modes. In thermodynamic equilibrium those chemical forces become zero. In search of a criterion which characterizes maximal relaxation of chemical forces it is tempting to describe the maximal relaxation of the system by minimal remaining chemical forces on its way to equilibrium, i.e. in the context here by minimal total ("integrated") curvature of trajectories defined by the objective function

$$\Phi(c(t)) = \|J(f(c)) \cdot f(c)\| \tag{5.7}$$

in the general optimization problem (5.1).
Interestingly, from a different point of view the objective function (5.7) can also be interpreted as minimizing the length of a trajectory in a suitable Riemannian metric.
For any continuously differentiable curve $\gamma(t)$ on a Riemannian manifold, the length L of γ is defined as

$$L(\gamma) = \int_\gamma \sqrt{g_{\gamma(t)}(\dot{\gamma}(t), \dot{\gamma}(t))}\, \mathrm{d}t \tag{5.8}$$

with $g_{\gamma(t)}$ being a scalar product defined on the tangent space of the curve in each point. If the Riemannian metric $g_{\gamma(t)}$ is chosen as

$$g_{\gamma(t)}(f, f) := f^T \underbrace{J^T J}_{\text{positive definite}} f \;=\; \|J\, f\|^2 \tag{5.9}$$

the "length-minimizing" objective functional equivalent to (5.7) is now

$$\min \int_0^T \sqrt{g_{\gamma(t)}(\dot{c}(t), \dot{c}(t))}\, \mathrm{d}t \ . \tag{5.10}$$

The solution trajectory of this problem can be interpreted as a geodesic, i.e. a curve which minimizes the length of the path between two points in a possibly curved manifold. Hence the "distance from equilibrium in a chemical sense" can be formulated here in an explicit mathematical form based on concepts from differential geometry.
To describe the distance of a chemical system from its thermodynamic equilibrium in a general way, the Riemannian metric

$$\hat{g}_{\gamma(t)}(f, f) := f^T \underbrace{J^T \cdot A \cdot J}_{\text{positive definite}} f \ =: \ \|J\, f\|_A^2 \ , \tag{5.11}$$

can be considered, where A is a positive definite matrix. A proposition for a possible choice of A is the diagonal matrix with the entries

$$a_{kk} = \sum_{j=1}^{n} \nu_{kj}\, \frac{\mathrm{d_i} S_j}{\mathrm{d}t} \qquad (k = 1, \ldots, m) \ . \tag{5.12}$$

which represents an anisotropic "kinetic weighting" of the phase space directions by including the entropy production rate. Here n is the number of reactions, ν_{kj} are the stoichiometric coefficients describing the degree (but not the direction), i.e. $\nu_{kj} \geq 0$ to which the chemical species k participates in reaction j, and $\mathrm{d_i} S_j/\mathrm{d}t$ is the entropy production rate of reaction j. The diagonal element a_{kk} of A is the sum of the entropy production rates of all elementary reactions in which species k takes part. A is positive definite since according to the Second Law of Thermodynamics $\mathrm{d_i} S_j/\mathrm{d}t > 0$ holds for any spontaneous process, and therefore $a_{kk} > 0$ for all $k = 1, \ldots, m$.
With this result an objective function in the general problem (5.1) is readily formulated as

$$\Phi(c(t)) = \|J\, f\|_A \tag{5.13}$$

which obviously includes formulation (5.7) for the choice $A = I_m$ (identity matrix).
Another possible choice for a Riemannian metric would be the (negative) second differential of entropy which is used for the so-called Shahshahani metric [81] and employed for model reduction purposes in [33]. A more detailed look at this metric will be given in Subsection 5.2.3.

Computation of Curvature

From a practical perspective, the computation of the Jacobian for the curvature expression in (5.5) is not necessary, as $\ddot{c}$ simply states a directional derivative of the right hand side of the ODE-system in the direction of the right hand side itself.
This directional derivative could also be evaluated using difference quotients [86], but a more appealing alternative is found in [85].
Instead of using the central difference formula

$$F'(x_0) \approx \frac{F(x_0 + \delta) - F(x_0 - \delta)}{2\delta} \tag{5.14}$$

for the approximation of the derivative of the real valued function $F(x)$, Squire and Trapp [85] suggest replacing δ with $\mathrm{i}\delta$ ($\mathrm{i} = \sqrt{-1}$). If F is an analytic function, (5.14) then reads

$$F' \approx \frac{\mathrm{im}\,(F(x_0 + \mathrm{i}\delta))}{\delta}, \tag{5.15}$$

which is called *complex-step derivative approximation.*
This result is especially appealing, as (5.15) does not contain a subtraction and hence eliminates cancellation errors. Therefore δ can be chosen as small as possible, hence making higher-order terms in the Taylor expansion negligible.
For the directional derivative $\ddot{c}$ at a point c_0 with c from $\dot{c} = f(c)$, (5.15) reads

$$\ddot{c}|_{c_0} \approx \frac{\mathrm{im}\,(f(c + \mathrm{i}\delta f(c)))}{\delta}. \tag{5.16}$$

Compared to using an exact Jacobian, the complexity for the evaluation of $\ddot{c}$ can be reduced from $O(n^2)$ to $O(n)$ using this complex variable approach. At the same time a high accuracy is guaranteed by the possibility of using an extremely small δ.
In principle, automatic (or algorithmic) differentiation (see [34]) could also be used for the computation of curvature, however this usually requires the inclusion of external program packages, while (5.15) can easily be implemented. A benefit of automatic differentiation compared to the complex step derivative approximation is the capability to compute higher-order derivatives, which is not necessary for the computation of curvature.

5.2.3 Length / Velocity

As stated in the previous subsection, the objective function (5.7) can also be interpreted as minimizing the length of a trajectory in a suitable Riemannian

metric, leading to an optimization functional

$$\Phi(c(t)) = \|f\|_B \tag{5.17}$$

where B is a positive definite matrix. Reinterpreting the curvature minimization from the previous subsection, this matrix can be chosen as

$$B = J^T A J. \tag{5.18}$$

However, including the Jacobian of the ODE system in the formulation of the minimization functional leads to an increase of computational demand. Another choice for the Riemannian metric is the so-called Shahshahani metric [81]. Shahshahani supposes the use of the metric defined by using

$$B = \operatorname{diag}\left(\frac{\|x\|}{x_i}\right), i = 1, ..., n. \tag{5.19}$$

The application of this metric for systems in a constant volume under a constant temperature (like the model hydrogen combustion mechanism in A.2) is based on the fact, that the unnormalized version of this metric (i.e. $\operatorname{diag}\left(\frac{1}{x_i}\right), i = 1, ..., n$) is found by the second differential of the Lyapunov function G of such systems

$$G = \sum_{i=1}^{n} x_i \left(\ln \frac{x_i}{x_i^{\mathrm{eq}}} - 1\right). \tag{5.20}$$

Using B as defined in (5.19) a minimization criterion can be stated as

$$\Phi(c(t)) = f^T \operatorname{diag}\left(\frac{\|x\|}{x_i}\right) f. \tag{5.21}$$

Having this functional, the length of a trajectory can be minimized. From a different point of view this minimization represents a velocity minimization, as (5.21) is the local speed of $c(t)$ as defined in Definition 3.20, evaluated in the Shahshahani metric. Moreover, the length of the trajectory is minimized on a constant time interval. Having these ideas in mind, a relation to "slow manifolds" is easily established.

Chapter 6

Results

> "What's good is bad,
> what's bad is good,
> you'll find out when you reach the top,
> you're on the bottom."
>
> *Bob Dylan,* 1975

In this chapter optimized trajectories as approximations of slow attracting manifolds for different model problems and reaction mechanisms (which are found in the Appendix of this work) are presented. These trajectories are solutions of the generalized trajectory-based optimization approach from Chapter 5 using relaxation criteria introduced in the same chapter.
This chapter is subdivided in four sections dealing with different aspects of the application of the trajectory-based optimization approach for model reduction. Section 6.1 deals with the generalization of the approach for multiple dimensions. For reasons of presentability the results concentrate on the construction of two-dimensional manifolds. Section 6.2 then focuses on different ways to improve relaxation criteria with respect to the consistency property from Definition 5.1. The behaviour of the presented approach for temperature dependent systems is treated in Section 6.3. Section 6.4 deals with challenges that are faced when applying the approach to large-scale systems.
Results are generally shown as phase space plots, i.e. dependent variables representing the concentration of chemical species are plotted against each other, with time being eliminated from the system. For the two-dimensional manifolds in Section 6.1, the x- and y-axes depict the concentrations of progress variables, whereas the free variables are plotted on the z-axis. Generally these phase plots nicely depict the dynamical behaviour of the system.

6.1 Two-dimensional Manifolds

Lebiedz presented the approach of computing minimal entropy production trajectories (MEPT) in 2004 [50]. This approach has been first applied for the construction of an invariant manifold of higher dimension in [53].
This section focuses on the construction these higher-dimensional manifolds and for reasons of presentability especially on two-dimensional manifold

6.1.1 Entropy Production

Here results for a simplified six species isothermal hydrogen combustion reaction mechanism are shown. The mechanism comprises six species and twelve (six forward and six reverse) reactions and two conservation laws. Due to these conservation laws, the number of remaining degrees of freedom is four. Details about the mechanism are found in Section A.2 of the appendix.

Standard Approach

In Figure 6.1, the solutions of the general approach (5.1) with entropy production as the relaxation criterion $\Phi = \frac{\mathrm{d_i}S}{\mathrm{d}t} = \sum_{k=1}^{m} R(R_\mathrm{f} - R_\mathrm{r}) \log\left(\frac{R_\mathrm{f}}{R_\mathrm{r}}\right)$ as discussed in Subsection 5.2.1 are depicted. These results have been presented in [51, 53].
As explained in Subsection 5.1.1, the final time T is fixed to a value large enough for the species concentrations to approximately reach equilibrium. This means that (5.1d) will be fulfilled in general and can be omitted in the problem formulation (5.1).
The optimization problem whose solution is presented in Figure 6.1 can be stated as

$$\min_c \int_0^T \sum_{j=1}^{m} R(R_{\mathrm{f},j} - R_{\mathrm{r},j}) \log\left(\frac{R_{\mathrm{f},j}}{R_{\mathrm{r},j}}\right) \mathrm{d}t \tag{6.1a}$$

subject to

$$\frac{\mathrm{d}c_k}{\mathrm{d}t} = f_k(c), k = 1, ..., n \tag{6.1b}$$

$$c_k(0) = c_k^0, \quad k \in I_\mathrm{fixed} \tag{6.1c}$$

$$T \text{ fixed, sufficiently large} \tag{6.1d}$$

$$\begin{aligned} 2c_{\mathrm{H}_2} + 2c_{\mathrm{H}_2\mathrm{O}} + c_\mathrm{H} + c_\mathrm{OH} &= C_1 \\ 2c_{\mathrm{O}_2} + c_{\mathrm{H}_2\mathrm{O}} + c_\mathrm{O} + c_\mathrm{OH} &= C_2 \end{aligned} \tag{6.1e}$$

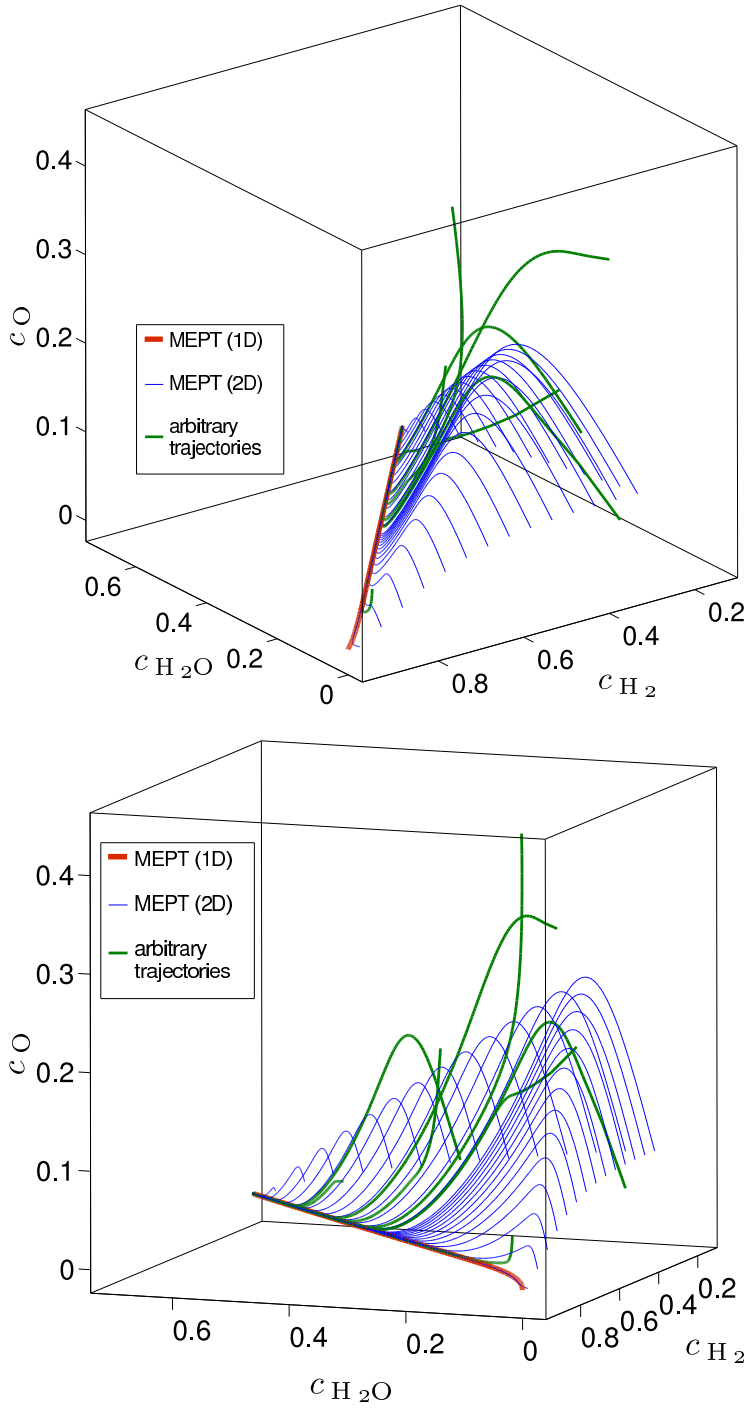

Figure 6.1: Two different views on MEPTs in their original formulation with two progress variables, H_2O and H_2. The union of the MEPTs spans an invariant manifold.

This problem has been solved for different fixed initial values. First, only c_{H_2O} has been fixed to $c_{H_2O} = 10^{-4}$, yielding the red trajectory, which represents a one-dimensional MEPT.
The two-dimensional manifold is created from the blue lines, which represent MEPTs with H_2O and H_2 chosen as progress variables. For the construction of the two-dimensional manifold first c_{H_2O} was set to 10^{-4} and c_{H_2} varied from 0.3 to 0.95, then c_{H_2} was set to 0.3 and c_{H_2O} varied from 0.05 to 0.65.
The green lines represent arbitrary trajectories relaxing to the two-dimensional manifold first, then relaxing to the one-dimensional MEPT and finally converging to equilibrium.
Hence by combining the MEPTs with H_2O and H_2 chosen as progress variables one obtains a manifold that is invariant by definition (as it is built from trajectories which are invariant by definition) and attracting at least close to equilibrium, as can be seen in Figure 6.1.

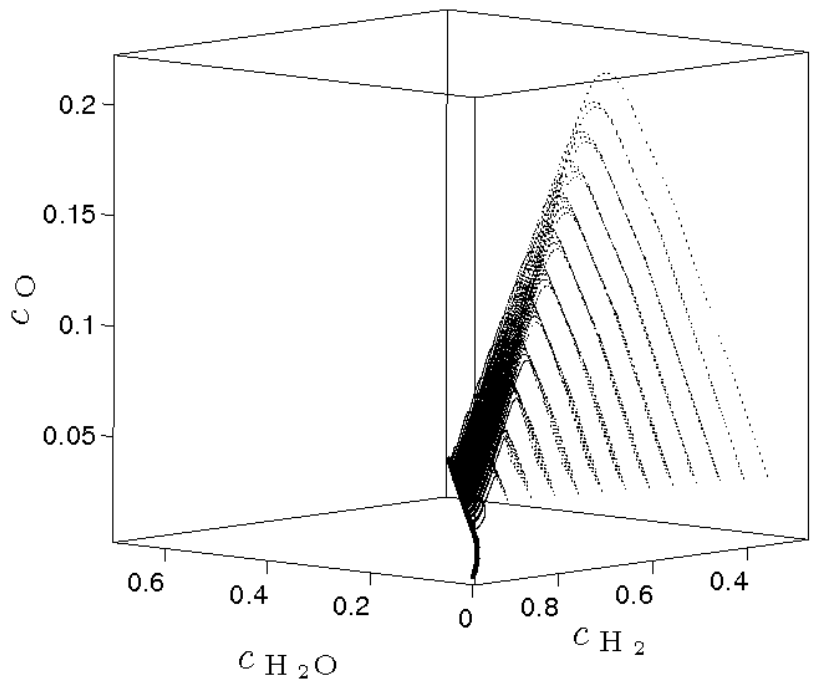

Figure 6.2: MEPTs computed as solutions to (6.1) on a grid including "inner points" as in Figure 5.1.

However, it looks like the MEPTs themselves are relaxing to an attracting manifold in their initial phase and then continue their course on this manifold. This in turn would mean that the consistency property from Section 5.2 (Definition 5.1) is not fulfilled for the so-computed MEPTs. This conclusion

is clearly confirmed by Figure 6.2, where MEPTs as solutions of (6.1) have been computed on a grid that includes "inner points" (cf. Figure 5.1). This violation of the consistency property motivates the search for alternative optimization criteria and for remedies in the computation of MEPTs that will be pursued in the subsequent paragraphs and sections.

Velocity Weighted Formulation

An improvement for the computation of minimal entropy production trajectories can be found by looking at the optimization functional

$$\int_0^T \sum_{j=1}^{m} \frac{\mathrm{d_i} S_j}{\mathrm{d}t} \, \mathrm{d}t \tag{6.2}$$

Using this formulation, entropy production is integrated over time. However,

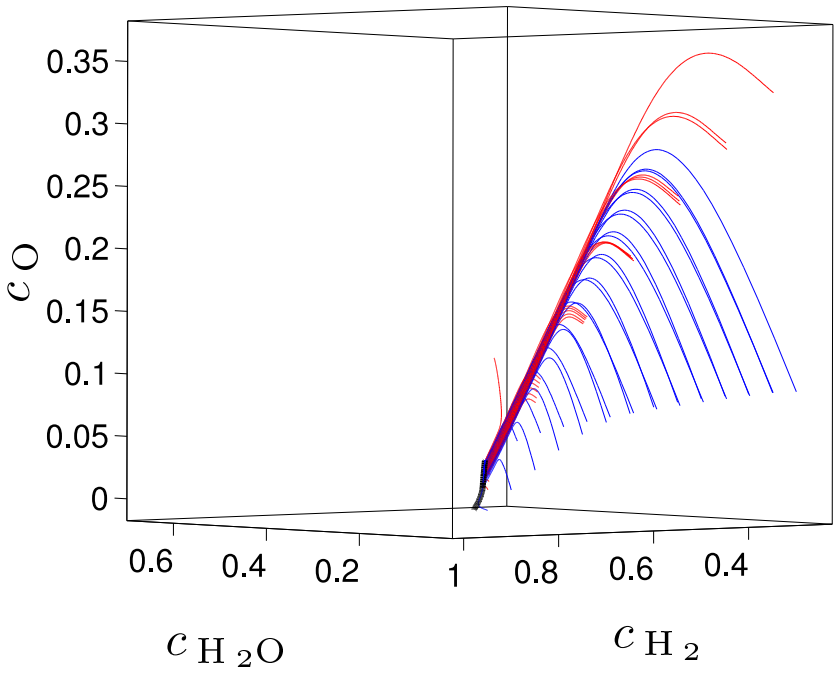

Figure 6.3: Comparison of MEPTs in the original formulation (blue lines, solutions of (6.1)) and "velocity weighted MEPTs" (red lines, solutions of (6.1) with modified optimization functional (6.6)). The trajectories computed by the velocity weighted problem start closer to the attracting manifold.

it would be more natural for the original task of minimizing entropy produc-

tion along a trajectory to consider a path integral from the initial value to equilibrium

$$\int_{s(0)}^{s(c^{\mathrm{eq}})} \sum_{j=1}^{m} \frac{\mathrm{d_i}S_j}{\mathrm{d}t}\, \mathrm{d}s(t), \tag{6.3}$$

where $s(t)$ is the length of the curve $c(t)$ at time t, which is given by (see Section 3.2)

$$s(t) = \int_0^t \|\dot{c}(\tau)\|_2 \mathrm{d}\tau. \tag{6.4}$$

Note that (6.3) is not simply a reparametrization of (6.2), as $\frac{\mathrm{d_i}S_j}{\mathrm{d}t}$ still depends on t and not on s. By differentiation of (6.4) one gets

$$\frac{\mathrm{d}s(t)}{\mathrm{d}t} = \|\dot{c}(t)\|_2 \quad \text{or} \quad \mathrm{d}s(t) = \|\dot{c}(t)\|_2 \mathrm{d}t. \tag{6.5}$$

As the derivative $\dot{c}(t)$ of the curve $c(t)$ is already given by the initial ODE $\dot{c}(t) = f(c)$, a modified version of the optimization functional can be given by

$$\int_0^T \sum_{j=1}^{m} \frac{\mathrm{d_i}S_j}{\mathrm{d}t}\, \|f(c(t))\|_2 \mathrm{d}t. \tag{6.6}$$

Thus, the initial integration phase, that corresponds to processes that are further away from equilibrium and hence generally faster, is weighted more than in the original formulation (6.2).
The results for the velocity weighted version of (6.1) – where (6.1a) simply has been replaced by (6.6) – are depicted in Figure 6.3 and can also be found in [74].

Short Integration Times

Another alternative for the application of entropy production as a relaxation criterion is closely related to the velocity weighting argument from the last paragraph. One problem in the original formulation of minimal entropy production trajectories lies in the "underweighting" of the initial fast motion towards the slow attracting manifold described above. This "underweighting" can be conceptually avoided by using the above velocity weighting. Another possibility to deal with this situation is to minimize the optimization functional only on the initial trajectory piece.
For the optimization problem this means choosing a smaller value for T which obviously has the appealing side-effect that the solution of (6.1) will be less demanding in terms of computation time. Although this formulation violates the condition (5.1d) of the original trajectory-based optimization problem,

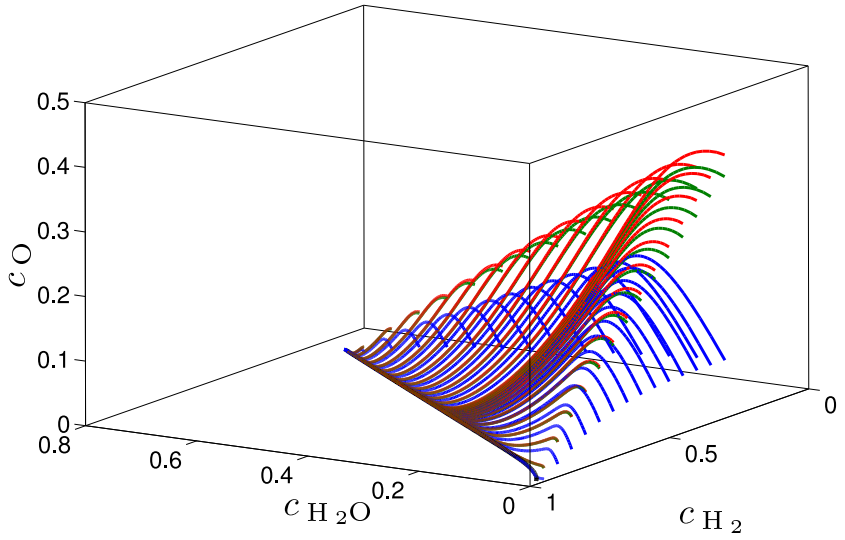

Figure 6.4: Original MEPTs as solutions of (5.1) (blue lines) in comparison with trajectories starting from initial points from MEPTs with a fixed integration time $T = 10^{-4}$ (green lines) and $T = 10^{-6}$ (red lines).

the results in Figure 6.4 demonstrate that this change in the philosophy of evaluation of the general problem (5.1) yields better results.
Note that the green and red lines in Figure 6.4 are not solutions of (5.1). Instead, (5.1) has been solved on a very small integration horizon $[0, T]$ ($T = 10^{-4}$ and $T = 10^{-6}$ respectively). In general, the end-point $c(T)$ of a solution to an optimization problem with such an integration horizon is not close to equilibrium. The trajectories in Figure 6.4 are trajectories that are integrated from the initial values $c(0)$ of these solutions.

6.1.2 Curvature Based Methods

In the last section, the computation of minimal entropy production trajectories for a model hydrogen combustion system has been demonstrated. A couple of improvements that can be found for the problem that the resulting trajectories do not completely lie on the slow invariant manifold have been shown in that section. However, none of these remedies resulted in "perfect" trajectories fulfilling the consistency property from Section 5.2, which should be the ultimate goal for all modifications of the general problem. Another possibility for the adaptation of the general problem (5.1) lies in the modification of the relaxation criterion $\Phi(c(t))$ in (5.1a).

In [73, 97], a novel optimization criterion for model reduction based on the minimization of curvature has been introduced. A detailed explanation on the implications of curvature for model reduction can be found in these references and in Subsection 5.2.2.
Results achieved with criteria based on curvature are reviewed in this section. Before turning to more realistic scenarios and to the computation of two-dimensional manifolds with curvature as the relaxation criterion, a simple two-dimensional model problem is used to demonstrate the conceptual power of the curvature approach.

Davis-Skodje Problem

A simple two-dimensional model that can be used as a benchmark is the model of Davis and Skodje from [16], which is given by

$$\begin{aligned} \frac{\mathrm{d}y_1}{\mathrm{d}t} &= -y_1 \\ \frac{\mathrm{d}y_2}{\mathrm{d}t} &= -\gamma y_2 + \frac{(\gamma-1)y_1 + \gamma y_1^2}{(1+y_1)^2}, \end{aligned} \tag{6.7}$$

where $\gamma > 1$ is a measure of stiffness for the system (the stiffness of the system grows with γ).
An exact slow invariant manifold and an analytical ILDM can be found for this system. The equations for these manifolds and further details on the model can be found in the appendix (Section A.1).
To demonstrate the behaviour of the minimal curvature method compared to the ILDM method, minimally curved trajectories in an Euclidian norm formulation ($A = I_n$ in (5.13)) have been computed, i.e.

$$\int_0^1 \|J(f(y))f(y)\|_2 \mathrm{d}y \tag{6.8}$$

has been minimized subject to the usual constraints.
The trajectories computed by this procedure are compared to the exact slow invariant manifold (SIM) and the ILDM in Figure 6.5. Note that stiffness often supports model reduction methods (especially those directly based on the separation of time-scales), as it allows for a decoupling of slow and fast subsystems. This can also be seen in the fact that both the ILDM and the minimal curvature method show an increased accuracy for growing γ.
Even though the minimally curved trajectories do not exactly represent the slow invariant manifold for small values of γ, they are always closer to the SIM than the ILDM is. A modified matrix A in the norm used in (5.13) may lead to even better results.

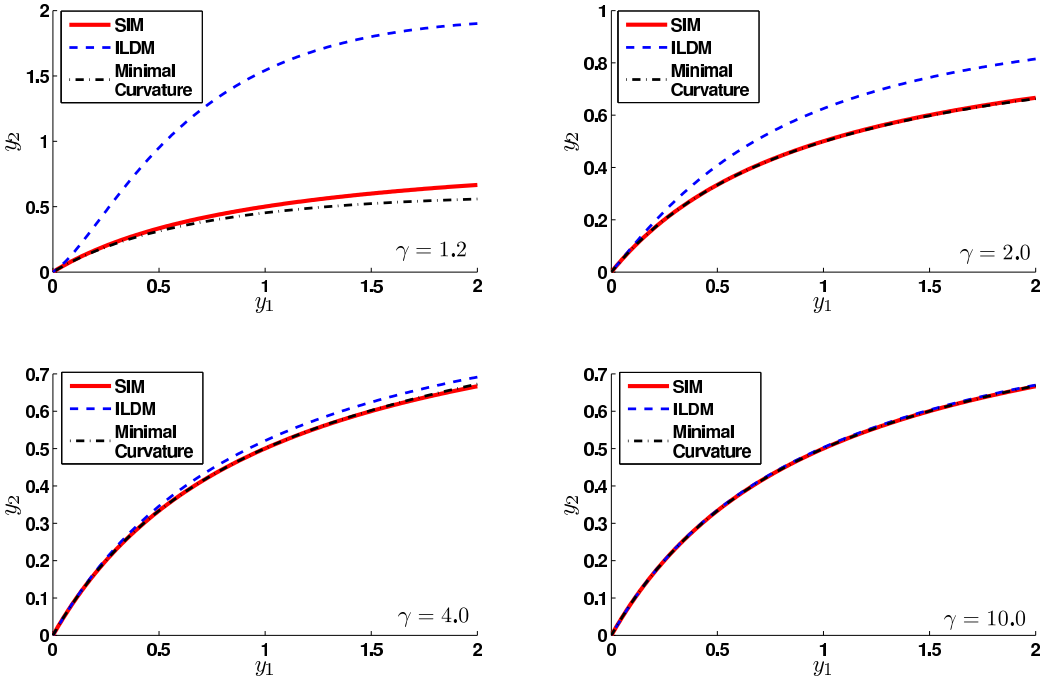

Figure 6.5: Results for the Davis-Skodje problem for different values of γ. Minimally curved trajectories are found to be closer to the true slow invariant manifold than the ILDM solution.

However, the entropy production based choice (5.12) of A is not feasible in this case, as there is no obvious formulation for entropy production in this system.

Model mechanism

The promising results for the Davis-Skodje problem suggest the applicability of the curvature minimization to more realistic situations. Here the six-species model reaction mechanism from A.2 is considered as the example application, allowing for the computation of a two-dimensional manifold approximating the SIM.
For this mechanism the entropy production is well defined, hence the curvature

$$\|Jf\|_A = \sqrt{f^T J^T A J f} \tag{6.9}$$

in the modified norm formulation with $A = \mathrm{diag}(a_k)$, $a_k = \sum_{j=1}^{m} \nu_{kj} \frac{\mathrm{d_i} S_j}{\mathrm{d}t}$ from (5.12) can be minimised subject to the usual constraints.
For the results presented here, the same variables have been used as progress variables as for the MEPT-approach in Section 6.1.1, making the results

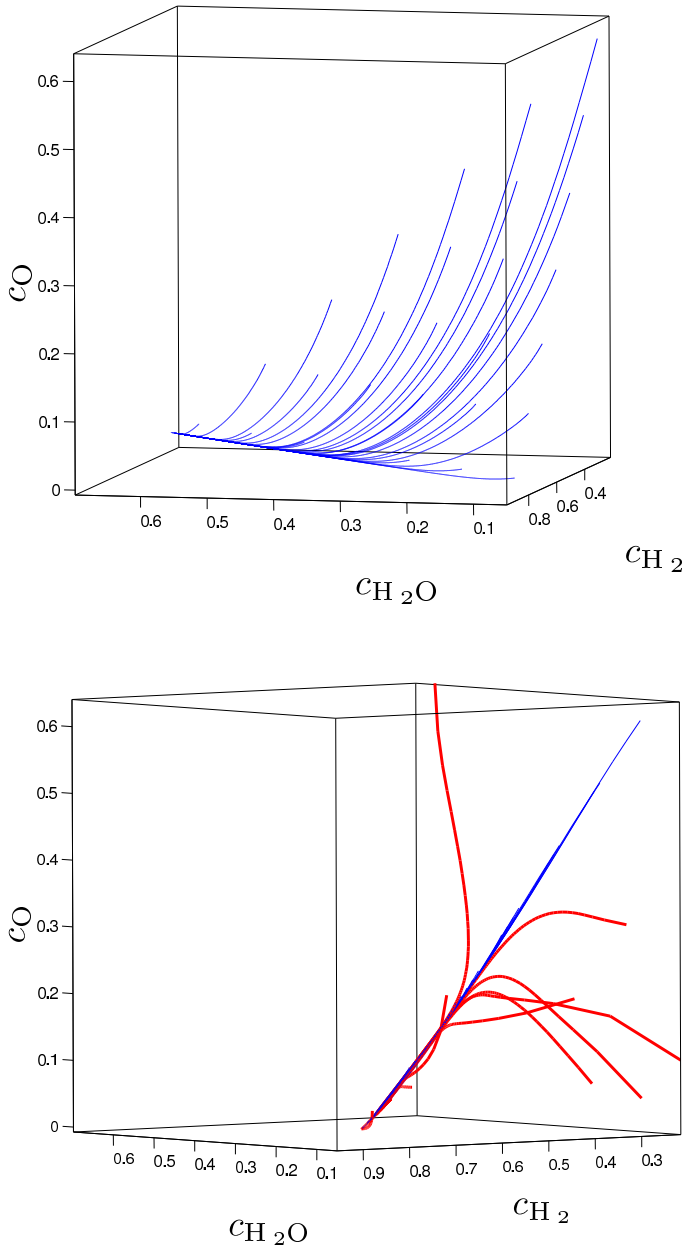

Figure 6.6: Results for the model hydrogen combustion mechanism using the curvature minimization from Subsection 5.2.2. Red lines represent arbitrary trajectories relaxing to the attracting manifold spanned by the blue minimal curvature trajectories.

comparable. The results of this computation are depicted in Figure 6.6. Again, the fixed initial concentration of H_2 is varied between 0.3 and 0.95 and the initial concentration of H_2O is varied between 0.05 and 0.65. However, compared to the results from Figure 6.1, the results here also include "inner points", whereas the MEPT manifold in Figure 6.1 has been computed just by trajectories starting from the boundary of a predefined domain. It is especially this inclusion of inner points that demonstrates the high extent of relaxation, as it allows for an optical verification of the consistency property. The results in Figure 6.6 suggest that the minimization of curvature in the modified formulation (6.9) at least approximately fulfils the consistency property from Section 5.1 and hence can be used for local species reconstruction for the given mechanism.

6.2 Towards Consistent Reduction Criteria

The previous section describes the general application of the trajectory-based optimization approach and especially for the construction of two-dimensional manifolds. By using the improved reduction criterion based on the minimization of curvature, a manifold that at least approximately fulfils the consistency criterion has been created using this approach.
This section focuses on the investigation of reduction criteria in the light of the consistency criterion from Definition 5.1. To guide the way towards criteria that fulfil the consistency criterion, this section concentrates on the computation of one-dimensional manifolds for the model hydrogen combustion mechanism from A.2. For a one-dimensional manifold – which is simply a trajectory – the consistency of the reduction criterion can be "optically" analyzed by looking at two-dimensional phase space plots.
All figures presented in this section follow the same idea: Optimized trajectories are computed for each of the following initial concentrations of H_2O: $c_{H_2O}(0) \in \{10^{-4}, 0.1, 0.2, 0.3, 0.4, 0.5, 0.6, 0.8, 0.9, 0.99\}$. The initial concentration $c_{H_2O}(0) = 0.7$ is not considered, as it corresponds to the equilibrium concentration of H_2O. For a perfect optimization criterion satisfying the consistency property, all trajectories computed for these initial values would lie on the same 1-dimensional manifold, i.e. on the same line. For an accurate comparison between different criteria, the species concentrations of all other species are plotted against the concentration of the progress variable c_{H_2O}. Additionally the optimization criterion (or a related function) is depicted as a function of c_{H_2O} as well. Hence the figures in this section present a way of validating the consistency of an optimization criterion by eye inspection.
Special attention has to be paid to the initial values $c_{H_2O} > 0.7$. From a phys-

ical perspective these initial values are not meaningful, as the main product (H_2O) of the reaction is being consumed and the main reactants (H_2 and O_2) are produced. However, from a mathematical point of view, the underlying ODE system can be integrated to equilibrium from these unphysical initial conditions and it is of special interest whether the consistency of the reduction criteria holds even in this region.

6.2.1 Standard Evaluation

Three different relaxation criteria for the trajectory-based optimization approach are introduced in Chapter 5, entropy production, curvature and arc length. These basic criteria are reviewed in this subsection.

Entropy Production

The first relaxation criterion used in the context of the trajectory-based optimization approach was entropy production, introduced in [50] and reviewed in Section 5.2.1. Results for the minimization of entropy production along trajectories are shown in Figure 6.7. Instead of leaving the overall integration time T free for the optimizer and demanding the final point to be sufficiently close to the equilibrium point by (5.1d), a fixed integration horizon $[0, 1]$ is chosen here. This integration horizon has turned out to be sufficient to approximately reach equilibrium.
Figure 6.7 depicts results of the optimization problem (5.1a–5.1c), where the relaxation criterion Φ is

$$\Phi(c(t)) = \frac{\mathrm{d}S}{\mathrm{d}t} = R \sum_{j=1}^{m} \frac{\mathrm{d_i}S_j}{\mathrm{d}t} \tag{6.10}$$

i.e. entropy production, with $\frac{\mathrm{d_i}S_j}{\mathrm{d}t}$ from (5.2).
One can see that the manifold resulting from the solution of this problem does not fulfil the consistency criterion – the optimized trajectories contain an initial relaxation phase especially in the radical species O and H. Regarding the behaviour of entropy production in dependence of c_{H_2O} an interesting fact can be noticed that has also been observed in [97]: In an initial phase of the trajectories an entropy production rate higher than necessary is accepted. A possible explanation to this behaviour is the weighting of the relaxation criterion along the trajectories which are parametrized by time – the optimizer can decrease the overall entropy production by increasing entropy production on a short (w.r.t. time) initial phase, keeping the entropy production lower for the rest of the time interval.

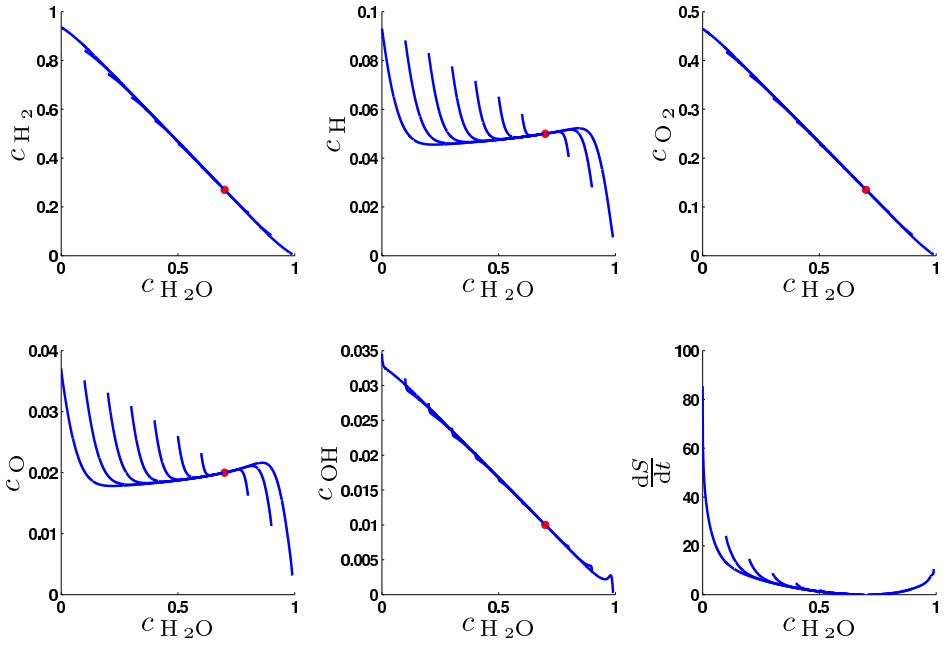

Figure 6.7: MEPTs for Φ from (6.10) on a fixed time horizon $[0, 1]$ with only H_2O as a progress variable. A strong initial relaxation phase is found for H and O.

Curvature

In [73, 97], curvature has been introduced as a relaxation criterion (see Section 5.2.2). Motivated by the promising results presented for the Skodje-Davis system in Subsection 6.1.2 and the results presented in [97], curvature as a relaxation criterion is investigated with respect to the consistency property here.
Figure 6.8 shows trajectories with minimized curvature in the Euclidian metric, i.e.

$$\Phi(c(t)) = \|J(f(c(t))) \cdot f(c(t))\|_2 \tag{6.11}$$

has been used as objective functional for problem (5.1a–5.1c) with a fixed integration time of $T = 1$.
Similar to the results presented for the Skodje-Davis system in Subsection 6.1.2 and the results presented in [97], Figure 6.8 shows that the trajectories computed with this curvature minimization start reasonably close to the one-dimensional SIM. Nevertheless Figure 6.8 also shows that the curvature minimization does not fulfil the consistency criterion, making improvement indispensable. A possible explanation to the violation of the consistency criterion may be that curvature is evaluated in a metric that is not adequate

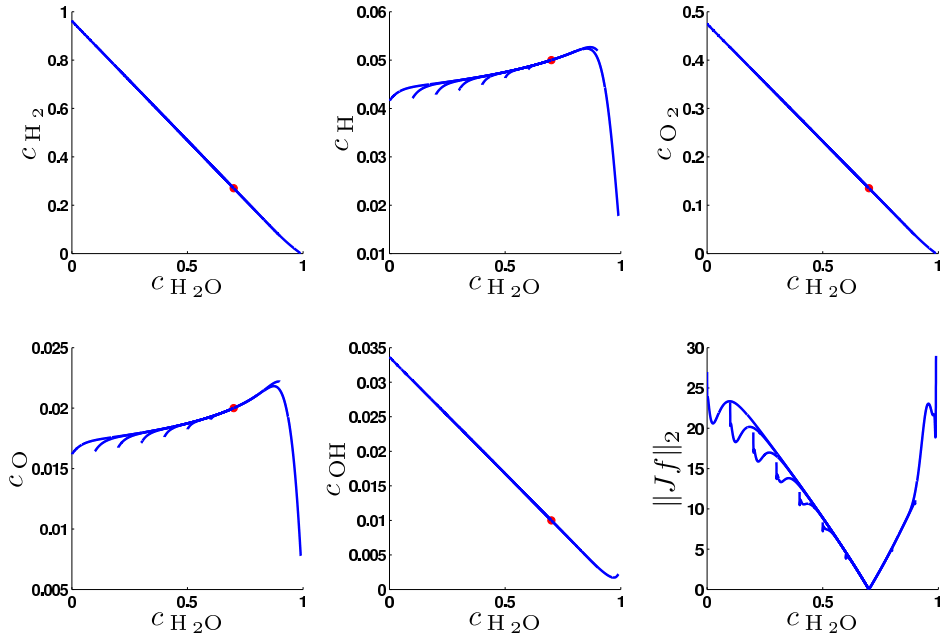

Figure 6.8: Curvature minimization results with Φ from (6.11) for H_2O as a progress variable on a fixed time horizon $[0, 1]$. Trajectories start reasonably close to the one-dimensional SIM.

in the phase space of the given system with respect to its thermodynamic and kinetic properties.

Length / Velocity

The third relaxation criterion presented in Chapter 5 is the speed of the trajectories, which by integration leads to an arc length minimization. As this minimization takes place on a constant time interval, the resulting trajectories can either be interpreted as shortest trajectories or a relation to "slow manifolds" can be established. Figure 6.9 depicts these shortest trajectories in the sense of a minimal arc length in an Euclidian norm formulation (cf. Subsection 5.2.3).
The trajectories in this figure are solutions to the optimization problem (5.1a–5.1c) on the fixed time horizon $[0, 1]$ using the criterion

$$\Phi(c(t)) = \|\dot{c}(t)\|_2 = \|f(c(t))\|_2 = \sqrt{f^T f}. \tag{6.12}$$

The resulting trajectories are very similar to the minimal entropy production trajectories from Figure 6.7 – a large initial relaxation period can be

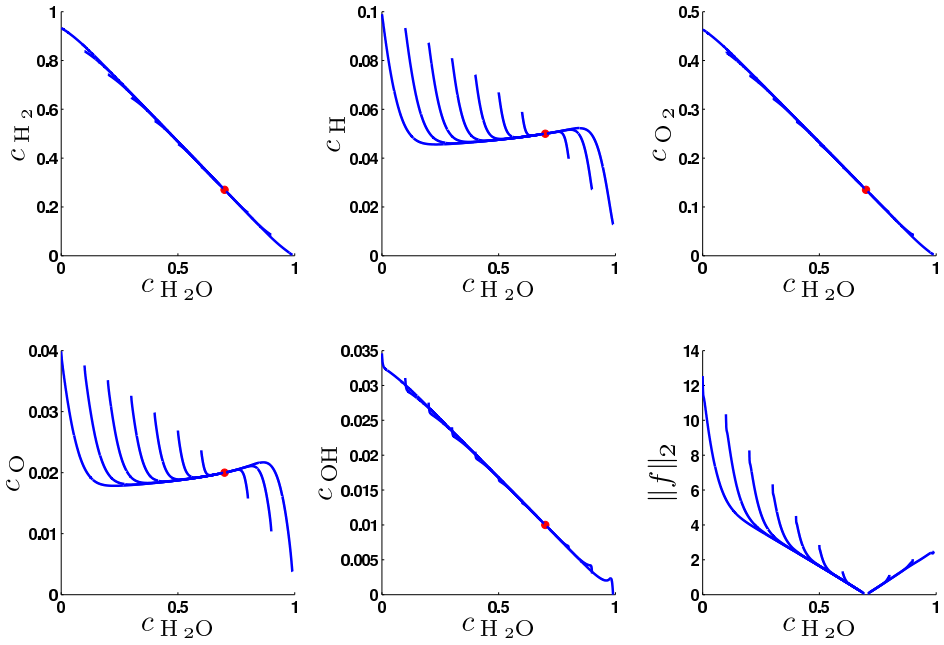

Figure 6.9: Shortest trajectories in the sense of minimal arc length in an Euclidian norm formulation – i.e. Φ from (6.12) on a fixed time horizon $[0, 1]$.

observed especially for the radical species O and H. Again this violation of the consistency property may be explained by inadequate metrics for the evaluation of the velocity $\|f\|_2$.

6.2.2 Improving Relaxation Criteria

The previous subsection shows that all three presented relaxation criteria – entropy production, curvature and speed/arc length – violate the consistency property. In this subsection possibilities to mitigate these violations are presented and investigated. Two possible explanations to the violation of the consistency criterion by the presented relaxation criteria have already been stated in Section 6.1 – an underweighting of the relaxation criterion on the initial trajectory piece and the usage of inadequate metrics in phase space.

A remedy for the underweighting of the initial trajectory piece can be found by multiplication of the relaxation criterion $\Phi(c(t))$ with a suitable weighting function $g(c(t))$, i.e.

$$\tilde{\Phi}(c(t)) := \Phi(c(t))g(c(t)). \tag{6.13}$$

The idea of finding a suitable metric for the kinetic phase space is conceptually similar, but additionally allows for different weightings of the different species. As stated in Section 5.2, the key idea is to replace the Euclidian metric $\|x\|_2 := \sqrt{x^T x}$ by

$$\|x\|_A := \sqrt{x^T A x}, \tag{6.14}$$

where A is a symmetric, positive definite matrix. Two such matrices are proposed in the equations (5.12) and (5.19).
Generally such matrices are based on properties concerning the species, but the computation of entropy production is not based on *species* but on *reactions* (more precisely on pairs of forward and reverse reactions). Hence the use of a different metric based on species – as all modified metric used in this work – is not meaningful in the context of entropy production as a relaxation criterion. Hence in the sequel the weighting function $g(c(t))$ will primarily be used in the entropy production context, while modified metric formulations will be used for the modification of arc length and curvature as relaxation criteria.

Arc Length in Different Metrics

As stated in Subsection 5.2.3, the length of a trajectory can be computed in terms of different Riemannian metrics by adapting the Euclidian scalar product and its induced norm. A choice of Riemannian metric that has been used in model reduction [33] before is the so-called Shahshahani metric. Figure 6.10 shows minimal-length trajectories in this metric.
These trajectories have been computed as solutions of the optimization problem (5.1a–5.1c) on the fixed time horizon $[0, 1]$ using the criterion

$$\Phi(c(t)) = \|\dot{c}(t)\|_B = \|f(c(t))\|_B = \sqrt{f^T \cdot B \cdot f} \tag{6.15}$$

with $B = \operatorname{diag}\left(\frac{1}{c_i}\right)$ corresponding to the Shahshahani metric discussed in 5.2.3.
Figure 6.10 shows that using the Shahshahani metric, the initial relaxation period can be largely diminished – the resulting trajectories start very close to the SIM even for the radical species O and H. For the other species there is no visible deviation from the SIM. Even though the deviations for O and H demonstrate that the consistency property is still violated, the velocity property $\|\dot{c}(t)\|_B$ can also be useful for model reduction, e.g. as a weighting function $g(c(t))$ for entropy production.
Note that due to the large range of values of the relaxation criterion a logarithmic scale has been chosen for the plot of $\|f\|_B$ against $c_{\mathrm{H_2O}}$ in Figure 6.10.

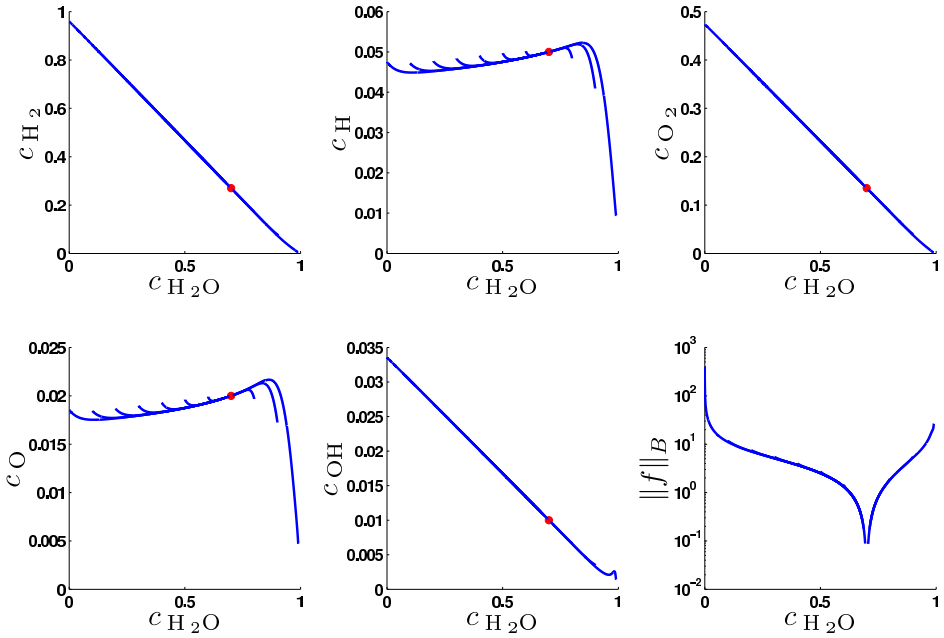

Figure 6.10: Shortest trajectories in the sense of minimal arc length in a Shahshahani metric formulation – i.e. Φ from (6.15) with $B = \operatorname{diag}\left(\frac{1}{c_i}\right)$ on a fixed time horizon $[0, 1]$. A logarithmic scale has been chosen for the plot of $\|f\|_B$ against $c_{\mathrm{H_2O}}$.

Weighting Functions for Entropy Production

As discussed above, weighting functions can help to improve relaxation criteria based on entropy production. In the sequel potential weighting functions helping to improve (in terms of the consistency) entropy production as an optimization criterion are introduced.

Velocity Weighting The idea that weighting functions can help to improve relaxation criteria is that due to the dissipative nature of the underlying dynamical systems, fast time-scales are underweighted if no weighting function is used. Due to this underweighting an excess in the relaxation criterion can be compensated by quickly reaching a longer (with respect to time) period close to equilibrium. A self-evident weighting function that serves for a kinetic weighting of the criterion with respect to the arc length of the trajectory is the velocity along the trajectory, i.e.

$$g(c(t)) := \|\dot{c}(t)\|_2 = \|f(c(t))\|_2. \tag{6.16}$$

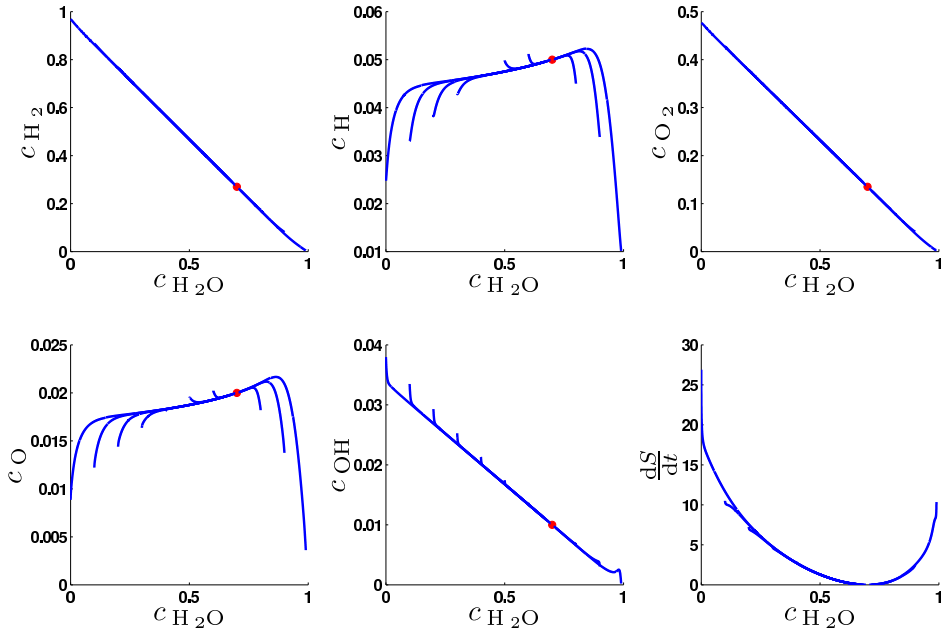

Figure 6.11: MEPTs weighted by velocity – i.e. for Φ from (6.17) on a fixed time horizon $[0, 1]$. The initial relaxation phase has been reduced but not eliminated compared to Figure 6.7.

Using velocity as a weighting function the weighted entropy production criterion Φ for (5.1a–5.1c) is

$$\Phi(c(t)) = \frac{\mathrm{d}S}{\mathrm{d}t}\|f\|_2 = R\sum_{j=1}^{m}\frac{\mathrm{d_i}S_j}{\mathrm{d}t}\|f\|_2. \tag{6.17}$$

Figure 6.11 shows minimal entropy production trajectories for this weighted entropy production criterion.

Compared to Figure 6.7 one can see that the initial relaxation period has been reduced, but not completely eliminated. The two-dimensional manifold in Figure 6.3 confirms this impression. Interestingly, whereas Figure 6.7 exhibited an excess of entropy production in the initial relaxation phase, Figure 6.11 shows that the entropy production in the initial phase is actually less than for the one-dimensional SIM. Hence by the velocity weighting the problem of the initial excess entropy production has been solved, but nevertheless the SIM is not well approximated.

As the arc length minimization using the Shahshahani metric showed promising results, it is reasonable to use this metric for the velocity weighting as

well, i.e. to use

$$g(c(t)) := \|\dot{c}\|_B = \|f\|_B,\ B = \mathrm{diag}\left(\frac{1}{c_i}\right), \quad i = 1, ..., n. \tag{6.18}$$

Figure 6.12 shows results for the minimal entropy production weighted by velocity evaluated using the Shahshahani metric, i.e. for the minimization of

$$\Phi(c(t)) = \frac{\mathrm{d}S}{\mathrm{d}t}\|f\|_B = R\sum_{j=1}^{m}\frac{\mathrm{d_i}S_j}{\mathrm{d}t}\|f\|_B \tag{6.19}$$

with $\|.\|_B$ being the Shahshahani metric induced by $B = \mathrm{diag}\left(\frac{1}{c_i}\right)$ and discussed in 5.2.3.

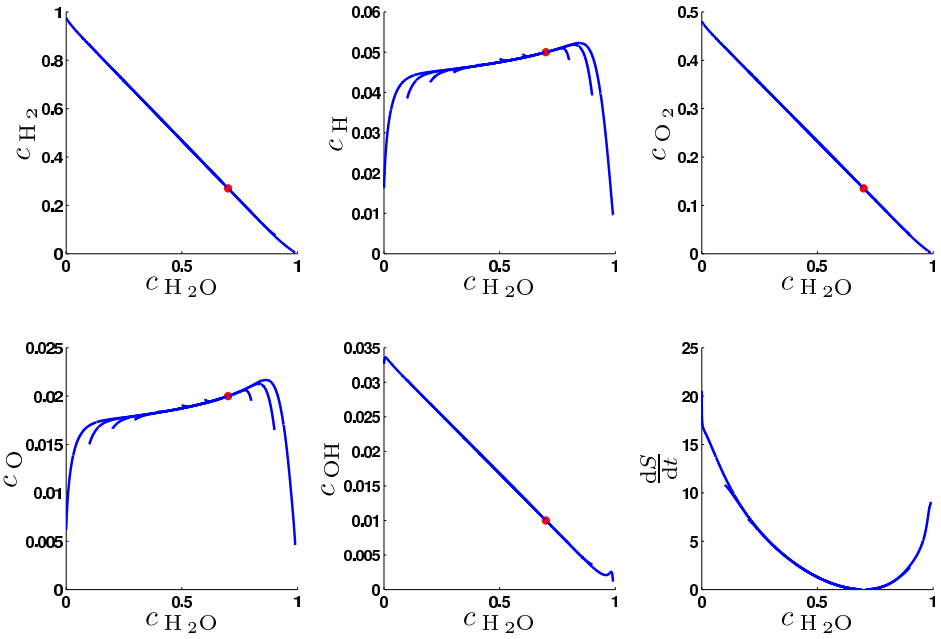

Figure 6.12: MEPTs weighted by velocity in Shahshahani metric – i.e. for Φ from (6.19) on a fixed time horizon $[0, 1]$. Trajectories start closer to the SIM than those computed with the Euclidian metric velocity weighting in Figure 6.11.

In both Figure 6.11 and Figure 6.12, the large relaxation phases present in the "pure" entropy production minimization could be decreased – especially close to equilibrium. However, for the Euclidian metric formulation results depicted in Figure 6.11, the deviations from the one-dimensional SIM are

larger than for the Shahshahani metric in Figure 6.12. This can especially be seen by comparing the results for the radical species OH. A further observation that can be made is that further away from equilibrium the shortest trajectories in Shahshahani metric from Figure 6.10 start closer to the SIM than the velocity-weighted MEPTs.

Curves of Minimal Energy While a velocity weighting of the arc length optimization criterion does not seem meaningful at first sight, a second view reveals another picture. As a velocity weighting is simply achieved by multiplying the original criterion by $\|f\|_2$, a velocity weighted criterion based on arc length is obtained as

$$\Phi(c(t)) = \|f(c(t))\|_2^2. \tag{6.20}$$

Integrating this criterion leads to $\int_0^T \|f\|_2^2 \mathrm{d}t$, which by Definition 3.22 is the *energy of the curve* described by the underlying ODE system $\dot{c} = f(c)$. Hence optimizing (5.1a–5.1c) with Φ from 6.20 as the relaxation criterion amounts to a computation of curves of minimal energy.

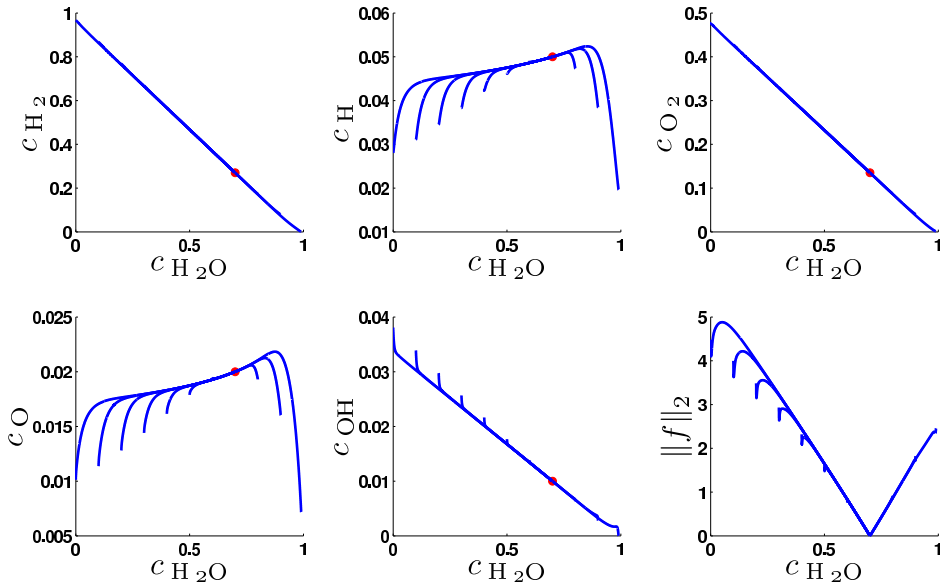

Figure 6.13: Trajectories with minimal energy – i.e. for Φ from (6.20) on a fixed time horizon $[0, 1]$. The results are comparable to the velocity weighted MEPTs in Figure 6.11.

Results achieved using this energy minimization are depicted in Figure 6.13. These results are roughly comparable to the velocity weighted MEPTs in

Figure 6.11 which was to be expected as the results for minimal entropy production trajectories and arc length minimization are very similar (cf. Figures 6.7 and 6.9).

Restricted Velocity Weighting A problem resulting from a pure velocity weighting as in the previous paragraph is that both the dynamics for the progress variables and for the other species are uniformly weighted. However, from a model reduction point of view, the dynamics for the progress variables should not be weighted at all. An approach to have the weighting function depend on the choice of progress variables is simply not to use the progress variables for the weighting, i.e. to use the seminorm

$$\|x\|_{2,\text{non-rpv}} := \sqrt{\sum_{\substack{i=1 \\ i \notin I_{\text{fixed}}}}^{n} x_i^2}. \tag{6.21}$$

Note that the case $\|x\|_{2,\text{non-rpv}} = 0$ for $x \neq 0$ will only occur if the progress variable concentrations are set such that all other species concentrations are zero – a case that can be avoided by the user. With this seminorm, a restricted weighting function can be stated as

$$g(c(t)) := \|f(c)\|_{2,\text{non-rpv}}. \tag{6.22}$$

Using this weighting function, Figure 6.14 shows results for the optimization problem (5.1a–5.1c) with the optimization functional

$$\Phi(c(t)) = \frac{\mathrm{d}S}{\mathrm{d}t}\|f\|_{2,\text{non-rpv}}. \tag{6.23}$$

Compared to the results from Figure 6.11 with a pure velocity weighting, the results in Figure 6.14 are improved far away from equilibrium, while close to equilibrium the trajectories start further away from the one-dimensional SIM.
A seminorm similar to the one from (6.21) can also be introduced using the Shahshahani metric. This seminorm then is written as

$$\|x\|_{B,\text{non-rpv}} := \sqrt{\sum_{\substack{i=1 \\ i \notin I_{\text{fixed}}}}^{n} b_i \cdot x_i^2}, \tag{6.24}$$

with $b_i > 0$ being the diagonal entries of matrix B from equation (6.18).

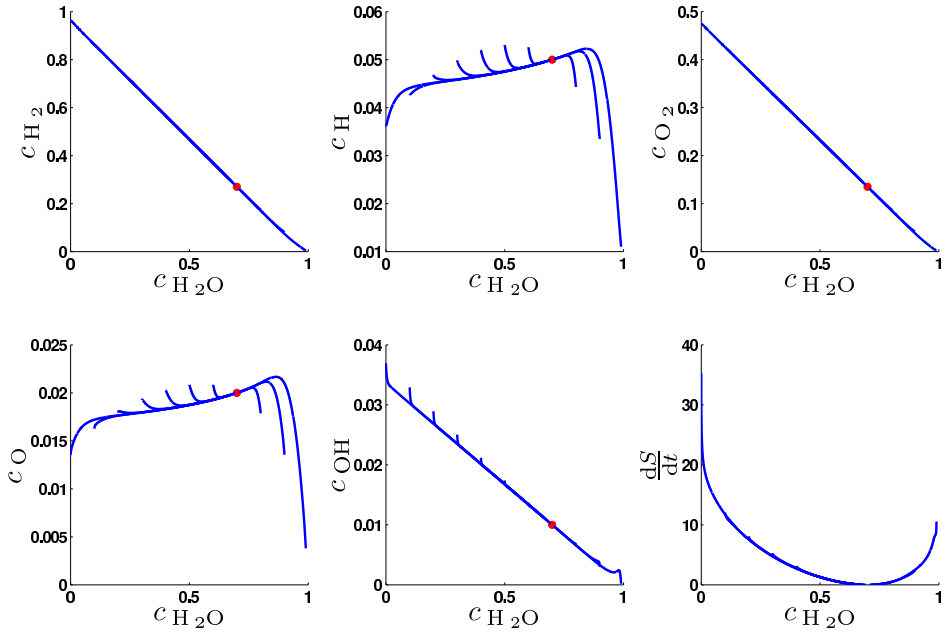

Figure 6.14: MEPTs weighted by restricted velocity – i.e. for Φ from (6.23) on a fixed time horizon $[0, 1]$. Compared to the Euclidian metric velocity weighting in Figure 6.11, the results are improved only far away from equilibrium, while close to equilibrium the deviations from the SIM are larger.

Results for the minimization of

$$\Phi(c(t)) = \frac{\mathrm{d}S}{\mathrm{d}t}\|f\|_{B,\text{non-rpv}} \tag{6.25}$$

are shown in Figure 6.15.
While the results for H_2O as the progress variable in Figure 6.15(a) look very promising, Figure 6.15(b) at least partly disproves this impression. For high concentrations of H_2 an initial relaxation phase can be noticed. This is not surprising, because the dynamics on the SIM are most likely not governed by a *user-defined* progress variable.
A weighting function that is capable of distinguishing between the dynamics *on* an *towards the* SIM will probably have to include time-scale information to determine the true parameter of the SIM. However, getting this information involves the expensive computation of eigenvalues and hence is infeasible in this context. Nevertheless the results in Figure 6.15(a) demonstrate the potential of a weighting function that depends on the parametrization of the SIM.

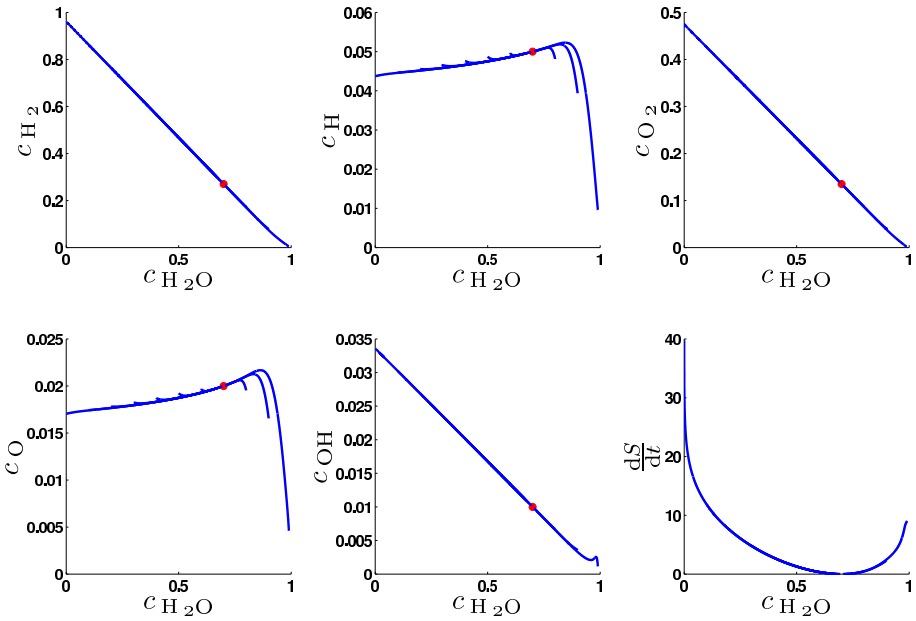

(a) H_2O as progress variable.

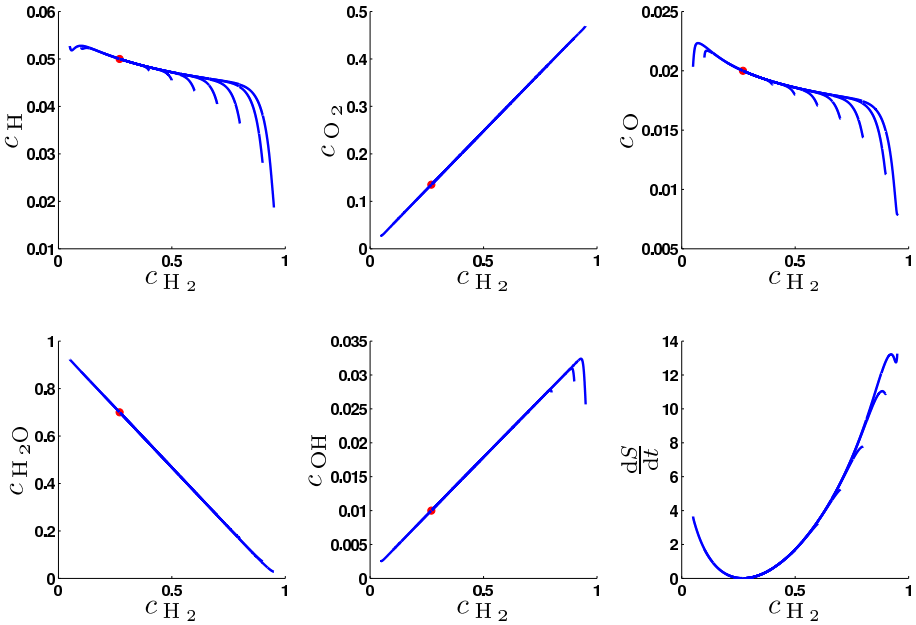

(b) H_2 as progress variable.

Figure 6.15: MEPTs weighted by restricted velocity in Shahshahani metric – i.e. for Φ from (6.25) for the reaction progress variables H_2O (a) and H_2 (b). The consistency property seems to be nearly satisfied for the results depicted in (a), while the results depicted in (b) exhibit more deviations from the SIM.

Curvature in Different Metrics

As discussed in Subsection 5.2.2 and demonstrated in the results from [73] in Section 6.1, a possible way of diminishing the small initial relaxation phase of the curvature minimization results in Figure 6.8 is to choose a different norm in (6.11). While this procedure is conceptually comparable to the use of a weighting function as above, it also allows for the different weighting of different phase space directions which seems to be advantageous.
Using this strategy results for the minimized curvature

$$\Phi(c(t)) = \|J(f(c)) \cdot f(c)\|_A \tag{6.26}$$

with the norm $\|.\|_A$ based on the diagonal matrix $A = \mathrm{diag}\,(a_{kk})\,, \quad a_{kk} = \sum_{j=1}^{m} \nu_{kj} \frac{\mathrm{d_i}S_j}{\mathrm{d}t}, \; k = 1, ..., n$ are depicted in Figure 6.16.

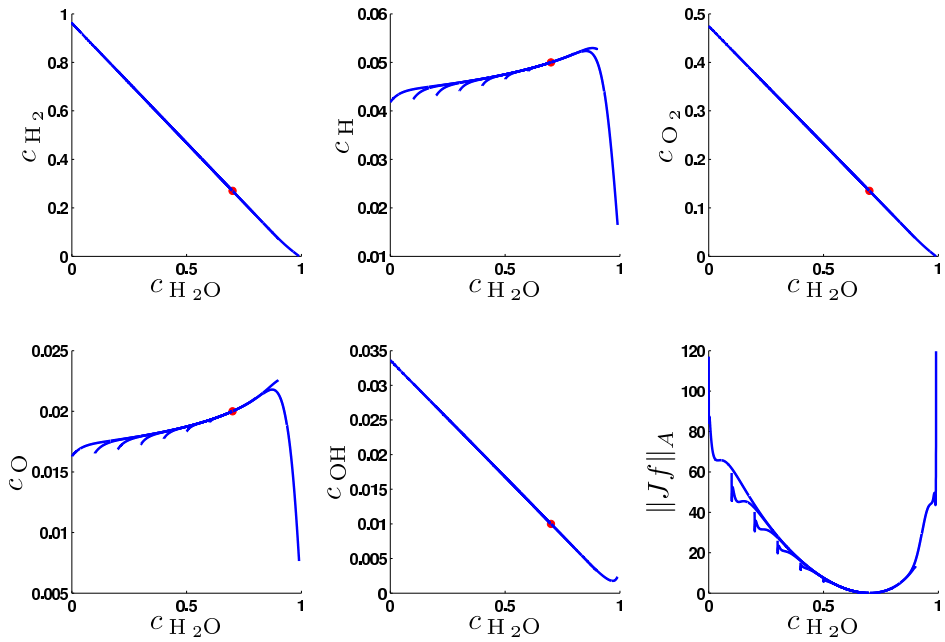

Figure 6.16: Curvature minimization results in entropy production metric with Φ from (6.26) for H_2O as a progress variable on a fixed time horizon $[0, 1]$. No clear improvement compared to the results in Figure 6.8 is found.

While this procedure leads to a minimal relaxation phase for the two-dimensional manifold in Subsection 6.1.2 (cf. [97]), no clear improvement can be found for the results in Figure 6.16 compared to the results in Figure 6.8.

However, choosing the Shahshahani metric instead, i.e. minimizing

$$\Phi(c(t)) = \|J(f(c)) \cdot f(c)\|_B \tag{6.27}$$

with $\|x\|_B = x^T \mathrm{diag}\left(\frac{1}{x_i}\right) x$, leads to the improved results shown in Figure 6.17.

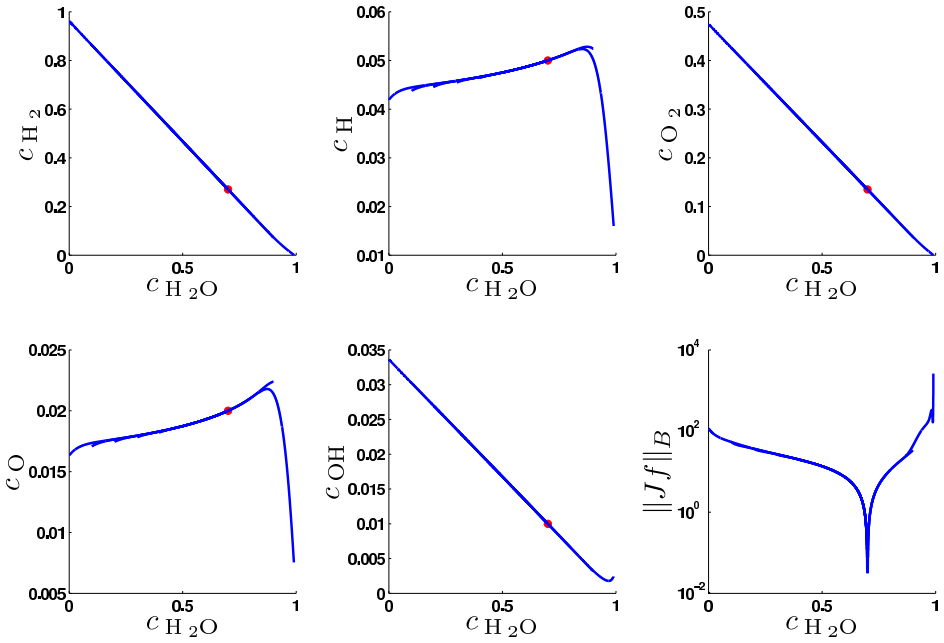

Figure 6.17: Curvature minimization results in Shahshahani metric with Φ from (6.27) for H_2O as a progress variable on a fixed time horizon $[0, 1]$. Trajectories start very close to the SIM, but the range of values for the relaxation criterion is extremely large.

The latter results look very promising and demonstrate the potential of the curvature minimization approach. However, it has to be noted that the range of values that the relaxation criterion takes is extremely large compared to the other criteria entropy production, arc length and even curvature in other metrics. Due to this reason the relaxation criterion is plotted on a logarithmic scale in the bottom right plot of Figure 6.17. In large scale model reduction this range of values may lead to numerical problems, especially as the relaxation criterion and its derivatives may take even larger values during the optimization.
Another point that has to be mentioned is that the second differential of entropy – the Shahshahani metric – takes this simple diagonal form only due

to the fact that the underlying system is regarded for constant volume and constant temperature. For other conditions the matrix B may be much more complicated and the user could even be forced to rely on approximations that would have to be assured to lead to a positive definite matrix.

6.2.3 A Modified Problem Formulation Using an Additive Initial Value Term

In the previous subsection, a way to improve the consistency of the minimal curvature criterion by evaluating curvature in a different geometry has been discussed. Another possibility for improvement is to add an initial value term to the integral formulation, i.e.

$$\min_{c_k} \int_0^T \Phi(c(t))\ \mathrm{d}t - \varphi(c(0)) \tag{6.28a}$$

subject to

$$\frac{\mathrm{d}c_k}{\mathrm{d}t} = f_k(c), \qquad k = 1, ..., n \tag{6.28b}$$

$$c_k(0) = c_k^0, \qquad k \in I_{\text{fixed}} \tag{6.28c}$$

$$\begin{aligned} 2c_{\mathrm{H_2}} + 2c_{\mathrm{H_2O}} + c_{\mathrm{H}} + c_{\mathrm{OH}} &= C_1, \\ 2c_{\mathrm{O_2}} + c_{\mathrm{H_2O}} + c_{\mathrm{O}} + c_{\mathrm{OH}} &= C_2. \end{aligned} \tag{6.28d}$$

A (heuristic) motivation for this procedure might be found in the idea that $\varphi(c(0))$ may represent the past or history of the trajectory. For $\Phi(c) = \|\ddot{c}\|_2$, this idea suggests the choice of $\varphi(c) = \|\dot{c}\|_2$. Results for this choice of $\Phi(c), \varphi(c)$ are depicted in Figure 6.18.
While the initial relaxation phase seems to be completely eliminated for the values $c_{\mathrm{H_2O}}(0) \in \{10^{-4}, 0.1, 0.2, 0.3, 0.4, 0.5, 0.6\}$, the (unphysical) results to the right of the equilibrium point do not look satisfying in terms of the consistency criterion. Interestingly, a remedy for this is found in a change of sign in $\varphi(c)$ for values of $c_{\mathrm{H_2O}}(0) > \bar{c}_{\mathrm{H_2O}} = 0.7$.
A more general expression for the change of sign in $\varphi(c)$ is found as follows: As the mechanism is based on the overall reaction $2\,\mathrm{H_2} + \mathrm{O_2} \rightarrow 2\,\mathrm{H_2O}$, its equilibrium constant (see Section 3.3) is

$$K_C = \frac{\bar{c}_{\mathrm{H_2O}}^2}{\bar{c}_{\mathrm{H_2}}^2 \bar{c}_{\mathrm{O_2}}},$$

where $\bar{c}$ denotes the equilibrium concentration. Choosing the sign of φ according to the sign of the difference between this equilibrium constant and

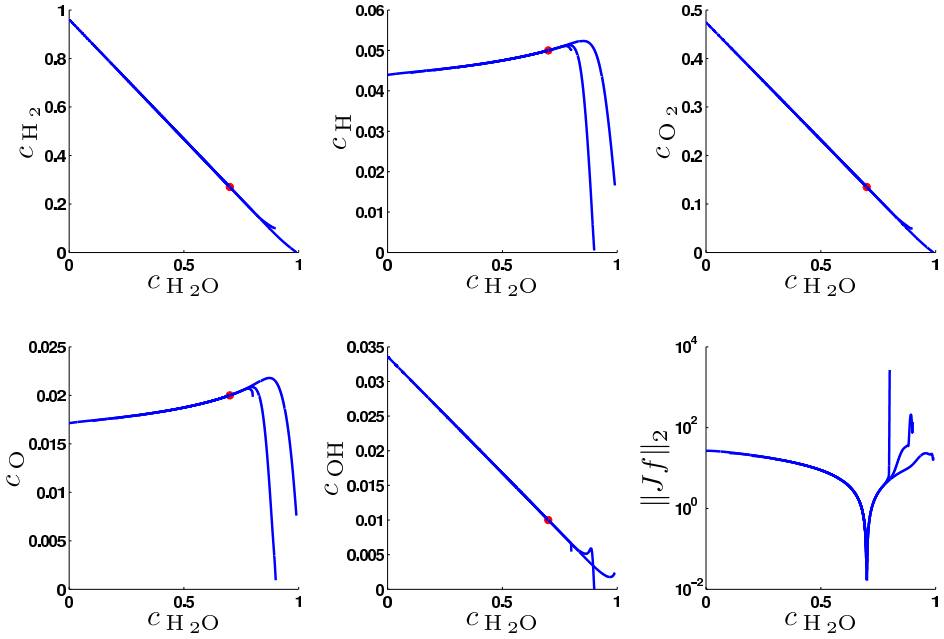

Figure 6.18: Optimal trajectories as solutions of the additive initial value term problem (6.28) with $\Phi = \|\ddot{c}\|_2$ and $\varphi = \|\dot{c}\|_2$ for H_2O as the progress variable. For $c_{H_2O}(0) < 0.7$, the trajectories seem to completely reside on the SIM, for (the unphysical region) $c_{H_2O}(0) > 0.7$ a large initial relaxation phase is observed.

the mass action coefficient yields a negative sign for an excess of products (and a deficit of reactants) and a positive sign for an excess of reactants (and a deficit of products). For the mechanism treated here, this difference is

$$\frac{\bar{c}_{H_2O}^2}{\bar{c}_{H_2}^2 \bar{c}_{O_2}} - \frac{c_{H_2O}^2}{c_{H_2}^2 c_{O_2}}.$$

Using

$$\varphi(c(0)) = \text{sign}\left(\frac{\bar{c}_{H_2O}^2}{\bar{c}_{H_2}^2 \bar{c}_{O_2}} - \frac{c_{H_2O}^2(0)}{c_{H_2}^2(0) c_{O_2}(0)}\right) \|f(c(0))\|_2, \tag{6.29}$$

the results depicted in Figure 6.19(a) are achieved.
While the initial relaxation phase of the trajectories in Figure 6.19(a) seems to be completely eliminated, the the bottom right plot of curvature of Figure 6.19(a) indicates that the computed trajectories are not completely identical to the SIM.
Nevertheless this result shows that a very good approximation of the SIM is possible with the trajectory-based optimization approach used in this work.

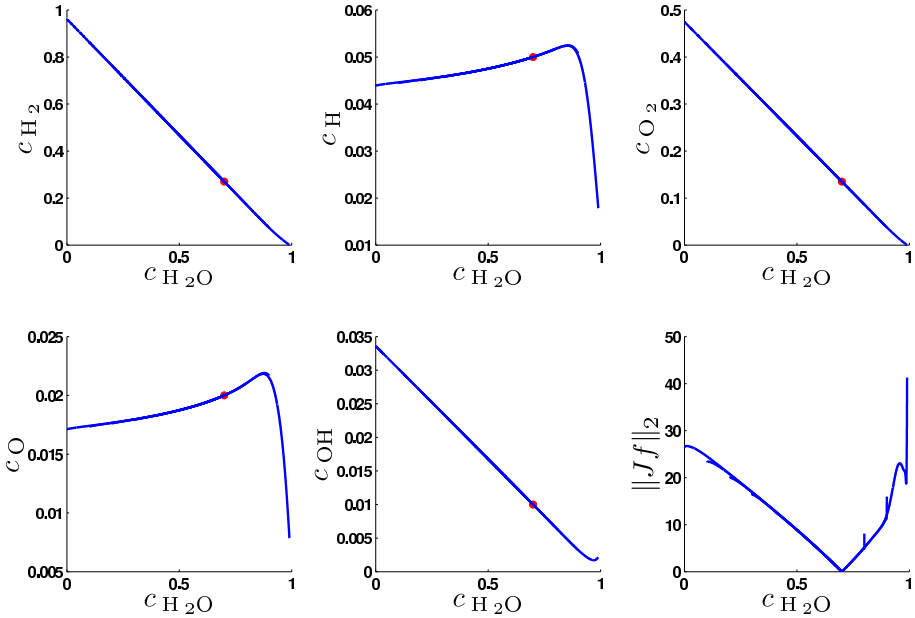

(a) H_2O as progress variable

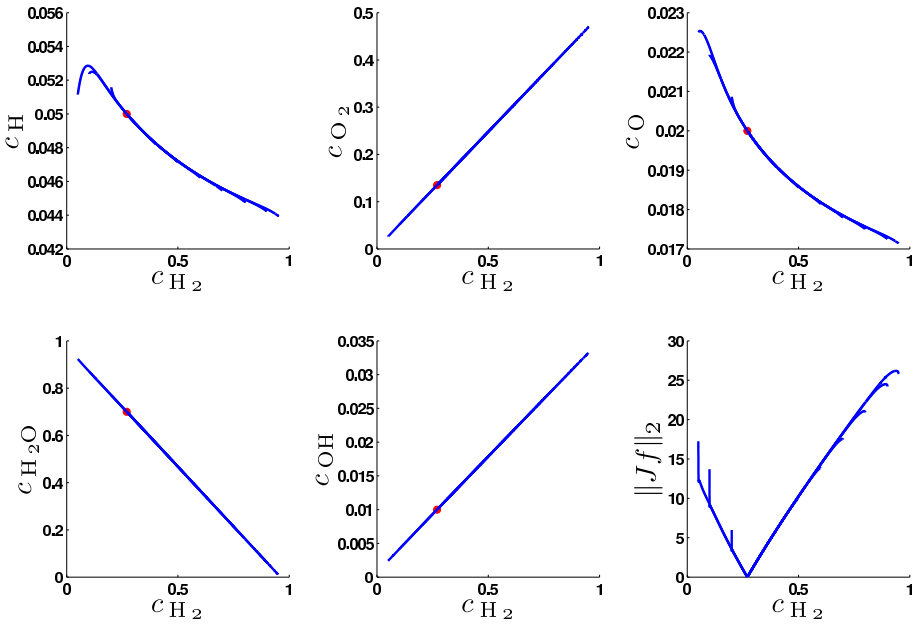

(b) H_2 as progress variable

Figure 6.19: Optimal trajectories as solutions of problem (6.28) with $\Phi = \|\ddot{c}\|_2$ and φ from (6.29) for different progress variables (H_2O and H_2). Trajectories form an excellent approximation of the SIM. A small remaining deviation is visible for the bottom right plot of curvature in (a) and for some plots of species in (b).

Additionally, using this strategy good results can also be achieved for different scenarios. For example Figure 6.19(b) shows that even for a change of the progress variable the solutions to problem (6.28) still result in a good approximation of the SIM. The same problem (i.e. solve (6.28) with $\Phi = \|\ddot{c}\|_2$ and $\varphi(c(0)) = \|\dot{c}(0)\|_2$) has been treated for these results, except that instead of initial concentrations of H_2O, initial concentrations of H_2 have been fixed – i.e. $c_{H_2}(0) \in \{0.05, 0.1, 0.2, 0.4, 0.5, 0.6, 0.7, 0.8, 0.9, 0.95\}$. Note that in Figure 6.19(b) the axes have been chosen according to the modified choice of the progress variable.

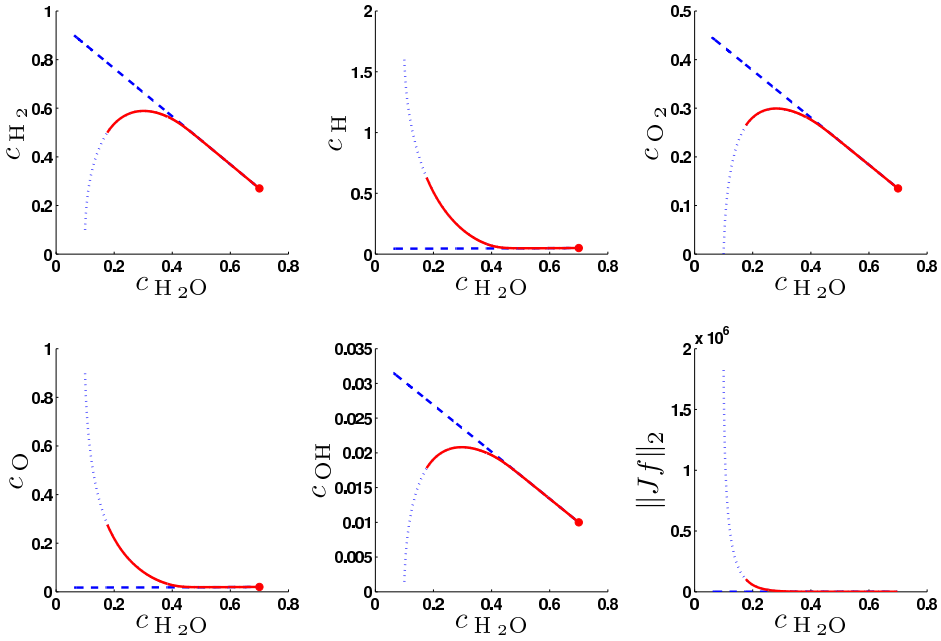

Figure 6.20: Optimal trajectories as solutions of problem (6.28) with $\Phi = \|\ddot{c}\|_2$ and φ from (6.29). Dashed lines denote the solution for only H_2 as a progress variable ($c_{H_2}(0) = 0.9$), dotted lines the solution for $c_{H_2}(0) = c_{H_2O}(0) = 0.1$ and solid red lines the solution for initial values of H_2 and H_2O taken from the dotted trajectory. These results demonstrate an excellent approximation of the two-dimensional SIM by the additive initial value term approach.

Moreover, solving problem (6.28) with $\Phi = \|\ddot{c}\|_2$ and φ from (6.29) also gives an excellent approximation of a SIM of dimension two. As a demonstration of this, the results depicted in Figure 6.20 have been computed in the following fashion:
First a solution of (6.28) has been computed for the initial values of H_2 and

H_2O set to 0.1 (blue dotted line). An arbitrary point from this solution (i.e. $c(t_1)$ for an arbitrarily t_1) has been chosen and the concentrations $c_{H_2}(t_1)$ and $c_{H_2O}(t_1)$ have been chosen as new initial values for H_2 and H_2O. For these new initial values, a new solution of (6.28) has been computed (red solid line). The one-dimensional SIM (blue dashed line) (for $c_{H_2}(0) = 0.9$) is included in Figure 6.20 for comparison.
In other words, the idea of the consistency property from Definition 5.1 has been analyzed for a two-dimensional case and the results underline that the criterion chosen in (6.28) with $\Phi = \|\ddot{c}\|_2$ and φ from (6.29) is very close to being consistent as judged by eye-inspection for the two-dimensional case.

6.2.4 Discussion

The aim of Section 6.2 was a detailed overview over different relaxation criteria and their modifications with the ultimate goal of finding a (possibly universal) criterion that satisfies the consistency property from Definition 5.1. Although no general relaxation criterion satisfying this property is found, some trends can be seen from the results presented here.
As a general trend it can be stated that criteria based on curvature as introduced in Subsection 5.2.2 seem to be more successful than those based on entropy production as introduced in Subsection 5.2.1 or arc length as introduced in Subsection 5.2.3.
The minimization of curvature without any modifications (see Figure 6.8) already shows results that are closer to the SIM than nearly any result based on minimizations of modified entropy production. However, there is one exception – the minimization of entropy production parametrized by a progress-variable-dependent arc length in a different metrics (see Figure 6.15). While this seems complicated at first sight, the idea of including a dependence on the parametrization of the SIM in the minimization (e.g. via a weighting function $g(c(t))$) is an idea that is worth to be pursued in the future. The main advantage is that relaxation criteria based on this idea need not include derivatives of the reaction rates as the curvature minimization does.
For the curvature minimization, two basic directions for modifications have been inspected – a change of the metric and the addition of an optimization objective for the initial point – both with encouraging results.
While the entropy production metric, introduced and successfully used for a two-dimensional manifold in [97], does not seem to help in the one-dimensional case, minimizing curvature in the Shahshahani metric leads to an improved approximation of the SIM in the one-dimensional case as seen in Figure 6.17. The use of different metrics in the formulation of curvature certainly seems to be a promising way of improving the curvature minimization

criterion. However, the search for an "optimal geometry" in phase-space of chemical reaction mechanisms (and in other settings, too) remains an open question for future work.
The most encouraging result in this work probably is the inclusion of an additive initial value term in the formulation of curvature minimization – i.e. the modified problem (6.28). The results achieved with this strategy are depicted in Figures 6.19 and 6.20 and show a very good approximation for the SIM for different choices of progress variables and manifold dimensions. It also has to be noted that preliminary tests of the combination (6.28) with $\Phi = \|\ddot{c}\|_2$ and φ from (6.29) with other systems (e.g. the Skodje-Davis problem) do not give results of the same quality as the ones presented here for the model hydrogen combustion mechanism. Nevertheless, the general strategy of adding an initial value optimization term to the trajectory-based optimization approach seems promising, which is confirmed by the results for the ozone combustion reaction mechanism in Subsection 6.3.2.

6.3 Temperature Dependence

The results in the previous sections have been achieved with model reaction mechanisms that did not include any temperature dependence. The focus of this section lies on detailed chemical reaction mechanisms that include temperature dependence in terms of the Arrhenius law (see Section 3.3).

6.3.1 Short Integration Horizon

To demonstrate the capability of the general trajectory-based optimization approach, a detailed reaction mechanism including temperature dependence is investigated here. The mechanism for ozone combustion consists of three species and one conservation relation and therefore has two degrees of freedom. Hence the investigation is based on a reduction to a one-dimensional manifold only. Details on the reaction mechanism are found in A.3.
The methodology used for the approximation of the SIM here is based on the curvature minimization idea and the unit-speed parametrization. However, instead of integrating the system for a fixed time horizon, a fixed arc length is chosen.
There are two general ideas how to achieve this. One way is to introduce an additional differential state $\frac{\mathrm{d}s}{\mathrm{d}t} = \|f(c)\|$ to the original problem formulation along with two equality constraints $s(0) = 0$ and $s(T) = s^{\mathrm{f}}$.
However, a more convenient way might be to replace the governing ODE $\dot{c}(t) = f(c)$ by a "normalized" version $\dot{c} = \frac{f(c)}{\|f(c)\|}$, whose solutions are curves

in unit-speed parametrization.

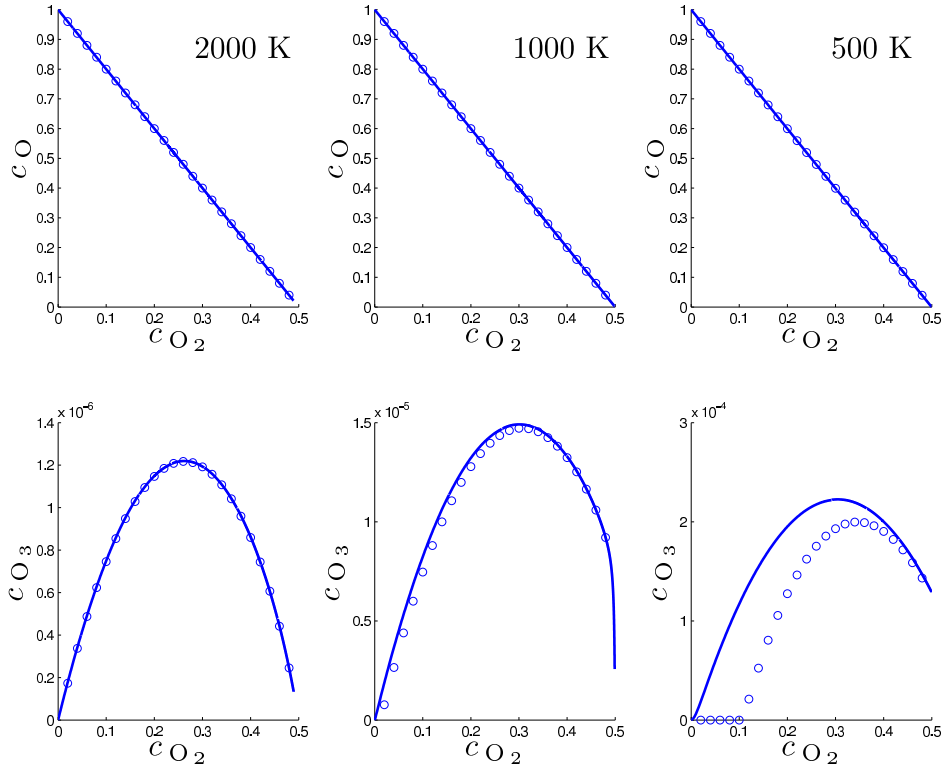

Figure 6.21: Ozone mechanism at three different temperatures, 2000 K, 1000 K and 500 K with the relaxation criterion $\Phi = \|\ddot{c}\|_2$. The solid lines depict the trajectory computed from the initial values of the solution of (6.30) for $c_{\mathrm{O}_2}(0) = 10^{-4}$. The dots correspond to the initial values of solutions of (6.30) on an equidistant grid. Deviations from the SIM are found away from equilibrium for 1000 K and 500 K.

The reparametrized problem is then written as

$$\min_{c_k} \int_0^{s^{\mathrm{f}}} \Phi(c(s))\mathrm{d}s \tag{6.30a}$$

subject to

$$\frac{\mathrm{d}c_k}{\mathrm{d}s} = \frac{f_k(c)}{\|f(c)\|}, \qquad k = 1, ..., n \tag{6.30b}$$

$$c_k(0) = c_k^0, \qquad k \in I_{\mathrm{fixed}}. \tag{6.30c}$$

Note that in this formulation t and T have been replaced by s and s^{f}, representing the arc length of the trajectory. It turns out, that short trajectory

pieces $c(s)$, $s \in [0, s^{\mathrm{f}}]$ are sufficient for the optimizer to find accurate reduced descriptions. s^{f} is generally chosen as 10^{-3} in this section.

The optimization criterion Φ is chosen as curvature $\|J(f(c))f(c)\| = \|\ddot{c}\|$. Note that the derivative $\ddot{c} = \frac{\mathrm{d}^2 c}{\mathrm{d}t^2}$ is taken w.r.t. time. Figure 6.21 shows results for the minimization of curvature by solving problem (6.30).

There the solid line depicts a trajectory integrated from the initial values of a solution of problem (6.30) for $c_{\mathrm{O}_2}(0) = 10^{-4}$ and the circles denote initial values from solutions of problem (6.30) on an equidistant grid for the fixed initial values $c_{\mathrm{O}_2}(0)$ with a spacing of 0.02. The results at 2000 K look very promising, all computed points share the same trajectory, suggesting that the consistency property is fulfilled. However, this is not the case for lower temperatures. This can be seen in the plots for 1000 K and 500 K in Figure 6.21, where the initial values from the solutions of (6.30) show deviations from the SIM especially further away from equilibrium.

However, similar to the previous sections, curvature in a special metric can again be used to improve these results. In this case

$$\Phi(c) = \|\ddot{c}\|_D \tag{6.31}$$

is chosen with the positive definite matrix

$$D = \mathrm{diag}\,(d_{kk})\,,\ d_{kk} = \frac{\|f\|}{\|f_k\|}. \tag{6.32}$$

Similar to the entropy production metric from (5.12), this modified metric yields a kinetic weighting. While the choice of the matrix D is to some extent heuristic, the results for this optimization – given in Figure 6.22 – clearly suggest that the consistency property is also fulfilled for the lower temperature values 1000 K and 500 K. With this the successful application of the chosen approach using the metric $\|.\|_D$ with D from (6.32) for a wide range of different temperatures seems to be possible at least for the given mechanism.

Nevertheless, a drawback of this optimization strategy also has to be mentioned: Due to the small integration horizons, the strategy is highly dependent on good initial values and hence also depends on a good numerical continuation strategy.

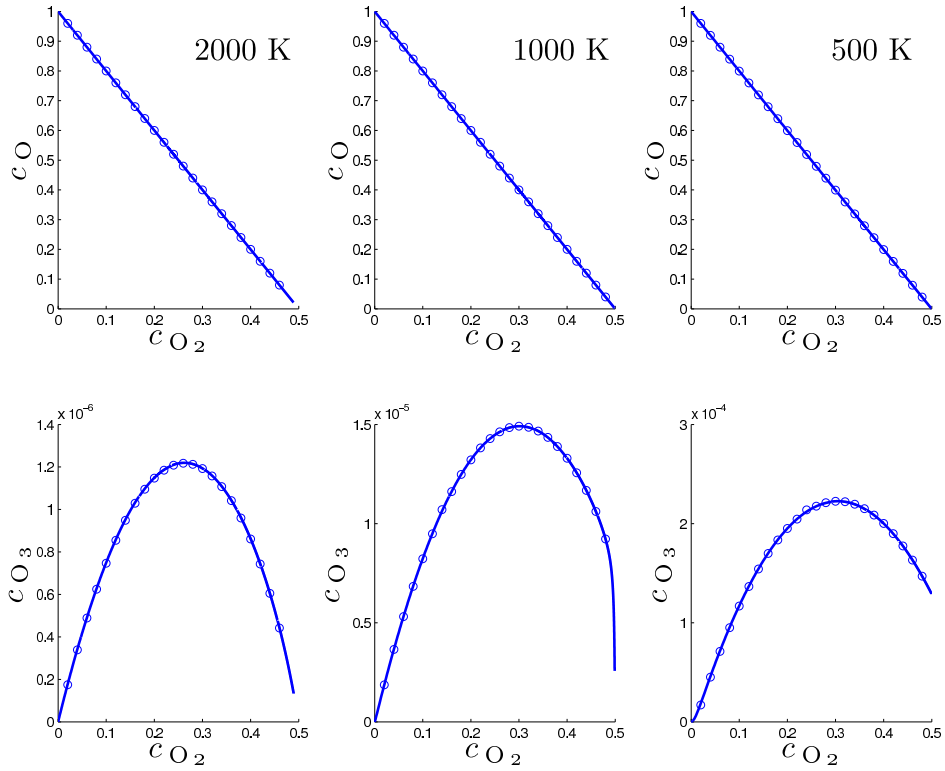

Figure 6.22: Ozone mechanism at three different temperatures, 2000 K, 1000 K and 500 K with the relaxation criterion $\Phi = \|\ddot{c}\|_D$ and D from (6.32). The solid lines depict the trajectory computed from the initial values of the solution of (6.30) for $c_{\mathrm{O}_2}(0) = 10^{-4}$. The dots correspond to the initial values of solutions of (6.30) on an equidistant grid. Deviations from the SIM are not visible.

6.3.2 Additive Initial Value Term Strategy

In Subsection 6.2.3 the modified problem formulation (6.28) was used, that includes an additive initial value term. In this subsection the same strategy is used for the computation of optimal trajectories for the ozone combustion reaction mechanism from A.3 that has also been used in the previous subsection. Note that this means that as opposed to the results in Subsection 6.3.1, the ODE is written in its standard (time-parametrized) formulation again and the integration horizon $[0, T]$ is chosen such that $c(T)$ is approximately the equilibrium concentration. For the computations in this Subsection, $T = 0.1$ has been chosen.

As in Subsection 6.2.3, $\Phi(c(t)) = \|\ddot{c}(t)\|_2$ and $\varphi(c(0)) = \|\dot{c}(0)\|_2$ are used.

Having all this, the results depicted in Figures 6.23 and 6.24 are computed as solutions of

$$\min_{c_k} \int_0^T \|\ddot{c}(t)\|_2 \, \mathrm{d}t - \|\dot{c}(0)\|_2 \tag{6.33a}$$

subject to

$$\frac{\mathrm{d}c_k}{\mathrm{d}t} = f_k(c), \qquad k = 1, ..., n \tag{6.33b}$$

$$c_k(0) = c_k^0, \qquad k \in I_{\text{fixed}} \tag{6.33c}$$

$$c_{\mathrm{O}} + 2c_{\mathrm{O}_2} + 3c_{\mathrm{O}_3} = C. \tag{6.33d}$$

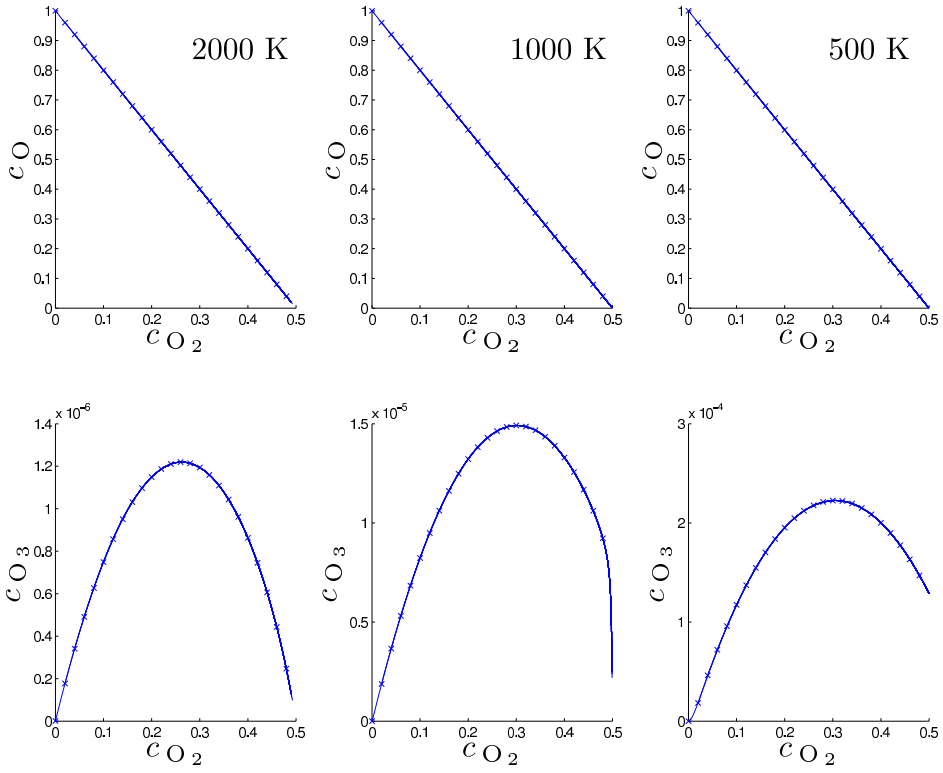

Figure 6.23: Solution of the additive initial value term problem (6.33) for the ozone reaction mechanism from A.3 at three different temperatures, 2000 K, 1000 K and 500 K. Crosses denote initial points of computed trajectories. All trajectories emanating from these points are plotted and approximately lie on the same manifold which is expected to be the SIM.

In other words, the results depicted in Figures 6.23 and 6.24 are *trajectories* (and their initial values, marked by crosses) that are computed as optimal

solutions of problem (6.33) while the results depicted in Figures 6.21 and 6.22 are *initial points* of small trajectory pieces.
The results depicted in Figure 6.23 demonstrate that the additive initial value strategy – successfully applied to the model hydrogen combustion mechanism in Subsection 6.2.3 – also yields very good results for the ozone combustion reaction mechanism for different temperatures. The trajectories depicted in the figures in this subsection are computed on the same grid for the progress variable O_2 as used for the results in Subsection 6.3.1 and the initial values of these trajectories are marked by crosses. For the temperatures 500 K, 1000 K

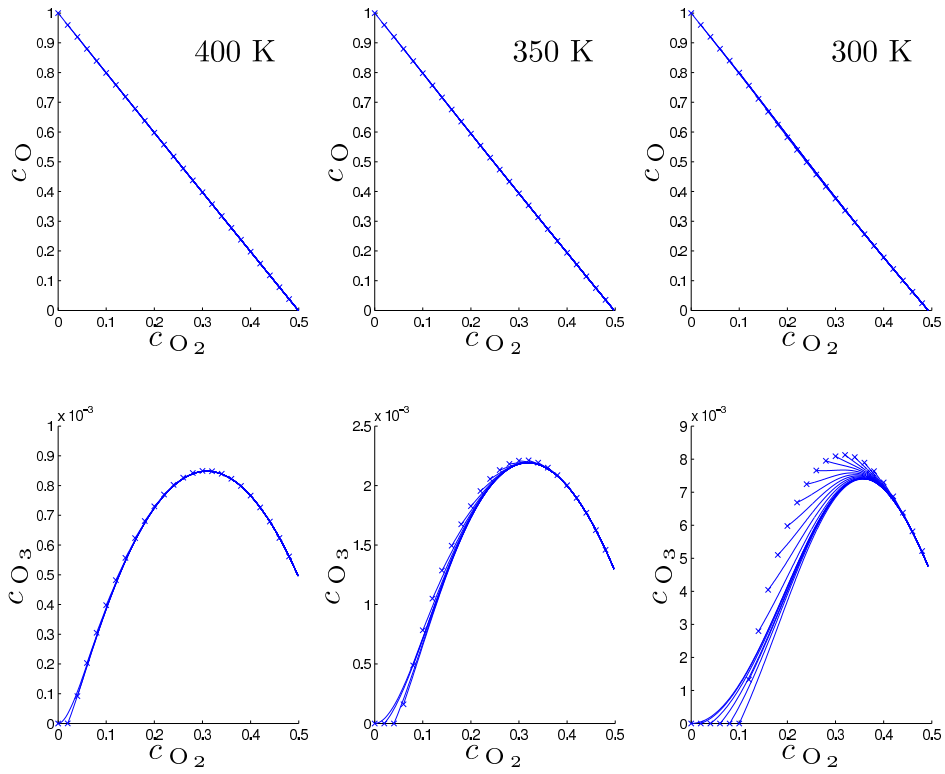

Figure 6.24: Solution of the additive initial value term problem (6.33) for the ozone reaction mechanism from A.3 at three different temperatures, 400 K, 350 K and 300 K. Crosses denote initial points of computed trajectories. All trajectories emanating from these points are plotted, growing deviations from the SIM are observed for decreasing temperature.

and 2000 K the resulting trajectories are found to satisfy the consistency property by eye-inspection. The results for these temperatures are depicted in Figure 6.23.

However, if the temperature is decreased to 400 K and below, deviations from the SIM are found for the progress variable concentrations further away from equilibrium. These deviations can be observed in the results depicted in Figure 6.24 especially for the solutions of (6.33) for 300 K – a condition which states a strong demand for all model reduction techniques, as it amounts to approximately 27°C. At such low temperatures the chemical kinetics are extremely slow and a clear separation of time-scales can not be guaranteed. While the results in Figure 6.24 question the generality of using problem (6.33) to approximate the SIM for all temperatures, a wide range of temperatures for which the consistency property is observed to be satisfied is found in Figure 6.23. Together with the promising results presented in Subsection 6.2.3, the results depicted in Figure 6.23 demonstrate the potential of the additive initial value term strategy for the approximation of the SIM.

6.4 Large-Scale Mechanisms

The mechanism in A.4 is a realistic reaction mechanism for the combustion of hydrogen in pure oxygen consisting of 8 species and 60 reactions. Compared to the other test-cases used in this work, this hydrogen combustion mechanism provides a substantial step towards large-scale application of the methods derived in this work.

No results as solutions of optimization problems are presented in this work for this mechanism, but some statements on trajectories shall be made here. These statements may be of importance for the transfer of the methods derived in this work to realistic large-scale reaction mechanisms. The insight given here is illustrated by the trajectories in Figure 6.25.

Three trajectories are displayed in this figure. The first one (solid blue, c^1) starts from the initial point where only the reactants H_2 and O_2 have a non-zero concentration ($c_{H_2}(0) = \frac{1}{6}$, $c_{O_2}(0) = \frac{1}{3}$).

The second trajectory (dashed blue, c^2) starts from the point where the initial concentrations $(c_H(0), c_O(0), c_{OH}(0), c_{HO_2}(0), c_{H_2O_2}(0), c_{O_2}(0), c_{H_2}(0), c_{H_2O}(0))$ are $(.441, .217, 6 \times 10^{-3}, 10^{-5}, 5 \times 10^{-5}, .05, .1, .01)$. This point is chosen arbitrarily but consistent with the conservation equations (A.8) and (A.9) with $C_1 = \frac{2}{3}$ and $C_2 = \frac{1}{3}$. The third trajectory (solid red, c^3) is the part of the first trajectory that can be interpreted as a part of the one-dimensional SIM*.

In the computations performed in this work, the Lagrange-type optimization criterion usually has been included in the ODE system as an additional state,

*Remember that all trajectories relax towards the one-dimensional SIM and hence there exists a point in time t_0 from which on the curve $c(t)$, $t \in [t_0, T]$ is reasonably close to the one-dimensional SIM.

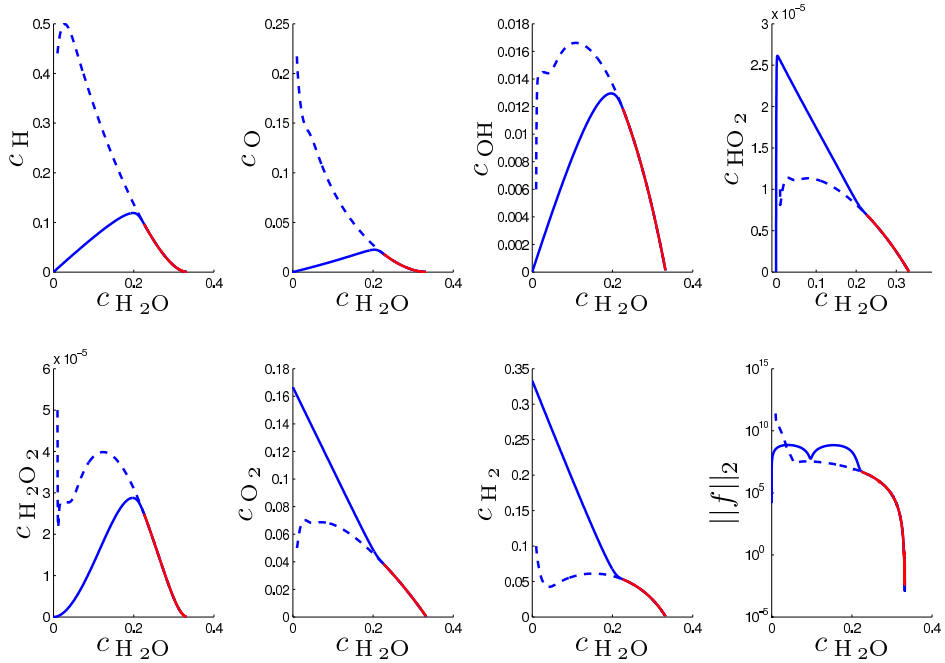

Figure 6.25: Three different trajectories for the detailed hydrogen mechanism from A.4 at 1500 K. The solid blue and dashed blue lines denote trajectories (c^1 and c^2 respectively) from arbitrary initial values consistent with the conservation relations. The red line (c^3) can be interpreted as a part of the one-dimensional SIM.

i.e.

$$\begin{aligned} \dot{c}(t) &= f(c(t)) \\ \dot{m}(t) &= \Phi(c(t)), \end{aligned} \tag{6.34}$$

with $m(0) = 0$.

If this procedure is applied to the eight species reaction mechanism, some difficulties arise.

The number of time steps and minimal time step for the solution of the original ODE system $\dot{c} = f(c)$ using a standard integrator (`ode15s`) from MATLAB® are shown in Table 6.1.

Integrating (6.34) with the same integrator as the ODE system, about ten times as many time steps and minimum time steps occur that are smaller by a factor of 10^{-3}. The detailed results of these integration are shown in Table 6.2.

In particular the fact that even the integration of the (non-stiff) SIM (solid red line) needs so many timesteps causes concern. However, if trajectories are

Trajectory	Time Steps	Minimal Time Step
c^1	632	2.6832×10^{-7}
c^2	674	8.1777×10^{-11}
c^3	396	1.8600×10^{-8}

Table 6.1: Number of time steps and minimal time step for the integration of $\dot{c}(t) = f(c(t))$.

Trajectory	Time Steps	Minimal Time Step
c^1	6577	2.4269×10^{-10}
c^2	5641	1.0224×10^{-14}
c^3	5358	4.1808×10^{-11}

Table 6.2: Number of time steps and minimal time step for the integration of (6.34).

computed as solutions of the original ODE $\dot{c} = f(c)$ only and the relaxation criterion is evaluated along these trajectories, the accuracy of the computed trajectories may be to low for an accurate evaluation of the relaxation criterion. These inaccuracies in the evaluation of the relaxation criterion may in turn lead to problems in the optimization. An alternative optimization strategy for large-scale problems avoiding these integration difficulties may be found using a fixed discretization of the trajectories (possibly in terms of an arc length parametrization) within a collocation method (see [86, p. 595]).

Chapter 7

Summary, Conclusion and Outlook

7.1 Summary

This work deals with the problem of model reduction in chemical kinetics. The main task of model reduction is the provision of low-dimensional descriptions of high-dimensional systems for the efficient application within computationally demanding multi-scale numerical simulations. In the context of this work the systems to be reduced are dissipative systems described by Ordinary Differential Equation (ODE) systems. Due to their dissipative nature, phase trajectories in these systems tend to relax to invariant manifolds of decreasing dimension, the so-called Slow Invariant Manifolds (SIM) and finally to equilibrium, which can be interpreted as a zero-dimensional Slow Invariant Manifold (SIM). These SIMs can be employed for model reduction as they are parametrized by a small number of parameters – the so-called progress variables, which are often chosen as certain species concentrations – but contain information about the long-term behaviour of all species present in the system. Therefore most modern model reduction methods are based on computing approximations of these SIMs.

For this purpose a novel approach introduced by Lebiedz [50] for the approximation of SIMs is pursued and examined for increasingly realistic reaction mechanisms and higher-dimensional manifolds in this work. The basis for this approach is the computation of optimal trajectories via suitable optimization criteria that can be achieved by sophisticated numerical tools. Methodologically the optimization criteria are supposed to describe the extent of relaxation, as trajectories on the SIM can be interpreted as "maximally relaxed" trajectories.

Mathematically, the basis for this novel model reduction approach is its formulation as a variational Boundary Value Problem (BVP), introduced in Chapter 5 and its solution via a Nonlinear Programming Problem (NLP) formulation. The tools for the solution of the variational BVP – which are discussed in Chapter 4 – are based on a direct multiple shooting discretization [7, 8] that subdivides the integration horizon into several subintervals on each of which an independent Initial Value Problem (IVP) is solved. The resulting NLP is then solved by Sequential Quadratic Programming (SQP), a standard approach for such problems. As the underlying ODE systems in this work are usually stiff systems (for the description of chemical kinetics), the IVPs are integrated using the implicit Differential Algebraic Equation (DAE) solver DAESOL [2, 4, 5] which is integrated in the software package MUSCOD-II [54, 55, 56, 57] that is used to solve the variational BVP.

For the construction of invariant manifolds of dimension $n > 1$, the general trajectory-based optimization approach has to be formulated as a parametrized problem family with the different initial concentrations parametrizing the manifold.For this formulation, an efficient initial value embedding strategy can be applied, which has been used before for Nonlinear Model-Predictive Control (NMPC) [20, 21]. Using this initial value embedding strategy, neighbouring problems can be solved efficiently, leading to a powerful continuation strategy for the construction of low-dimensional manifolds.

Using this numerical optimization framework, this work presents the approximation of SIMs by the means of minimizing different criteria describing the relaxation of chemical forces. The original criterion – entropy production – is fundamentally rooted in the field of thermodynamics. However, as it turns out that the minimization of entropy production along trajectories is not sufficient, Chapter 5 and 6 of this work focus on the derivation of alternative criteria to be used in the context of the trajectory-based optimization approach and on the introduction of a kinetic weighting in these criteria. The aim of these considerations is to improve the approximations of the SIM achieved with these criteria.

For this purpose, a qualitative way of evaluating the performance of the criteria is introduced in Section 5.2 – the consistency property. This property allows for the analysis of different criteria by eye-inspection, a path that has been followed in Section 6.2. The results presented in that section demonstrate the potential of the trajectory-based optimization approach, especially if curvature in a modified metric formulation* is used as the relaxation criterion. Apart from analyzing different criteria and kinetic weightings, a modification of the original optimization approach is presented in Subsection

*The modified metric formulations represent one possibility of a kinetic weighting.

6.2.3. This approach, which introduces an additive term that is evaluated at the initial point of the integration horizon, leads to very promising results for the mechanism discussed in that subsection. These results demonstrate that a very good approximation of the SIM is possible via trajectory-based optimization.

7.2 Conclusion

As alternative approaches to model reduction exist which are introduced in Chapter 2, two concluding questions shall be addressed here:

- How can the approach presented in this thesis be compared to other approaches?
- Why is the presented approach reasonable?

The overview of model reduction algorithms in Chapter 2 shows that many modern model reduction methods are based on finding or approximating slow invariant manifolds, which is a point that is shared by the trajectory-based optimization approach proposed in this thesis. In fact, the only (modern) approach presented here that does not rely on the computation or approximation of invariant manifolds is the RCCE method discussed in 2.1.4.
Instead the RCCE method locally reconstructs predefined minor species by locally maximizing entropy for fixed concentrations of the major species. The original MEPT method follows a similar idea by the minimization of an integral over entropy production.
However, the pointwise maximization of entropy bears the same problems as the initial phase of original minimal entropy production trajectories. The maximum entropy compositions do not lie close to the slow invariant manifold. Hence the RCCE method will, in general, only provide good results when the concentrations of the progress variables are close to their equilibrium values. For the original MEPT method this problem can at least be attenuated by starting trajectories from the boundary of a predefined computational domain and combining them to an invariant manifold.
This construction of a manifold from trajectories emanating from the boundary of a predefined computational domain is the exact idea of the ICE-PIC method. A manifold created like this is at least invariant by definition, as it consists of trajectories.
Nevertheless, an invariant manifold is not necessarily the Slow Invariant Manifold. Basing the manifold generation on trajectories serves for invariance, finding the SIM itself is usually more complicated. Iterative methods

have been introduced for this task and are discussed in Chapter 2. An interesting similarity of ideas can be found in the Constrained Runs Schemes, where the $m + 1^{\text{st}}$ time derivative of the free variables is computed to be zero. For $m = 1$, this idea (although applied locally) is conceptually close to the curvature minimization presented in this work as the same directional derivatives occur in this context.
Summarizing the findings, it is clear that the approach pursued in this work shares some ideas with other model reduction approaches, but is unique in its idea of optimizing trajectories in such a way that the resulting trajectories approximate the SIM. With this optimization – based on sophisticated numerical tools – the approach bears potential to overcome at least some of the drawbacks of other approaches for the approximation of slow invariant manifolds in chemical kinetics for the purpose of model reduction.

7.3 Outlook

While substantial steps towards the generalization of trajectory-based optimization for model reduction have been taken within the scope of this work, future work may include the further optimization of relaxation criteria as well as the implementation of these methods for large-scale automatic model reduction. Some issues that may be of importance for these future developments are discussed in this section.

7.3.1 Criteria and Evaluation

In Chapter 5, three important criteria for the reduction of chemical reaction mechanisms via optimization of trajectories have been presented: entropy production, curvature of trajectories and length of trajectories – in a suitable metric.
In principle other reduction criteria are conceivable. Lemma 3.18, for example, relates the volume of the phase space to the divergence of the r.h.s. of the ODE-system. This relationship can also form an important background to a successful model reduction criterion, as the phase space volume is related to the dissipativity of the underlying system by Definition 3.17. One problem of this formulation is the integration of the divergence over a domain as opposed to a pure time integration.
Apart from choosing different reduction criteria, modifications of these criteria as e.g. a kinetic weighting can enhance the quality of the resulting reduced models. For example the velocity weighting that has been used e.g. for the results in Figure 6.3 can be interpreted as a modification of a given reduc-

tion criterion (here: entropy production). By the implementation of time transformations the same idea can also be directly applied to the differential equation system: conceptually, transforming the standard time t to a new time variable τ

$$\tau = \frac{t}{\|f(t)\|} \tag{7.1}$$

can be achieved by a normalization of the ODE system

$$\dot{c} = \frac{f(c)}{\|f(c)\|} \tag{7.2}$$

and if now the original (time-dependent) relaxation criterion is minimized subject to this normalized ODE system, the same velocity weighting as used in Chapter 6 is achieved. [39] uses similar methods to transform systems in a way that allows for the use of constant step-size methods for the solution of ODE systems.
While a unit-speed parametrization of the solutions of the ODE system is appealing for a trajectory-based method, problems arise by the singularity of the equilibrium point. A method making use of the normalized ODE system (7.2) has to be constructed in such a way that it avoids integration horizons that are too large. First steps into this direction have been taken for the results in Section 6.3.1.

7.3.2 Practical Issues

To make the methods developed in this work available for large-scale automatic model reduction of chemical reaction mechanisms in combustion, some further steps have to be taken. This subsection focuses on key issues on the way towards an automatic large-scale model reduction method based on the optimization of trajectories.

Automatic Model Reduction

For applications the automatization of a model reduction method is of particular importance. The aim of automatic model reduction is to provide reduced descriptions of reaction mechanisms based on as little input of the user as necessary. Generally, the user will supply a mechanism file and the physical conditions for which a reduced description shall be computed.

Mechanism Parser A mechanism parser is necessary for the conversion of large amounts chemical data to the right hand side of an autonomous ODE as (3.1).

The Arrhenius parameters A, b, E_a from (3.25) which determine the chemical source terms for an elementary reaction are generally stored in reaction mechanism files. Along with thermodynamical and molecular data, these parameters determine the reaction velocity for elementary reactions.

Parametrization by Chemical Properties Large scale model reduction tables of reduced chemistry can – in addition to the parametrization by reaction progress variables – also be parametrized by chemical properties. In practice, this parametrization leads to additional tabulation axes. The most common properties used for tabulation are temperature, pressure and mixture fraction (fuel-to-oxidizer ratio).
In the context of the method proposed in this work, these parameters generally enter the problem formulation (5.1) as equality constraints

$$\begin{aligned} T &= p_{\mathrm{T}}. \\ \mathrm{p} &= p_{\mathrm{p}} \\ \xi &= p_{\xi}, \end{aligned} \tag{7.3}$$

i.e. an additional parameter p_{T}, p_{p} or p_{ξ} enters the parametric optimization family of variational boundary value problems, for the parametrization by temperature, pressure and mixture-fraction respectively.
The only difference for the parametrization by pressure as opposed to the parametrization by temperature lies in the reaction mechanism parser, which is required to be able to treat pressure-dependent reactions, e.g. by the Troe formalism from [29, 87].
The mixture fraction parametrization is a way to express changes in the systems element composition (e.g. in the constants C_1 and C_2 of the conservation laws of the mechanisms in Sections A.2 and A.4) in one parameter, the fuel-oxidizer-ratio. This expression is possible if the configuration under consideration can be treated as coflow between fuel and oxidizer as e.g. for simple nonpremixed flames. The fuel-oxidizer-ratio is commonly written as the mixture fraction ξ, which is defined as

$$\xi = \frac{Z_i - Z_{i2}}{Z_{i1} - Z_{i2}}, \tag{7.4}$$

where

$$Z_i := \sum_{j=1}^{S} \mu_{ij} w_j \tag{7.5}$$

is the element mass fraction of the i-th element, computed as the sum of the species mass fractions w_j, weighted by μ_{ij}, the mass proportion of the

element i in species j. Z_{i1} and Z_{i2} denote the element mass fractions of the two streams. For equal diffusivities the mixture fraction is independent of the choice of the element $i, i = 1, ..., M$. More details on the mixture fraction parametrization can be found for example in [95].

Fast Manifold For practical computational fluid dynamics simulations, transport processes drive the physical states away from those on the SIM. Hence, not only the SIM itself is needed there, but also a way of projecting states back on the SIM (see [83]). In [11], Bykov et al. present a method suitable for these projections, if the directions of fast motion towards the SIM are known. It is conceivable that this method can be coupled with the method derived in this work if a trajectory-based optimization approach can be modified in such a way that the fast directions are computed.

Large-Scale Model Reduction

A method that is suitable for large-scale model reduction needs to be able to compute reduced descriptions for a large set of parameters in as little time as possible. Good strategies for continuation, storage and parallelization of the computation of reduced descriptions can help to achieve this goal.

Continuation A continuation strategy for trajectory-based model reduction is described in [73] and in this work, Section 5.1.2. As the basis of the model reduction approach lies in the optimization of trajectories, founding a continuation strategy in parametric optimization is self-evident.

Storage The efficient storage of computed manifolds is a field on its own that is not addressed here. However, it should be noted that in the presented approach one trajectory can serve as a representation for multiple points on the low-dimensional manifold.
For more details on the storage of tables of reduced chemistry, the reader is referred to [64, 71, 80].

Parallelization A parallelization strategy for the trajectory-based optimization approach can generally be similar to parallelization strategies used for the tabulation of ILDM-reduced chemistry, e.g. the parallelization proposed in [80]. There a master-slave approach is chosen – a master processor administers lists of already computed reduced descriptions and those parameter sets that have to be computed. The slave processors receive parameter sets and initial values from the master and carry out the actual computations

of single reduced descriptions. The storage of the table is also carried out by the master.

Appendix A

Test Problems and Reaction Mechanisms

A.1 The Davis-Skodje Problem

In [16], Davis and Skodje presented a test example for the generation of low-dimensional slow manifolds. This example, which has also been applied in [83] is particularly useful, as an exact slow manifold can be calculated for it. The model of a spatially homogeneous premixed reactor that consists of a two-dimensional system is given by

$$\begin{aligned} \frac{\mathrm{d}y_1}{\mathrm{d}t} &= -y_1 \\ \frac{\mathrm{d}y_2}{\mathrm{d}t} &= -\gamma y_2 + \frac{(\gamma-1)y_1 + \gamma y_1^2}{(1+y_1)^2}, \end{aligned} \tag{A.1}$$

where $\gamma > 1$ is a measure of stiffness for the system. Stiffness is increased by increasing γ.
The exact slow invariant manifold is given by

$$y_2 = \frac{y_1}{1+y_1} \tag{A.2}$$

and the system has a stable equilibrium point at $y_1 = y_2 = 0$.
Furthermore an analytical description of the ILDM (see Section 2.1.2) can be explicitly calculated as

$$y_2 = \frac{y_1}{1+y_1} + \frac{2y_1^2}{\gamma(\gamma-1)(1+y_1)^3} \tag{A.3}$$

for this system.

A.2 Model Hydrogen Combustion Mechanism

One mechanism used for the calculations in this work is the following six-species reaction mechanism

$$\begin{array}{lcll} \mathrm{H_2} & \overset{k_{\pm 1}}{\leftrightharpoons} & 2\,\mathrm{H}, & k_1 = 2.0, \quad k_{-1} = 216.0 \\ \mathrm{O_2} & \overset{k_{\pm 2}}{\leftrightharpoons} & 2\,\mathrm{O}, & k_2 = 1.0, \quad k_{-2} = 337.5 \\ \mathrm{H_2O} & \overset{k_{\pm 3}}{\leftrightharpoons} & \mathrm{H} + \mathrm{OH}, & k_3 = 1.0, \quad k_{-3} = 1400.0 \\ \mathrm{H_2} + \mathrm{O} & \overset{k_{\pm 4}}{\leftrightharpoons} & \mathrm{H} + \mathrm{OH}, & k_4 = 1000.0, \quad k_{-4} = 10800.0 \\ \mathrm{O_2} + \mathrm{H} & \overset{k_{\pm 5}}{\leftrightharpoons} & \mathrm{O} + \mathrm{OH}, & k_5 = 1000.0, \quad k_{-5} = 33750.0 \\ \mathrm{H_2} + \mathrm{O} & \overset{k_{\pm 6}}{\leftrightharpoons} & \mathrm{H_2O}, & k_6 = 100.0, \quad k_{-6} = 0.7714 \end{array} \tag{A.4}$$

or its kinetic model given by

$$\begin{aligned} \frac{\mathrm{d}c_{\mathrm{H_2}}}{\mathrm{d}t} &= -k_1 c_{\mathrm{H_2}} + k_{-1} c_{\mathrm{H_2}}^2 - k_4 c_{\mathrm{H_2}} c_{\mathrm{O}} + k_{-4} c_{\mathrm{H}} c_{\mathrm{OH}} \\ &\quad - k_6 c_{\mathrm{H_2}} c_{\mathrm{O}} + k_{-6} c_{\mathrm{H_2O}} \\ \frac{\mathrm{d}c_{\mathrm{H}}}{\mathrm{d}t} &= 2k_1 c_{\mathrm{H_2}} - 2k_{-1} c_{\mathrm{H_2}}^2 + k_3 c_{\mathrm{H_2O}} - k_{-3} c_{\mathrm{H}} c_{\mathrm{OH}} \\ &\quad + k_4 c_{\mathrm{H_2}} c_{\mathrm{O}} - k_{-4} c_{\mathrm{H}} c_{\mathrm{OH}} - k_5 c_{\mathrm{O_2}} c_{\mathrm{H}} + k_{-5} c_{\mathrm{O}} c_{\mathrm{OH}} \\ \frac{\mathrm{d}c_{\mathrm{O_2}}}{\mathrm{d}t} &= -k_2 c_{\mathrm{O_2}} + k_{-2} c_{\mathrm{O}}^2 - k_5 c_{\mathrm{H}} c_{\mathrm{O_2}} + k_{-5} c_{\mathrm{O}} c_{\mathrm{OH}} \\ \frac{\mathrm{d}c_{\mathrm{O}}}{\mathrm{d}t} &= 2k_2 c_{\mathrm{O_2}} - 2k_{-2} c_{\mathrm{O}}^2 - k_4 c_{\mathrm{H_2}} c_{\mathrm{O}} + k_{-4} c_{\mathrm{H}} c_{\mathrm{OH}} \\ &\quad + k_5 c_{\mathrm{H}} c_{\mathrm{O_2}} - k_{-5} c_{\mathrm{O}} c_{\mathrm{OH}} - k_6 c_{\mathrm{H_2}} c_{\mathrm{O}} + k_{-6} c_{\mathrm{H_2O}} \\ \frac{\mathrm{d}c_{\mathrm{H_2O}}}{\mathrm{d}t} &= -k_3 c_{\mathrm{H_2O}} + k_{-3} c_{\mathrm{H}} c_{\mathrm{OH}} + k_6 c_{\mathrm{H_2}} c_{\mathrm{O}} - k_{-6} c_{\mathrm{H_2O}} \\ \frac{\mathrm{d}c_{\mathrm{OH}}}{\mathrm{d}t} &= k_3 c_{\mathrm{H_2O}} - k_{-3} c_{\mathrm{H}} c_{\mathrm{OH}} + k_4 c_{\mathrm{H_2}} c_{\mathrm{O}} - k_{-4} c_{\mathrm{H}} c_{\mathrm{OH}} \\ &\quad + k_5 c_{\mathrm{H}} c_{\mathrm{O_2}} - k_{-5} c_{\mathrm{O}} c_{\mathrm{OH}}. \end{aligned} \tag{A.5}$$

Together with the conservation relations

$$\begin{aligned} 2\,c_{\mathrm{H_2}} + 2\,c_{\mathrm{H_2O}} + c_{\mathrm{H}} + c_{\mathrm{OH}} &= C_1 \\ 2\,c_{\mathrm{O_2}} + c_{\mathrm{H_2O}} + c_{\mathrm{O}} + c_{\mathrm{OH}} &= C_2 \end{aligned} \tag{A.6}$$

this mechanism yields a system with four degrees of freedom.
For the results in Section 6.1.1 and 6.1.2 computed for this mechanism $C_1 = 2.0$ and $C_2 = 1.0$ have been chosen.

A.3 Detailed Ozone Combustion Mechanism

The following mechanism from [61] is a small, but realistic reaction mechanism for the combustion of ozone. The Arrhenius parameters are given in Table A.1.

Reaction			A [cm, mol, s]	b	E_a [$\frac{kJ}{mol}$]
$O + O + M$	$\rightarrow$	$O_2 + M$	2.9×10^{17}	-1.0	0.0
$O_2 + M$	$\rightarrow$	$O + O + M$	6.81×10^{18}	-1.0	496.0
$O_3 + M$	$\rightarrow$	$O + O_2 + M$	9.5×10^{14}	0.0	95.0
$O + O_2 + M$	$\rightarrow$	$O_3 + M$	3.32×10^{13}	0.0	-4.9
$O + O_3$	$\rightarrow$	$O_2 + O_2$	5.2×10^{12}	0.0	17.4
$O_2 + O_2$	$\rightarrow$	$O + O_3$	4.27×10^{12}	0.0	413.9

Table A.1: Ozone Combustion Mechanism from [61]. Rate coefficient $k = AT^b \exp(-E_a/RT)$. Collision efficiencies in reactions including M: $f_O = 1.14$, $f_{O_2} = 0.40$, $f_{O_3} = 0.92$.

Together with the element conservation law

$$c_O + 2c_{O_2} + 3c_{O_3} = C, \tag{A.7}$$

this mechanism yields a system with two degrees of freedom. Without loss of generality, $C = 1$ can be chosen.

A.4 Detailed Hydrogen Combustion Mechanism

The reaction mechanism presented here consists of 8 species and 60 reactions (counting both forward and reverse reactions as well as counting third-body reactions as three reactions – once for each third-body). In Table A.2, the Arrhenius parameters A, E_a, b are shown for the forward reactions only. The parameters for the reverse reactions can be computed as follows: For two different temperatures T_1, T_2, the equilibrium constant $K(T)$ is computed by (3.39). Using (3.20), the equations

$$k_i^{(r)} = \frac{k_i^{(f)}}{K(T_i)}, \qquad i = 1, 2$$

are obtained. As b is identic for the forward and reverse reaction, these equations state a two-dimensional equation system with two unknowns.

Reaction			A [cm, mol, s]	b	E_a [$\frac{kJ}{mol}$]
$H + O_2$	$\rightleftharpoons$	$O + OH$	2.060×10^{14}	-0.10	62.85
$O + H_2$	$\rightleftharpoons$	$H + OH$	3.820×10^{12}	0.00	33.26
$O + H_2$	$\rightleftharpoons$	$H + OH$	1.020×10^{15}	0.00	80.23
$OH + H_2$	$\rightleftharpoons$	$H + H_2O$	2.170×10^{8}	1.52	14.47
$2\,OH$	$\rightleftharpoons$	$O + H_2O$	3.350×10^{4}	2.42	-8.06
$2\,H + M_1$	$\rightleftharpoons$	$H_2 + M_1$	1.020×10^{17}	-0.60	0.00
$2\,O + M_1$	$\rightleftharpoons$	$O_2 + M_1$	5.400×10^{13}	0.00	-7.40
$H + OH + M_2$	$\rightleftharpoons$	$H_2O + M_2$	5.560×10^{22}	-2.00	0.00
$H + O_2$	$\rightleftharpoons$	HO_2	2.650×10^{17}	-2.20	0.56
$H + O_2$	$\rightleftharpoons$	HO_2	2.730×10^{17}	-2.20	0.07
$H + HO_2$	$\rightleftharpoons$	$2\,OH$	4.460×10^{14}	0.00	5.82
$H + HO_2$	$\rightleftharpoons$	$O_2 + H_2$	1.050×10^{14}	0.00	8.56
$H + HO_2$	$\rightleftharpoons$	$O + H_2O$	1.440×10^{12}	0.00	0.00
$O + HO_2$	$\rightleftharpoons$	$OH + O_2$	1.630×10^{13}	0.00	-1.86
$OH + HO_2$	$\rightleftharpoons$	$O_2 + H_2O$	9.280×10^{15}	0.00	73.25
$2\,HO_2$	$\rightleftharpoons$	$H_2O_2 + O_2$	4.220×10^{14}	0.00	50.14
$2\,HO_2$	$\rightleftharpoons$	$H_2O_2 + O_2$	1.320×10^{11}	0.00	-6.82
$2\,OH$	$\rightleftharpoons$	H_2O_2	6.400×10^{17}	-1.80	4.13
$H + H_2O_2$	$\rightleftharpoons$	$HO_2 + H_2$	1.690×10^{12}	0.00	15.71
$H + H_2O_2$	$\rightleftharpoons$	$OH + H_2O$	1.020×10^{13}	0.00	14.97
$O + H_2O_2$	$\rightleftharpoons$	$OH + HO_2$	4.220×10^{11}	0.00	16.63
$O + H_2O_2$	$\rightleftharpoons$	$O_2 + H_2O$	4.220×10^{11}	0.00	16.63
$OH + H_2O_2$	$\rightleftharpoons$	$HO_2 + H_2O$	1.640×10^{18}	0.00	123.04
$OH + H_2O_2$	$\rightleftharpoons$	$HO_2 + H_2O$	1.920×10^{12}	0.00	1.78

Table A.2: Reaction mechanism for the combustion of hydrogen. Rate coefficient $k = AT^b \exp(-E_a/RT)$. Collision efficiencies in reactions including M_1: $f_{H_2} = 1.0, f_{H_2O} = 6.5, f_{O_2} = 0.4$. Collision efficiencies in reactions including M_2: $f_{H_2} = 1.0, f_{H_2O} = 2.55, f_{O_2} = 0.4$.

The conservation equations for this reaction mechanism are given by

$$c_H + c_{OH} + c_{HO_2} + 2c_{H_2O_2} + 2c_{H_2} + 2c_{H_2O} = C_1 \tag{A.8}$$

$$c_O + c_{OH} + 2c_{HO_2} + 2c_{H_2O_2} + 2c_{O_2} + c_{H_2O} = C_2. \tag{A.9}$$

Using only the 8 species $H, O, OH, HO_2, H_2O_2, O_2, H_2$ and H_2O, the mechanism in Table A.2 describes the combustion of hydrogen in pure oxygen. By adding the inert species N_2, the mechanism can also be used for the combustion of hydrogen in "clean" air (79% of N_2 and 21% of O_2). Nitrogen has

to be included in the computations of the third-bodies M_1 and M_2 with a collision efficiency of $f_{N_2} = 0.4$.

Bibliography

[1] R. Aglave. "CFD Simulation of Combustion Using Automatically Reduced Reaction Mechanisms: A Case for Diesel Engine". Ph.D. thesis, University of Heidelberg, 2007.

[2] J. Albersmeyer. "Effiziente Ableitungserzeugung in einem adaptiven BDF-Verfahren". Master's thesis, University of Heidelberg, 2005.

[3] P. Atkins and J. de Paula. *Atkins' Physical Chemistry*. Oxford University Press, 8th edn., 2006.

[4] I. Bauer. "Numerische Verfahren zur Lösung von Anfangswertaufgaben und zur Generierung erster und zweiter Ableitungen mit Anwendungen bei Optimierungsaufgaben in Chemie und Verfahrenstechnik". Ph.D. thesis, University of Heidelberg, 1999.

[5] I. Bauer, H. G. Bock, and J. P. Schlöder. "DAESOL – a BDF-code for the numerical solution of differential algebraic equations". Internal report, IWR, SFB 359, University of Heidelberg, 1999.

[6] E. D. Bloch. *A First Course in Geometric Topology and Differential Geometry*. Birkhäuser Boston Basel Berlin, 1997.

[7] H. G. Bock. *Randwertproblemmethoden zur Parameteridentifizierung in Systemen nichtlinearer Differentialgleichungen*, *Bonner Mathematische Schriften*, vol. 183. University of Bonn, 1987.

[8] H. G. Bock and K. J. Plitt. "A multiple shooting algorithm for direct solution of optimal control problems". In "Proc. 9th IFAC World Congress Budapest", Pergamon Press, 1984.

[9] M. Bodenstein. "Zur Kinetik des Chlorknallgases". *Z. Phys. Chem.*, vol. 85, pp. 329–397, 1913.

[10] M. Bodenstein and H. Lütkemeyer. "Die photochemische Bildung von Bromwasserstoff und die Bildungsgeschwindigkeit der Brommolekel aus den Atomen". *Z. Phys. Chem.*, vol. 114, pp. 208–236, 1924.

[11] V. Bykov, V. Gol'dshtein, and U. Maas. "Simple global reduction technique based on decomposition approach". *Combustion Theory and Modelling*, 2008.

[12] M. P. do Carmo. *Differential Geometry of Curves and Surfaces*. Prentice Hall, Englewood Cliffs, 1976.

[13] D. Chapman and L. Underhill. "The interaction of chlorine and hydrogen. The influence of mass." *J. Chem. Soc. Trans.*, vol. 103, pp. 496–508, 1913.

[14] E. Chiavazzo, A. N. Gorban, and I. V. Karlin. "Comparison of Invariant Manifolds for Model Reduction in Chemical Kinetics". *Commun. Comput. Phys.*, vol. 2(5), pp. 964–992, October 2007.

[15] C. Correa, H. Niemann, B. Schramm, and J. Warnatz. "Reaction Mechanism Reduction for Higher Hydrocarbons by the ILDM Method". In "Proceedings of the Combustion Institute", vol. 28, pp. 1607–1614, 2000.

[16] M. J. Davis and R. T. Skodje. "Geometric investigation of low-dimensional manifolds in systems approaching equilibrium". *J. Chem. Phys.*, vol. 111, pp. 859–874, 1999.

[17] S. Delhaye, L. M. T. Somers, J. A. van Oijen, and L. P. H. de Goey. "Simulating transient effects of laminar diffusion flames using flamelet libraries". In "Proceedings of the Third European Combustion Meeting", ECM, 2007.

[18] P. Deuflhard. "A Comparison of Related Concepts in Computational Chemistry and Mathematics". ZIB-Report 02-46, December 2002.

[19] P. Deuflhard, J. Heroth, and U. Maas. "Towards Dynamic Dimension Reduction in Reactive Flow Problems". In J. Warnatz and F. Behrendt, eds., "Modelling of Chemical Reaction Systems, Proceedings of an International Workshop, Heidelberg, Federal Republic of Germany, September 1-5, 1980", Springer, July 1996.

[20] M. Diehl, H. G. Bock, and J. P. Schlöder. "A real-time iteration scheme for nonlinear optimization in optimal feedback control". *SIAM Journal on Control and Optimization*, vol. 43(5), pp. 1714–1736, 2005.

[21] M. M. Diehl. "Real-Time Optimization for Large Scale Nonlinear Processes". Ph.D. thesis, University of Heidelberg, 2001.

[22] T. de Donder and P. van Rysselberghe. *Thermodynamic Theory of Affinity: A Book of Principles*. Stanford University Press, Menlo Park CA, 1936.

[23] A. Einstein. "Die Grundlage der allgemeinen Relativitätstheorie". *Ann. Phys.*, vol. 49, pp. 769–822, 1916.

[24] R. Fletcher. *Practical methods of optimization*. Wiley, John Wiley & Sons Chichester, second edn., 2001.

[25] T. Frankel. *The Geometry of Physics*. Cambridge University Press, Cambridge, New York, 1997.

[26] S. J. Fraser. "The steady state and equilibrium approximations: A geometrical picture". *J. Chem. Phys.*, vol. 88, pp. 4732–4738, 1988.

[27] C. W. Gear, T. J. Kaper, I. G. Kevrekidis, and A. Zagaris. "Projecting to a Slow Manifold: Singularly Perturbed Systems and Legacy Codes". *SIAM Journal on Applied Dynamical Systems*, vol. 4(3), pp. 711–732, 2005.

[28] C. Geiger and C. Kanzow. *Numerische Verfahren zur Lösung unrestringierter Optimierungsaufgaben*. Springer-Verlag Berlin Heidelberg New York, 1999.

[29] R. Gilbert, K. Luther, and J. Troe. "Theory of Thermal Unimolecular Reactions in the Fall-off Range. II. Weak Collision Rate Constants". *Ber. Bunsenges. Phys. Chem.*, vol. 87, pp. 169–177, 1983.

[30] H. Goldstein. *Classical mechanics*. Addison-Wesley, Reading, Mass., second edn., 1980.

[31] A. Gorban, I. Karlin, and A. Zinovyev. "Invariant Grids: Method of Complexity Reduction in Reaction Networks". *Complexus*, vol. 2, pp. 110–127, 2004/2005.

[32] A. N. Gorban and I. V. Karlin. *Invariant Manifolds for Physical and Chemical Kinetics*, *Lecture Notes in Physics*, vol. 660. Springer-Verlag Berlin Heidelberg New York, 2005.

[33] A. N. Gorban, I. V. Karlin, and A. Y. Zinovyev. "Constructive methods of invariant manifolds for kinetic problems". *Phys. Rep.*, vol. 396, pp. 197 – 403, 2004.

[34] A. Griewank. *Evaluating Derivatives: Principles and Techniques of Algorithmic Differentiation*. No. 19 in Frontiers in Appl. Math., SIAM, Philadelphia, PA, 2000.

[35] C. Großmann and J. Terno. *Numerik der Optimierung*. B.G. Teubner Stuttgart, second edn., 1997.

[36] J. Guddat, F. Guerra Vasquez, and H. T. Jongen. *Parametric Optimization: Singularities, Pathfollowing and Jumps*. B.G. Teubner, John Wiley & Sons, 1990.

[37] E. Hairer, S. P. Nørset, and G. Wanner. *Solving Ordinary Differential Equations I – Nonstiff Problems*, *Springer Series in Computational Mathematics*, vol. 8. Springer, Berlin, second edn., 1993.

[38] E. Hairer and G. Wanner. *Solving Ordinary Differential Equations II – Stiff and Differential-Algebraic Problems*, *Springer Series in Computational Mathematics*, vol. 14. Springer, Berlin, second edn., 1996.

[39] E. Hairer, G. Wanner, and C. Lubich. *Geometric Numerical Integration*. Springer Series in Computational Mathematics, Springer-Verlag Berlin Heidelberg New York, 2002.

[40] D. Hamiroune, P. Bishnu, M. Metghalchi, and J. C. Keck. "Rate-controlled constraint-equilibrium method using constraint potentials". *Combust. Theor. Model.*, vol. 2, pp. 81–94, 1998.

[41] J. Kammerer. "Numerische Verfahren zur dynamischen Komplexitätsreduktion biochemischer Reaktionssysteme". Ph.D. thesis, University of Heidelberg, 2007.

[42] H. G. Kaper and T. J. Kaper. "Asymptotic Analysis Of Two Reduction Methods For Systems Of Chemical Reactions". *Physica D*, vol. 165, pp. 66–93, 2002.

[43] J. C. Keck and D. Gillespie. "Rate-controlled partial-equilibrium method for treating reacting gas mixtures". *Combust. Flame*, vol. 17, pp. 237–241, 1971.

[44] H. B. Keller. *Numerical Solution of Two Point Boundary Value Problems.* No. 24 in Regional Conference Series in Applied Mathematics, SIAM, Philadelphia, 1976.

[45] E. L. King. "Unusual Kinetic Consequences of Certain Enzyme Catalysis Mechanisms". *J. Phys. Chem.*, vol. 60(10), pp. 1378–1381, 1956.

[46] E. L. King and C. Altman. "A Schematic Method of Deriving the Rate Laws for Enzyme-Catalyzed Reactions". *J. Phys. Chem.*, vol. 60(10), pp. 1375–1378, 1956.

[47] D. Kondepudi and I. Prigogine. *Modern thermodynamics.* WILEY-VCH Verlag GmbH, Weinheim, 1998.

[48] S. Lam. *Recent Advances in the Aerospace Sciences*, chap. Singular Perturbation for Stiff Equations using Numerical Methods, pp. 3–20. Plenum Press, New York and London, 1985.

[49] S. H. Lam and D. A. Goussis. "The CSP Method for Simplifying Kinetics". *Int. J. Chem. Kinet.*, vol. 26, pp. 461–486, 1994.

[50] D. Lebiedz. "Computing minimal entropy production trajectories: An approach to model reduction in chemical kinetics". *J. Chem. Phys.*, vol. 120, pp. 6890–6897, 2004.

[51] D. Lebiedz. "Optimal Control, Model- and Complexity-Reduction of Self-Organized Chemical and Biochemical Systems: A Scientific Computing Approach". Habilitation Thesis Physical Chemistry, University of Heidelberg, 2006.

[52] D. Lebiedz, J. Kammerer, and U. Brandt-Pollmann. "Automatic network coupling analysis for dynamical systems based on detailed kinetic models". *Phys. Rev. E*, vol. 72, p. 041 911, 2005.

[53] D. Lebiedz, V. Reinhardt, and J. Kammerer. "Novel trajectory based concepts for model and complexity reduction in (bio)chemical kinetics". In A. Gorban, N. Kazantzis, I. Kevrekidis, H. Öttinger, and C. Theodoropoulos, eds., "Model reduction and coarse-graining approaches for multi-scale phenomena", pp. 343–364. Springer, Heidelberg, 2006.

[54] D. B. Leineweber. "The Theory of MUSCOD in a Nutshell". Master's thesis, University of Heidelberg, 1995.

[55] D. B. Leineweber. *Efficient reduced SQP methods for the optimization of chemical processes described by large sparse DAE models*. VDI Verlag, Düsseldorf, 1999.

[56] D. B. Leineweber, I. Bauer, H. G. Bock, and J. P. Schlöder. "An Efficient Multiple Shooting Based Reduced SQP Strategy for Large-Scale Dynamic Process Optimization. Part I: Theoretical Aspects". *Comput. Chem. Eng.*, vol. 27, pp. 157–166, 2003.

[57] D. B. Leineweber, I. Bauer, H. G. Bock, and J. P. Schlöder. "An Efficient Multiple Shooting Based Reduced SQP Strategy for Large-Scale Dynamic Process Optimization. Part II: Software Aspects and Applications". *Comput. Chem. Eng.*, vol. 27, pp. 167–174, 2003.

[58] U. Maas. "Coupling of Chemical Reaction with Flow and Molecular Transport". *Appl. Math.*, vol. 40, pp. 249–266, 1995.

[59] U. Maas. "Efficient Calculation of Intrinsic Low-Dimensional Manifolds for the Simplification of Chemical Kinetics". *Computing and Visualization in Science*, vol. 1, pp. 69–81, 1998.

[60] U. Maas and S. B. Pope. "Simplifying Chemical Kinetics: Intrinsic Low-Dimensional Manifolds in Composition Space". *Combust. Flame*, vol. 88, pp. 239–264, 1992.

[61] U. Maas and J. Warnatz. "Simulation of Thermal Ignition Processes in Two-Dimensional Geometries". *Z. Phys. Chem. NF*, vol. 161, pp. 61–81, 1989.

[62] L. Michaelis and M. L. Menten. "Die Kinetik der Invertinwirkung". *Biochem. Z.*, vol. 49, pp. 333–369, 1913.

[63] A. H. Nguyen and S. J. Fraser. "Geometrical picture of reaction in enzyme kinetics". *J. Chem. Phys.*, vol. 91, pp. 186–193, 1989.

[64] H. Niemann. "Niedrigdimensionale Modellierung Dynamischer Systeme am Beispiel reduzierter Reaktionsmechanismen". Ph.D. thesis, University of Heidelberg, 2002.

[65] J. Nieto-Villar, R. Quintana, and J. Rieumont. "Entropy Production Rate as a Lyapunov Function in Chemical Systems: Proof". *Physica Scripta*, vol. 68, pp. 163–165, 2003.

[66] J. Nocedal and S. M. Wright. *Numerical Optimization*. Springer Verlag, New York, 1999.

[67] J. A. van Oijen and L. P. H. de Goey. "Modelling of Premixed Laminar Flames using Flamelet-Generated Manifolds". *Combust. Sci. Technol.*, vol. 161, pp. 113–137, 2000.

[68] M. S. Okino and M. L. Mavrovouniotis. "Simplification of Mathematical Models of Chemical Reaction Systems". *Chem. Rev.*, vol. 98, pp. 391–408, 1998.

[69] V. Petrov, E. Nikolova, and O. Wolkenhauer. "Reduction of nonlinear dynamic systems with an application to signal transduction pathways". *IET Syst. Biol.*, vol. 1(1), pp. 2–9, 2007.

[70] K. J. Plitt. "Ein superlinear konvergentes Mehrzielverfahren zur direkten Berechnung beschränkter optimaler Steuerungen". Master's thesis, University of Bonn, 1981.

[71] S. B. Pope. "Computationally efficient implementation of combustion chemistry using in situ adaptive tabulation ". *Combustion Theory Modelling*, vol. 1, pp. 41–63, Mar. 1997.

[72] M. Powell. "A Fast Algorithm For Nonlinearly Constrained Optimization Calculations". In A. Dold and B. Eckmann, eds., "Numerical Analysis", *Lecture Notes in Mathematics*, vol. 630, pp. 144–157. Springer-Verlag Berlin, 1978.

[73] V. Reinhardt, M. Winckler, and D. Lebiedz. "Approximation of slow attracting manifolds in chemical kinetics by trajectory-based optimization approaches". *J. Phys. Chem. A*, vol. 112(8), pp. 1712–1718, 2008.

[74] V. Reinhardt, M. Winckler, J. Warnatz, and D. Lebiedz. "Kinetic Mechanism Reduction by Trajectory-Based Optimization Methods". In "Proceedings of the Third European Combustion Meeting", ECM, 2007.

[75] Z. Ren and S. Pope. "Species reconstruction using pre-image curves". In "Proceedings of the Combustion Institute", vol. 30, pp. 1293–1300, 2005.

[76] Z. Ren, S. B. Pope, A. Vladimirsky, and J. M. Guckenheimer. "The Invariant Constrained Equilibrium Edge Preimage Curve Method for the Dimension Reduction of Chemical Kinetics". *J. Chem. Phys.*, vol. 124, p. 114 111, 2006.

[77] M. R. Roussel and S. J. Fraser. "Accurate Steady-State Approximations: Implications for Kinetics Experiments and Mechanism". *J. Phys. Chem.*, vol. 95, pp. 8762–8770, 1991.

[78] M. R. Roussel and S. J. Fraser. "Invariant Manifold Methods for Metabolic Model Reduction". *Chaos*, vol. 11, pp. 196–206, 2001.

[79] M. R. Roussel and T. Tang. "The functional equation truncation method for approximating slow invariant manifolds: A rapid method for computing intrinsic low-dimensional manifolds". *J. Chem. Phys.*, vol. 125, p. 214 103, 2006.

[80] B. Schramm. "Automatische Reduktion chemischer Reaktionsmechanismen am Beispiel der Oxidation von höheren Kohlenwasserstoffen und deren Verwendung in reaktiven Strömungen". Ph.D. thesis, University of Heidelberg, 2003.

[81] S. Shahshahani. "A new mathematical framework for the study of linkage and selection". *Mem. Am. Math. Soc*, vol. 17(211), 1979.

[82] O. Shaik, J. Kammerer, J. Gorecki, and D. Lebiedz. "Derivation of a quantitative minimal model from a detailed elementary-step mechanism supported by mathematical coupling analysis". *J. Chem. Phys.*, vol. 123, p. 234 103, 2005.

[83] S. Singh, J. M.Powers, and S. Paolucci. "On slow manifolds of chemically reactive systems". *J. Chem. Phys.*, vol. 117(4), pp. 1482–1496, 2002.

[84] R. H. Snow. "A Chemical Kinetics Computer Program for Homogeneous and Free-Radical Systems of Reactions". *J. Phys. Chem.*, vol. 70(9), pp. 2780–2786, 1966.

[85] W. Squire and G. Trapp. "Using Complex Variables to Estimate Derivatives of Real Functions". *SIAM Rev.*, vol. 40(1), pp. 110–112, 1998.

[86] J. Stoer and R. Bulirsch. *Introduction to numerical analysis*. Springer, New York, 1996.

[87] J. Troe. "Theory of Thermal Unimolecular Reactions in the Fall-off Range. I. Strong Collision Rate Constants." *Ber. Bunsenges. Phys. Chem.*, vol. 87, pp. 161–169, 1983.

[88] T. Turányi, A. S. Tomlin, and M. J. Pilling. "On the error of the quasi-steady-state approximation". *Journal of Physical Chemistry*, vol. 97(1), pp. 163–172, 1993.

[89] F. Verhulst. *Nonlinear Differential Equations and Dynamical Systems*. Springer-Verlag, Springer-Verlag Berlin Heidelberg New York, 2006.

[90] W. Walter. *Gewöhnliche Differentialgleichungen*. Springer-Verlag Berlin Heidelberg New York, 7th edn., 2000.

[91] J. Warnatz. "Calculation of the Structure of Laminar Flat Flames I: Flame Velocity of Freely Propagating Ozone Decomposition Flames." *Ber. Bunsenges. Phys. Chem.*, vol. 82, pp. 193–200, 1978.

[92] J. Warnatz. "Calculation of the Structure of Laminar Flat Flames II: Flame Velocity of Freely Propagating Hydrogen-Air and Hydrogen-Oxygen Flames." *Ber. Bunsenges. Phys. Chem.*, vol. 82, pp. 643–649, 1978.

[93] J. Warnatz. "Calculation of the Structure of Laminar Flat Flames III: Structure of Burner-Stabilized Hydrogen-Oxygen and Hydrogen-Fluorine Flames." *Ber. Bunsenges. Phys. Chem.*, vol. 82, pp. 834–841, 1978.

[94] J. Warnatz. "Concentration-, Pressure-, and Temperature-Dependence of the Flame Velocity in Hydrogen-Oxygen-Nitrogen Mixtures". *Combustion Science and Technology*, vol. 26(5), pp. 203–213, 1981.

[95] J. Warnatz, U. Maas, and R. W. Dibble. *Combustion: Physical and Chemical Fundamentals, Modeling and Simulation, Experiments, Pollutant Formation*. Springer, Berlin, 2006.

[96] S. Wiggins. *Introduction to Applied Nonlinear Dynamical Systems and Chaos*. Springer-Verlag Berlin Heidelberg New York, 1996.

[97] M. Winckler. "Towards optimal criteria for trajectory-based model reduction in chemical kinetics via numerical optimization". Master's thesis, University of Heidelberg, 2007.

[98] A. Zagaris, C. W. Gear, T. J. Kaper, and I. G. Kevrekidis. "Analysis of the accuracy and convergence of equation-free projection to a slow manifold", 2007.

[99] A. Zagaris, H. Kaper, and T. Kaper. "Analysis of the Computational Singular Perturbation Reduction Method for Chemical Kinetics". *J. Nonlin. Sci.*, vol. 14, pp. 59–91, 2004.

[100] J. Zobeley, D. Lebiedz, J. Kammerer, A. Ishmurzin, and U. Kummer. "A new time-dependent complexity reduction method for biochemical systems". *Trans. Comput. Syst. Biol.*, vol. 1, pp. 90–110, 2005.

List of Figures

Index